The Dissertation Committee for Pravat Karki Certifies that this is the approved version of the following dissertation:

An Integrated Approach to Measure and Model Fatigue Damage and Healing in Asphalt Composites

Committee:

Amit Bhasin, Supervisor

Randy Machemehl

Jorge A. Prozzi

Zhanmin Zhang

Wei Li

An Integrated Approach to Measure and Model Fatigue Damage and Healing in Asphalt Composites

by

Pravat Karki, B.E.; M.S.

Dissertation

Presented to the Faculty of the Graduate School of

The University of Texas at Austin

in Partial Fulfillment

of the Requirements

for the Degree of

Doctor of Philosophy

The University of Texas at Austin

August 2014

Dedication

To my parents and wife

Acknowledgements

I would like to acknowledge everyone who has assisted throughout my graduate studies over the years. Fore and foremost, I want to thank Professor Amit Bhasin for generously serving as my research advisor and continuously providing me invaluable guidance, feedback and resources required for this research study. It has been my privilege to work with him in several different exciting and challenging research studies. I want to acknowledge here the Federal Highway Administration (Contract No. DTFH61-07-H-00009) and the National Science Foundation (CMMI Award No. 1053925) for providing the financial assistant required for this particular study.

I would also like to thank Professors Randy Machemehl, Jorge A. Prozzi, Zhanmin Zhang and Wei Li from the University of Texas at Austin, TX for serving as my dissertation committee members and helping me refine my overall research. I am also grateful to Professor Dallas N. Little from the University of Texas A&M at College Station, TX and Professor Youngsoo Richard Kim from North Carolina State University at Raleigh, N.C. for their invaluable feedback.

My special thanks goes to Sharmin Sultana and Zelalam Arega from the University of Texas at Austin, Nabaraj Banajara from the University of Nebraska-Lincoln, Soohyuk Im from Texas A&M University and Ruixia Li from Chang'an University for a great camaraderie and selfless help during my graduate study.

I also want to thank my parents and brothers back home in Katmandu, Nepal and in-laws in Biratnagar, Nepal for motivating me to pursue advanced degrees. Last but by no means least, a very cordial thanks to my dear wife Roshani Thapa for her continuous support, and understanding and above all, for her love.

An Integrated Approach to Measure and Model Fatigue Damage and Healing in Asphalt Composites

Pravat Karki, Ph.D.

The University of Texas at Austin, 2014

Supervisor: Amit Bhasin

This study presents a test and analysis method to determine both damage and healing characteristics of asphalt composites using the same test specimen. The test involves applying multiple stretches of load cycles, each separated by a period of zero load introduced at several different levels of reduced stiffness. The analytical procedure involves (1) using modified correspondence principles to transform the time-dependent physical quantities (stress, strain and energy density) into time-independent pseudo-elastic quantities, and then (2) using viscoelastic continuum damage mechanics to quantify damage and healing properties of the material based on the transformed quantities. The results obtained using two different asphalt mortars subjected to uniaxial and shear load cycles confirmed the findings from the previous researchers that the characteristic pseudo stiffness versus damage relationship for a given material is independent of testing conditions. More importantly, this study demonstrated that the aforementioned relationship was also independent of the rest periods introduced intermittently during the cyclic tests. Results also show that healing defined in terms of the change in the internal state variable for damage represents the true healing potential of a material. Furthermore, healing properties obtained using the proposed test method (a) agreed with the properties obtained using a more rigorous protocol with multiple test

specimens, and (b) were independent of the loading conditions used to induce fatigue damage. These observations strongly suggest that the proposed method can be used to predict damage and healing properties for any arbitrary loading condition from properties determined using the proposed protocol.

Table of Contents

List of Tables

List of Figures

Chapter 1: Introduction

1.1 BACKGROUND

Asphalt pavements continually experience physical and environmental loads due to repetitive traffic movements and the change in temperature. These loads instigate microcracks that initiate at imperfections and propagate through the pavement structure. The nucleation, coalition and growth of microcracks with time induces fatigue cracking in asphalt mixtures (Bhasin et al. 2009). The incessant fatigue cracking leads to structural and serviceability failures in the absence of timely and adequate maintenance. Laboratory tests have revealed that asphalt pavement mixtures not only lose their mechanical integrity during loading but also have capacity to recover this loss during periods of near zero loads (Bazin and Saunier 1967; Bhasin and Little 2007; Carpenter and Shen 2006; Kim 1988; Kim et al. 2003; Lee and Kim 1998a; b; Raithby and Sterling 1970; Tayebali et al. 1994). In-situ tests of asphalt pavement mixtures have also corroborated this phenomena of load-induced damage evolution and rest-induced stiffness recovery or healing (Little et al. 2001; Lytton et al. 2001a; b; Williams et al. 2001). The time gaps between the passages of successive wheel axles of the same or consecutive vehicles provide rest periods in pavements. These previous studies have also claimed that strength recovery during rest periods can increase fatigue lives of asphalt materials and pavements, thereby suggesting the importance of incorporating healing in prediction models. Lytton et al. (1993) exemplified the benefit of such inclusion by demonstrating a better prediction of pavement life with a shift factor dedicated to healing. Despite the convincing evidence of healing and its importance in accurately predicting the fatigue cracking life of asphalt mixtures, one can find only a few tests and methods to quantify healing along with damage.

1.2 PROBLEM STATEMENT

Test methods that are typically used to measure damage and healing properties of asphalt materials quantify them in terms of metrics that are affected by applied test conditions such as loading rate, loading magnitude, loading mode and test temperature (Ghuzlan and Carpenter 2000; Kim et al. 1997). Typical examples of such metrics include the number of load cycles to failure as a measure of fatigue cracking resistance (Aragao, Lee, et al. 2010; Kim et al. 2003; Reese 1997) and the percentage of stiffness recovery due to a rest period as a measure of healing capacity (Bazin and Saunier 1967; Kim 1988; Lee and Kim 1998a). As such, the metrics determined from one particular loading condition cannot be used to predict the response of the material at any other arbitrary loading condition. Therefore, damage and healing properties of asphalt materials determined from conventional methods cannot be treated as true material properties. Due to test condition dependency of such metrics, contemporary test methods require separate test specimens for each expected loading condition (Palvadi et al. 2012). Furthermore, these methods require tests without rest periods to quantify damage and separate tests with rest periods to quantify healing. To overcome these limitations, it is imperative to devise an efficient method that uses the minimum number of test specimens and test runs to characterize both damage and healing properties of asphalt materials in terms of metrics that are independent of test conditions.

1.3 RESEARCH OBJECTIVES AND SCOPE

The primary objective of this study was to devise and verify a method that can quantify both damage and healing properties of asphalt materials

- using the same specimen,
- using metrics that are independent of loading conditions, and
- that can be used in cyclic shear as well as cyclic uniaxial tests.

To achieve these objectives, this study makes use of the viscoelastic continuum damage mechanics (VECD) and associated metrics. This study proposes and verifies the hypothesis that the partially or fully healed materials recover their inherent damage evolution rate (i.e., the damage evolution rate without any rest period) after certain number of load cycles following the rest period. A corollary of this hypothesis is that multiple rest periods can be introduced during a fatigue test to evaluate both fatigue characteristics without any rest period as well as healing characteristics during the rest periods. In other words, it is hypothesized that the VECD-based pseudo-stiffness versus damage curve of a given material is independent of the number and duration of rest periods. This study investigates the validity of this hypothesis using three different asphalt composites and two different modes of fatigue cracking. This study also exploits this behavior to develop a very cost efficient yet accurate method of characterizing fatigue damage and healing.

The asphalt composites used in this study contain higher percentage and proportion of both binder and fine aggregates than the typical full asphalt mixtures, but follow the same material constitution, i.e. viscoelasticity (Karki, Li, et al. 2014; Kim et al. 2003; Li et al. 2014; Palvadi et al. 2012). Similarly, the modes of loading used in this study include cyclic shear (Chapter 3) and cyclic tension-compression (Chapter 4). For analytical purposes, this study quantifies fatigue and healing in terms of VECD-based internal state variable and its change due to rest periods. This study also verifies that the selected metrics are true material properties by demonstrating their independence under several different loading conditions. Also, this study investigated the influence of the duration and number of rest periods and the stiffness preceding the rest periods on the healing behavior of the materials.

1.4 DISSERTATION ORGANIZATION

This dissertation contains five different chapters, including the current one. As is seen, the first chapter introduces the need of a simplified test and analysis method that can quantify both damage and healing properties of asphalt composites using the same specimen in terms of metrics that are independent of the test conditions. This chapter also defines the objectives and the scope of this study. The second chapter reviews the merits and limitations of previous test methods and models used to measure or predict overall damage and healing properties of asphalt materials. The third chapter proposes a method to quantify both fatigue damage and healing properties of asphalt mixtures in torsional shear from the same specimen. Furthermore, this chapter verifies that the properties obtained using the proposed method are equivalent to the properties obtained using a more elaborate method that requires multiple specimens to measure similar properties. The fourth chapter then describes how the same method used in torsional shear mode can also be applied in uniaxial tension-compression mode. Both the third and the fourth chapters also include additional tests to verify the test condition independency of the proposed models. Furthermore, the fourth chapter also presents and verifies a procedure to predict the fatigue-cracking life of asphalt materials with and without rest periods using the test results obtained from the proposed method. The final and fifth chapter provides concluding remarks along with contributions of the proposed method.

Chapter 2: Literature Review

2.1 BACKGROUND

Over the years, researchers have developed several different test methods and analytical models to characterize fatigue behavior of asphalt materials subjected to different loading and temperature conditions, and use these measured properties to predict pavement lives. Typical laboratory test methods include the uniaxial tension-compression tests, the indirect tension tests, the torsional shear tests, the compact tension test and the bending beam tests. These tests usually simulate one mode of failure in asphalt pavements such as bottom-up cracking, top-down cracking, shear cracking, etc. (Figure 2.1). However, despite a wide variety of test methods and models, there still exists a significant amount of discrepancy between the pavement fatigue life predicted using laboratory-measured material properties and the actual pavement fatigue life (Kim and Little 1990; Lytton et al. 1993).

Lytton et al. (1993) mentioned that the use of shift factors are necessary to narrow the discrepancy between the predicted and actual pavement lives. However, to a large extent, these shift factors reflect the inadequacy of mechanistic or material constitutive models to accurately reflect true material behavior. For example, the effect of rest period between the passages of consecutive axles of the same or different vehicles is one of those mechanisms that are either completely ignored or inadequately accounted for in contemporary predictive models. Field (Little et al. 2001; Lytton et al. 2001a; b; Nishizawa et al. 1997; Williams et al. 2001) as well as laboratory (Bhasin et al. 2008; Kim et al. 2003; Lee and Kim 1998a) studies have verified that healing is an important mechanism that has a significant influence on the fatigue cracking life of asphalt mixtures. However, most of the current test methods quantify healing and damage using

separate specimens in terms of metrics that are dependent on loading or testing conditions, thereby necessitating separate tests at several different loading conditions that can be expected in the field.

The following sections will provide a synthesis from the review of the literature that focuses on (a) the evidence of healing in asphalt pavements and asphalt materials, (b) the micro-mechanical explanation of healing, and (c) the synopses of two broad major approaches to characterize overall damage and healing.

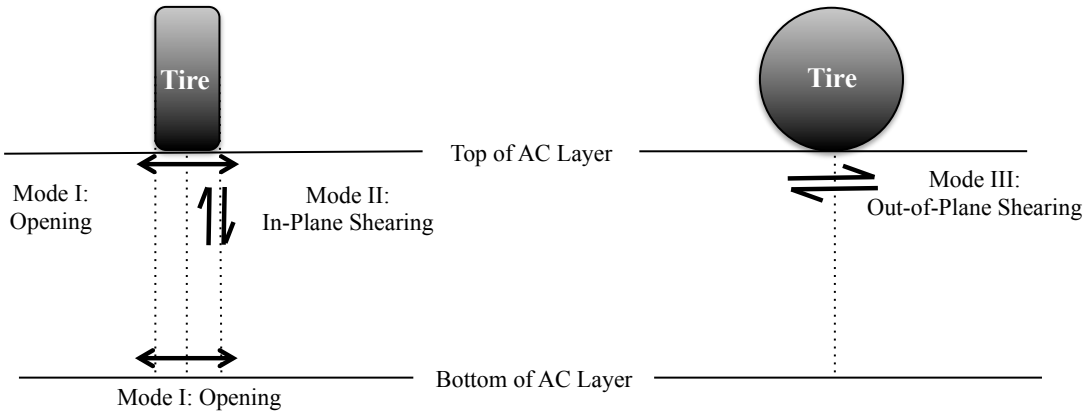

Figure 2.1: Schematic examples of different types of crack formation in asphalt pavements

2.2 HEALING: A SYNOPSIS

2.2.1 Healing in Asphalt Pavements

Several researchers have studied the impact of rest periods on overall properties and performance of asphalt pavements. For example, in an extensive field study, researchers (Little et al. 2001; Lytton et al. 2001a; b; Williams et al. 2001) investigated the effect of rest periods on the stiffness of four different pavement sections at the Accelerated Loading Facility of Turner-Fairbanks Highway Research Center. The

researchers performed surface wave tests along the wheel path before, during and after 24-hr long rest periods that were introduced between repetitive traffic load cycles. They were able to extract the change in overall stiffness by monitoring the change in wave speed. The researchers also performed similar tests at MnROAD pavement test track sections near Albertville, Minnesota and the pavement sections on U.S. Highway 70 in North Carolina. The researchers consistently observed a recovery in stiffness due to the introduction of rest period, and attributed this recovery to "microdamage healing". Moreover, the researchers also observed that the duration of rest period and the grade of binder influenced the overall stiffness. The researchers mentioned (a) the structural changes due to relaxation, (b) the steric hardening of binder due to molecular restructuring, and (c) the increase in stiffness as the main reasons behind the reversal of microdamage.

In another study, Nishizawa et al. (1997) studied the effect of rest periods on four thick pavement sections. The researchers remarked that microdamage healing capacity of asphalt materials can completely offset the fatigue-related damage at low strains by healing the microcracks and therefore can keep the pavements perpetually intact.

2.2.2 Healing in Asphalt Materials

Laboratory tests have also provided substantial proof of healing in asphalt binders, mortars and mixtures. In one of the early studies, Bazin and Saunier (1967) performed monotonic uniaxial tests and dynamic flexural tests on asphalt concrete beams to investigate the effect of rest periods. The researchers first performed these tests on the intact specimens until failure. They then kept the fractured faces of the specimens in contact with each other for different durations of rest periods (1-300 days) under various temperature-pressure conditions. Finally, they repeated the same tests on these

conditioned specimens. From the monotonic uniaxial tests, the researchers measured the tensile strength of beams before and after rest periods and determined an index for healing based on tensile strength. Similarly, from the dynamic flexural tests, the researchers measured the number of cycles required to create a rupture in the beams before and after applying a rest period. The researchers observed a recovery in the tensile strength of beams and an equivalent increase in fatigue life. For example, a 3-day long rest period recovered the tensile strength by 90% while a 1-day long rest period increased the fatigue life by 50%.

Similarly, Raithby and Sterling (1970) investigated the effect of rest period on fatigue life by performing stress-controlled uniaxial cyclic tests on asphalt concrete beams at different frequencies and temperatures. The researchers reported a recovery in strain energy and a longer fatigue cracking life due to the rest period. Only rest periods of significant durations resulted in a noticeable increase in fatigue life in their study.

In another study, McElvaney and Pell (1973) conducted uniaxial cyclic tests on asphalt concrete specimens at different stress amplitudes and studied the effect of rest period. The researchers mentioned that it is important to introduce a rest period before a certain level of damage to yield noticeable increase in fatigue life. The researchers found that only rest period with duration up to ten times the loading cycle increased the fatigue life. This observation suggested that there is an optimum value of rest duration that can show a significant increase in fatigue life.

Bonnaure et al. (1982) investigated the influence of rest period on fatigue life by conducting three-point bending beam tests on asphalt composites at different stress, strain and temperature conditions. When the researchers introduced rest periods of durations equal to 0-25 times the loading cycle, they observed an increasing trend of fatigue life with an increase in the duration of the rest period. The impact of rest periods was more

substantial in stress-controlled cyclic tests than in strain-controlled cyclic tests. This observation illustrated the influence of loading mode in addition to the duration of the rest period on the overall healing characteristics of the method.

Daniel and Kim (2002) conducted flexural fatigue tests on asphalt concrete beams with rest periods of variable durations at different test temperatures. They monitored the change in flexural stiffness using impact on resonance test. The researchers calculated the increase in the number of cycles to failure due to a rest period to determine the benefit of healing. Also, the researchers used the number of cycles endured at a particular rest period normalized with respect to the number of cycles to failure as the "damage indicator".

Similarly, Kim et al. (2003) investigated the effect of healing on overall properties of sand-asphalt matrices by performing cyclic shear tests with and without rest periods at 10 Hz and 25ºC using a dynamic mechanical analyzer. The researchers introduced 120-second long rest periods at ten different stiffness levels during the cyclic tests and reported the consequential increase in dynamic modulus, pseudo-stiffness and dissipated strain energy as healing indices. Equally important was the 9-24% rise in fatigue life due to the introduction of rest periods depending upon the applied strain amplitude and the binder. These results reconfirm the dependence of healing indices on loading mode and material type.

Carpenter and Shen (2006) studied the effect of rest periods on fatigue cracking life by subjecting four-point bending beams of asphalt composites to cyclic loads with rest periods of various duration (0 to 9 second) after each load cycle. In this work, the researchers monitored the ratio of dissipated energy change (RDEC) due to the rest period at 50% fatigue failure criteria as an indicator of the effect of rest period. The results showed that rest period have significant influence on the RDEC value. Roque et

al. (2006) also demonstrated that aggregate angularity, film thickness, and volume of mineral aggregates dictated the healing characteristics of an asphalt mixture.

In a recent study, Palvadi et al. (2012) reaffirmed the influence of rest period on the overall properties of fine aggregate matrices as well as the intrinsic properties of asphalt binders. The researchers reported these findings based on the tests conducted using two different fine aggregate matrices and the two different binders. The researchers also mentioned that the duration of rest period and the stiffness level preceding the rest period governed the healing capacity of the fine aggregate matrices.

The aforementioned extensive evidence of the effect of rest periods on the fatigue cracking life of asphalt composites highlights the importance of being able to quantify healing potential of asphalt materials and incorporate this potential into mixture response model, pavement response model and pavement performance model. The following section will provide the synopses of some research studies that described the mechanism of healing as a crack closing phenomenon.

2.3 Crack Opening and Closing Mechanisms

Both damage and healing are fundamentally the consequences of the change in the size of one or more microcracks. According to fracture damage mechanics, a microcrack initiates in a material when and where the applied load intensity exceeds a certain threshold value that is characteristic to a given loading condition and the material. The microcrack then propagates through the points that successively exceed this threshold value following a power relationship with the difference between the maximum and minimum stress intensities, ΔK (Paris and Erdogan 1963; Paris et al. 1961):

$$\frac{dc}{dN} = \beta . \Delta K^{\alpha} \qquad 2.1$$

In Equation 2.1, dc/dN denotes the rate of change of crack length, c with respect to the number of load cycles, N. The terms α and β are material-specific properties. Researchers have used different variations of this model to describe crack growth in elastic (Rice 1968) and inelastic materials (Schapery 1973, 1975a; b; c, 1984). For example, the dissipated strain energy per unit surface area of cracks ($J-$integral) describes the crack opening in elastic materials. Similarly, the pseudo-dissipated strain energy per unit surface area of cracks ($J_v - i$ntegral) explains the initiation and propagation of macro- or nano-crack in viscoelastic materials such as asphalt cements and composites. Schapery (1984) presented a Paris-law type power relation to describe rate of cracking in viscoelastic materials:

$$\frac{dc}{dt} = [f(J_v)]^k \qquad 2.2$$

In equation 2.2, k is a material specific property. A number of researchers have explained healing as a crack-closing phenomenon involving thermo-mechanics of crack surfaces and molecules. In one such study, Wool and O'Connor (1981) mentioned healing as a micromechanical phenomenon consisting of five separate steps. According to these researchers, microcrack surfaces first (i) readjust, (ii) approach and (iii) retouch each other due to inherent cohesion or externally applied pressure-temperature condition. Then, the molecules on crack surfaces (iv) diffuse across the wet surfaces and (v) randomly relocate to regain original structural configuration and intrinsic mechanical properties. The researchers modeled the total healing (R) due to crack closing as a convolution integral of a wetting distribution function (ϕ) that describes the effect of crack closing rate and an intrinsic healing function (R_h) that describes the recovery of mechanical properties over time (τ):

$$R = \int_{-\infty}^{t} R_h(t-\tau)\frac{d\phi(\tau)}{d\tau}d\tau \qquad 2.3$$

Wool and O'Connor (1981) mentioned that this intrinsic healing depends on the material-specific properties such as molecular weight, surface free energy or cohesive force and the intensity of external impetus such as temperature and pressure. Another work by Kim and Wool (1983) added that the diffusion and reorientation of surface molecules occurs across molecular chains of polymers and at or above the glass transition temperature of the polymer material. Kim et al. (1990) addressed the molecular chain requirement of healing (Kim and Wool 1983) by introducing healing process zone and the functional morphology in asphalt materials.

Similarly, Schapery (1984) derived an energy equilibrium relationship to describe crack opening using the first principles of fracture mechanics. This relationship states that the work required for structural changes in a material by a certain amount and the mechanical work available to cause that change are equal. Schapery (1984) used this concept to express total density of surface energy in a viscoelastic media due to crack growth (2Γ) as a function of the time-dependent creep compliance [$D(t)$] and the dissipated pseudo strain energy density per unit area of the material (J_v):

$$2\Gamma = f(Creep\ properties, Dissipated\ energy) = E_R D(t)\, J_v \qquad 2.4$$

The multiplier "2" in this energy balance relationship represents the involvement of two crack surfaces in fracture process. Important to note here is the use of pseudo strain energy variant (J_v) and pseudo-elastic modulus (E_R) based on Schapery's extended correspondence principles that allow the use of time-independent pseudo variables instead of time-dependent viscoelastic variables.

Schapery (1989) extended the aforementioned energy balance relationship (Schapery 1984) to derive the instantaneous rate of healing ($\dot{h_2}$) as a function of thermo-mechanical properties of a viscoelastic material, including surface energy (Γ_h):

$$\dot{h_2} = \frac{dh_2}{dt} = f(Creep\ and\ hysteresis\ properties, Surface\ energy) = \left[\frac{2\gamma_m E_R^2 D_{1c} \Gamma_h}{(1-\upsilon^2) C_m^{1/m} H_V}\right]^{1/m_c} \beta \quad 2.5$$

In this expression, D_{1c}, m_c and γ_m together describe the creep compliance of the material in compression, while υ, E_R, H_V, and C_m refer to Poisson's ratio, reference elastic modulus, stress-strain hysteresis integral and average length of crack in the material. Similarly, β refers to the length of the fracture or healing process zone as shown in Figure 2.2. However, in contrary to Schapery's energy-driven crack closing hypothesis (1989), Lytton et al. (1998) presented wetting surface energy as the deterrent of crack closing. Based on the energy-inhibited crack-closing hypothesis, Lytton et al. (1998) modeled long-term "healing speed" ($\dot{h_1}$) as an inverse function of surface energy (Γ_h) as given by:

$$\dot{h_1} = \frac{dh_1}{dt} = g\left(Creep\ and\ hysteresis\ properties, \frac{1}{Surface\ energy}\right) = \left[\frac{(k_{th}) D_{1c} E_R H_V}{2\Gamma_h}\right]^{1/m_c} \beta \quad 2.6$$

In this relationship, k_{th} represents a fitting constant, whereas other symbols carry the same meaning as in Schapery's short-term "healing speed" model (1989).

Later, Kim et al. (1988; 1990) described net healing as the cumulative effect of two mechanisms - mechanical healing due to viscoelastic relaxation of stresses in the materials, and chemical healing at the crack surfaces due to energy imbalance. The researchers (Kim 1988; 1990) quantified net healing in asphalt materials in terms of a

"healing index" (HI), which is defined as the ratio of recovered dissipated pseudo strain energy (Φ) due to rest period and the dissipated pseudo strain energy preceding the rest period:

$$HI = \frac{\Phi_{after\ rest} - \Phi_{before\ rest}}{\Phi_{before\ rest}} \quad 2.7$$

In their study, the researchers observed dependence of the healing index on the duration of rest period, the temperature during the rest period, and the chemistry and rheology of the binder.

Lytton (2000) mentioned that the difference between the available or stored surface energy density and the dissipated surface energy density per unit crack surface area dictates whether the material undergoes damage by increasing crack surfaces or healing by decreasing crack surfaces. The researchers also reinforced the earlier finding that healing depends on the length of rest period, the temperature during the rest period, and the binder itself. Similarly, Carpenter and Shen (2006) also used the energy balance concept between surface energy and the dissipated energy to explain both fracture damage and healing. The researchers stated that, when the stored surface energy is lower than the dissipated energy, a material increases the surface area of microcracks and therefore accumulates more damage. But, when the stored surface energy is higher than the dissipated energy, the material reduces the surface area of microcracks and partially heals the inherent material properties depending upon the length of rest period.

Bhasin et al. (2007; 2008, 2011; 2009) simplified Wool and O'Connor's intrinsic healing function (Wool and O'Connor 1981) and combined it with Schapery's crack-surface wetting distribution concept (Schapery 1989) to model intrinsic healing in asphalt materials. The simplified model captures all three parts of healing phenomenon - the effect of surface wetting, the instantaneous or short-term healing immediately after the

crack surfaces wet each other, and the constant or long-term healing due to relentless diffusion and molecule randomization across the wet crack surfaces. As shown in Figure 2.2, the researchers used the healing process zone (β) to describe micromechanical process of healing in asphalt materials as used earlier.

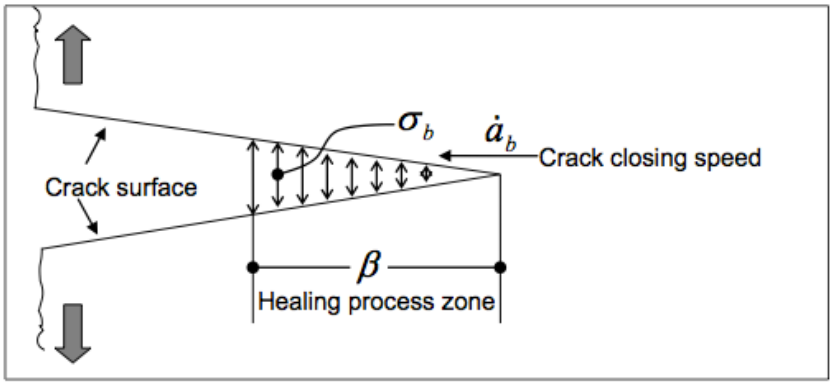

Figure 2.2: Schematic of crack closing phenomenon based on opening mode of fracture (Bhasin et al. 2008; Schapery 1989)

As evident from above research synopses, the inherent material properties as well as the external pressure and temperature govern the rate of crack closing and the net amount of intrinsic healing. The combined effect of wetting distribution and intrinsic healing involving one or more microcracks yields the overall healing. This dissertation is mainly focused on determining the overall or effective damage and healing.

2.4 Mechanistic Models

A number of studies have described micro-damage and micro-damage healing using two broad mechanistic approaches: (1) viscoelastic fracture damage mechanics, and (2) viscoelastic continuum damage mechanics.

2.4.1 Viscoelastic Fracture Damage Mechanics

Fracture damage mechanics is primarily founded on the Paris law of crack growth. Test methods that are based on fracture damage mechanics usually require compact test specimens with and without a pre-crack depending upon the intended mode of failure (e.g., opening, shearing and tearing). In the tests with a pre-crack, the crack tip opening displacement (CTOD) or the crack mouth opening displacement (CMOD), or simply the trajectory of a crack tip are continuously monitored. The two most common compact test specimens of asphalt materials include the compact tension specimens (Edwards and Hesp 2006; Wagoner et al. 2005a) and the single-edge notched flexural beam specimens (Wagoner et al. 2005b). In these tests, the change in mechanical properties and crack size due to the applied load, with and without rest periods are studied. However, the geometrical intricacy of asphalt composites creates discontinuities and unwarranted deviations in crack growth even if a pre-crack is installed (Jacobs et al. 1996), thus contradicting the basic concept of continuous crack growth with a well-defined geometry. In order to address the issue of heterogeneous composites, one needs to resort to computational micromechanics.

Computational micromechanics uses heterogeneous microstructures, laboratory-measured constituent properties, fracture damage mechanics models and numerical tools to predict the overall properties of the composites subjected to different boundary value problems. As such, the accuracy of such models primarily depends on the accuracy of laboratory-measured constituent properties. Also, the commonly used computational micromechanics models such as cohesive zone models (Barenblatt 1962; Tvergaard and Hutchinson 1992; Yoon and Allen 1999) usually address one or more of healing, anisotropy, aging and thermo-inelasticity but not all together. Dealing with each and

every constitutive mechanism simultaneously needs scrutiny and therefore complicates the simulation process.

Another limitation of computational micromechanics is that the heterogeneous microstructures need to be generated using digital images (Aragao, Kim, et al. 2010; Karki 2010; Karki, Kim, et al. 2014; Masad et al. 1999) or X-ray computed tomography images (Song et al. 2005; Wang et al. 2001; You et al. 2009) of actual asphalt concrete specimens. A recent study also proposed a virtually generated microstructure (Haft-Javaherian 2011) for such predictions. However, the size of microstructure that adequately replicates the representative volume and mechanical responses of the selected composites depends on the level of heterogeneity of the material. For example, a composite with higher heterogeneity requires a larger size of microstructure and consequently a higher resolution to capture the constituent material phases than a composite with a lower heterogeneity.

Computational fracture damage mechanics requires finite element methods (Dai et al. 2006; Guddati et al. 2002; Kim and Buttlar 2009; Masad et al. 2001; Sadd et al. 2003) or discrete element methods (Abbas et al. 2005; Buttlar and You 2001; Dai and You 2007) to simulate the boundary value problems in the microstructures. As a result, the computational effort required for optimized solutions increases with an increase in heterogeneity, and therefore might compromise efficiency.

Researchers have also attempted to reduce this inefficiency by assuming fewer phases of materials in asphalt composites. For example, recent studies predicted the linear viscoelastic properties (Aragao et al. 2010; Karki 2010; Karki et al. 2014) as well as damage properties (Aragao 2011) of asphalt composites using computational micromechanics assuming only two phases in full mixtures – the elastic phase of aggregates and the viscoelastic phase of fine aggregate-binder matrix. These studies

assumed that the aggregate and matrix phases of full mixtures share binder and air void contents based on an assumed thickness of binder film around the aggregates. Furthermore, the lack of aggregate-aggregate contact used in the studies limited the intended accuracy. In a recent study, Underwood and Kim (2013a) demonstrated that mechanical properties of fine aggregate matrix depends on the volumetric properties, and therefore the use of fine aggregate matrix in micromechanical models is justified only when the fabricated matrix truly replicates the corresponding phase in full mixtures. However, the studies have demonstrated that the consistently fabricated fine aggregate matrix can be used to analyze the influence of constituents binders (Li et al. 2014), as well as for model development (Palvadi et al. 2012).

2.4.2 Viscoelastic Continuum Damage Mechanics

Continuum damage mechanics assumes that the geometry of the continuum is much larger than the geometry of the microcrack and therefore the focus is to study the average state of damage in a continuum instead of monitoring the trajectory of individual cracks (Park and Schapery 1997; Park et al. 1996; Schapery 1975a). Viscoelastic continuum damage mechanics (VECD) describes damage and healing in viscoelastic materials using Schapery's extended correspondence principles (Schapery 1984) and Schapery's work potential theory based on irreversible thermodynamics (Schapery 1986, 1987). Schapery's extended correspondence principles translate the time-dependent stresses and strains of a viscoelastic material into time-independent pseudo stresses and pseudo strains of a reference elastic material. Similarly, Schapery's work potential theory provides a Paris-law type relationship of overall damage with the change in pseudo strain energy and the change in stress-strain history of a reference elastic material (Park and Schapery 1997; Park et al. 1996; Schapery 1986).

A number of researchers have applied viscoelastic continuum damage mechanics (VECD) approach to characterize fatigue damage and overall healing in asphalt materials. In one of the early works, Kim and Little (1990) studied the response of sand-asphalt composites subjected to multilevel load cycles with rest periods using the viscoelastic continuum damage mechanics model. The researchers identified viscoelastic relaxation and fatigue damage as the two key mechanisms that constitute the effective behavior of asphalt materials. Kim and Little (1990) adopted Schapery's second correspondence principle ($CP-II$) to separate the influence of hereditary viscoelastic effects on the overall damage or healing that involved the change in traction boundary. The researchers modeled effective damage due to fatigue as a power integral of pseudo strain (ε^R) over time (t).

$$S_p = \left(\int_0^t |\varepsilon^R|^p \, . \, dt \right)^{\frac{1}{p}} \qquad 2.8$$

In this cumulative damage model, the integral value (S_p) refers to an internal state variable for damage at time (t), and the slope parameter (p) refers to a material-specific parameter. The internal state variable (S_p) does not have any physical meaning but represents only the average state of damage. Kim and Little (1990) verified that the constitutive damage model developed from uniaxial tests could capture the effect of multilevel loading, the effect of sequence of multilevel loading, and the effect of rest periods.

In another study, Kim et al. (1995) used Schapery's extended elastic-viscoelastic correspondence principles to describe damage and healing behavior of densely graded asphalt concrete mixtures. The researchers applied haversine compressive stress cycles of three different amplitudes on the cylindrical specimens at 0.2 second/cycle loading rate and 25ºC with rest periods (1, 4, 8 and 6 seconds). For the purposes of analysis, the

researchers used Schapery's second correspondence principle and transformed the measured displacements and stresses into time-independent "pseudo-displacements" and "pseudo-stresses". Kim et al. (1995) successfully used the change in hysteresis behavior to describe damage due to load cycles and healing due to rest periods. However, the researchers did not use specific metrics to quantify damage and healing in this particular study.

Similarly, Park et al. (1996) applied the viscoelastic continuum damage mechanics to model the behavior of asphalt mixtures subjected to uniaxial tension. The researchers selected an internal state variable (S^*) to represent the overall state of damage in the material continuum. Defining pseudo strain energy density of material as a function of selected damage parameter and other associated variables, and using the Schapery's rate-type damage evolution law (Schapery 1986, 1987), Park et al. (1996) derived an integral relation for damage, wherein the slope parameter (α) is a material-specific parameter.

$$S^* = \left(\int_0^t |\varepsilon^R|^{2\alpha} . dt \right)^{\frac{1}{2\alpha}} \qquad 2.9$$

This viscoelastic constitutive model resembles the model developed earlier by Kim and Little (1990), except for the material parameters - p and α. Equally important, Park et al. (1996) also suggested that the proposed constitutive model bears a similar form when the reduced time was calculated using the time-temperature superposition principle (Ferry 1980) in lieu of the actual time. However, the researchers did not address healing in their study.

Lee and Kim (1998b) also used viscoelastic continuum damage mechanics to describe fatigue behavior of asphalt composites subjected to uniaxial load cycles. The researchers used an internal state variable (S_p) to represent overall damage and the slope

of hysteresis loop (S^R) to represent secant pseudo-stiffness. The secant pseudo-stiffness is defined as the ratio of pseudo stress and pseudo strain amplitudes and represents the stiffness of a reference elastic material based on Schapery's extended correspondence principles (1984). The researchers employed a function $[F(S_p)]$ to represent the change in secant pseudo-stiffness due to growing damage and another function (G) to account for the hysteresis behavior of stress-strain in each cycle. Lee and Kim (1998b) found that the curve constructed using the ratio of secant pseudo-stiffness (S^R) and the initial secant pseudo-stiffness (I) versus the ratio of damage parameter (S_p) at given number of cycle and the damage parameter corresponding to 50% fatigue life (S_f) is independent of loading modes (stress or strain amplitudes).

In a subsequent study, Lee and Kim (1998a) introduced rest periods during the strain-controlled uniaxial cyclic tests of asphalt mixtures, and extended the constitutive damage model (Lee and Kim 1998b) to study resultant healing effect. The researchers (1998a; b) once again defined overall damage in a continuum as the effective "structural changes except linear viscoelasticity contributing to the recovery of stiffness or strength during rest periods, such as fracture healing, steric hardening, nonlinear viscoelastic relaxation, and so forth". The constitutive model used for damage as used by Lee et al. (1998a; b) follows as:

$$S \cong \sum_{i=1}^{N} \left[\frac{1}{2}[\varepsilon_i^R]^{2\alpha}(C_{i-1} - C_i)\right]^{\frac{\alpha}{1+\alpha}} (t_i - t_{i-1})^{\frac{1}{1+\alpha}} \qquad 2.10$$

The notations S and C in this model refer to the internal state variable for damage and secant pseudo-stiffness. In this study, the researchers demonstrated a good agreement between the normalized secant pseudo-stiffness versus normalized damage parameter curves irrespective of the difference in applied loading modes, magnitudes and rates.

Additionally, the researchers observed an increase in pseudo-stiffness of the material after applying a rest period and defined this increase as healing ($H = \Delta S^R$). Healing due to each rest period increased the fatigue life by certain amount (ΔN_f). Furthermore, Lee and Kim (1998a) also observed two distinct portions in the reloaded curve – the initial portion corresponding to the re-establishment of damage in the healed zone and the tail portion corresponding to the damage growth in the virgin material. One limitation of this study is that the healing function depends on loading conditions, as does the secant pseudo-stiffness.

Similarly, Daniel et al. (2002) analyzed the fatigue damage response of uniaxially loaded asphalt mixtures using viscoelastic continuum damage mechanics model. The researchers found that the normalized pseudo-stiffness versus normalized damage parameter curve ($C_1 \, vs \, S_1$) is a material-specific characteristic and therefore, remains constant irrespective of the loading mode used to induce fatigue damage for a given material. The researchers used the initial pseudo-stiffness to normalize the secant pseudo-stiffness at each load cycles. Additionally, the characteristic $C_1 \, vs \, S_1$ curve revealed an inflection when the material lost its integrity due to localization of microcracks.

Researchers (Chehab 2002; Underwood et al. 2006) have also verified that the VECD model can be used to describe and predict the growth of damage in viscoelastic materials at different temperatures and loading rates by substituting the actual time (t) with the reduced time (ξ) calculated from time-temperature superposition shift factor (a_T). This observation is consistent with the previous suggestion by Park et al. (Park and Schapery 1997; 1996):

$$S \cong \sum_{i=1}^{N} \left[\frac{1}{2}[\varepsilon_i^R]^{2\alpha}(C_{i-1} - C_i)\right]^{\frac{\alpha}{1+\alpha}} (\xi_i - \xi_{i-1})^{\frac{1}{1+\alpha}} \qquad 2.11$$

In another study, Lundström and Isacsson (2003) characterized damage characteristics of asphalt composites subjected to both monotonic and cyclic tension tests using the viscoelastic continuum damage mechanics model. The researchers verified that the constitutive model based on continuum damage mechanics is independent of strain loading rates (e.g., 100, 800 με/sec.) in monotonic tests and also independent of stress-amplitudes (e.g. 800 MPa, 1000 MPa) and loading frequencies (e.g. 0.1 to 40 Hz) in uniaxial cyclic tests. Equally important, the researches also verified that damage model is independent of test temperature (0 to 30ºC). However, the pseudo-stiffness versus damage parameter curves obtained from monotonic tensile and cyclic tension-compression tests did not agree with each other despite the fact that both test involved cracking in tension mode. Additionally, researchers also did not investigate the healing potential of the materials in their study.

Kutay et al. (2008) also used VECD models to describe damage accumulation during uniaxial cyclic tests of six different types of asphalt mixtures subjected to various loading modes (stress and strain), frequencies and temperatures. The researchers verified that the stiffness history predicted using the constitutive model and the stiffness measured from laboratory tests agreed with each other.

Kutay et al. (2009) again used VECD models to investigate the possibility of using smaller specimens obtained from thinner field layers for tension-compression tests. The researchers conduced tests on test specimens with regular geometry (71.4 mm diameter and 150 mm height) as well as on test specimens with smaller geometry (38.1 mm diameter and 100 mm height) at different controlled stress and strain conditions. The VECD analyses of fatigue results obtained from the tests of both smaller and regular size specimens resulted in similar $C\ vs\ S$ curves. Furthermore, the researchers also showed that the fatigue damage behavior predicted from VECD models agreed with the field

observations. The use of VECD-based damage model to decide the representative specimen geometry exemplifies the robustness of the VECD method.

Recent studies have focused on simplfiying the test procedure and improving the accuracy of the viscoealstic continuum damage models. In one such work, Underwood et al. (2010) constructed a simplified viscoealstic continuum damage (SVECD) model to describe damage growth in a uniaxial test, and compared its accuracy with similar models presented earlier by Daniel and Kim (2002), Lee and Kim (1998a; b), Underwood et al. (Underwood et al. 2006), Kutay et al. (Kutay et al. 2008) and so forth. The researchers used the results from five different types of asphalt mixtures subjected to uniaxial monotonic and cyclic tests at various stress and strain conditions for verification purposes. Most importantly, the simplified model was claimed to be capable of capturing the transient effects and the specimen-to-specimen variation. Additionally, the proposed model accounts for the tensile part of stress-strain history that is responsible for fatigue cracking using a dedicated correction factor.

Underwood and Kim (2013b) evaluated whether the simplified viscoelastic continuum damage mechanics (S-VECD) model based on nonlinear viscoelasticity (NLVE) is more accurate than the VECD model based on linear viscoelasticity (LVE). In their study, the researchers assessed the fatigue response of asphalt mixtures subjected to monotonic tests using these two models at different stress and strain conditions. The researchers observed a discrepancy in the damage parameter predicted using the LVE and NLVE versions of S-VECD models. However, the modulus values predicted from both of these models agreed with each other.

In addition to uniaxial (monotonic or cyclic) loading, a few studies also have applied viscoelastic continuum damage mechanics to study fatigue cracking in other modes of loading such as torsional shear or flexural loading. In one such study, Kim et al.

(2003) applied Schapery's extended correspondence principles to evaluate the change in stiffness, pseudo-stiffness and pseudo strain energy of fine aggregate matrix subjected to torsional shear cycles and rest durations. Though the researchers could show the benefit of introducing rest periods by demonstrating an increase in the number of cycles to failure, they did not specifically characterize damage or healing in terms of any ISVs. The selected metrics (the change in stiffness, pseudo-stiffness and pseudo strain energy) depended on applied test conditions.

In another study, Palvadi et al. (2012) applied the VECD approach to characterize damage and healing behavior of fine aggregate matrices subjected to torsional shear with as well as without rest periods. The authors proposed an experimental method with four different durations of rest periods introduced at three different damage levels to quantify both damage and healing. The researchers constituted a VECD model for torsional shear and verified that the model produces material-specific $C\ vs\ S$ curves. Along with overall damage, Palvadi et al. (2012) also modeled overall healing in this study. The researchers quantified healing in terms of the ratio of recovered amount of damage due to a rest period and damage value preceding the rest period. As such, healing function inherits the independence of damage parameter from loading condition. In the study, Palvadi et al. (2012) also demonstrated that the healing potential of a material depends on the duration of the rest period, the damage preceding the rest period and the material itself. Despite the promising benefits of the analytical models for damage and healing, the experimental method proposed in this study required multiple specimens at each rest condition to compute the corresponding healing potential.

As evident from above synopses, most of the recent studies that use viscoelastic continuum damage mechanics quantify damage in terms of metrics that are independent of loading conditions. However, these studies quantify overall healing in terms of metrics

(e.g. the change in stiffness, pseudo-stiffness, pseudo strain energy, number of cycles) that depend not only on rest conditions but also on loading conditions used to induce fatigue damage preceding the rest period. Though a recent study (Palvadi et al. 2012) quantified healing in terms of metrics that are independent of the test conditions, the experimental method proposed in this study required multiple test specimens depending upon rest conditions. Therefore, the ensuing chapters will describe an integrated method that eliminates all the limitations of previous models. To this end, the integrated method uses the VECD-based metrics for analytical purpose and a single specimen for test purposes. The method also verifies the use of this methodology in torsion as well as tension-compression load cycles.

Chapter 3: Damage and Healing in Shear[1]

This chapter presents an integrated method to quantify both damage and healing properties of asphalt materials. The proposed method uses a same specimen to quantify:

- the fatigue damage characteristics that are independent of test conditions, and
- the fatigue healing characteristics that are independent of loading conditions but dependent on rest conditions - the length of rest period and the stiffness preceding the rest period.

The following sections will present the description of selected materials, methods and mechanics. The final section of this chapter will discuss the interpretation of results obtained from these tests.

3.1 Theoretical Background

The response of asphalt materials (asphalt cements and composites) differs with applied stress and strain rates, magnitudes and temperatures. Viscoelastic continuum damage (VECD) mechanics is extensively used to model the damage response of asphalt materials. The following sections will give a background required to understand linear viscoelastic responses, the use of correspondence principles and work potential theory as required for VECD damage and healing models.

3.1.1 Linear Viscoelastic Constitutive Model

The linear viscoelastic property of an asphalt material represents its time- or rate-dependent mechanical response at low stresses or strains that do not induce damage to the material. In torsional shear mode of loading, the physical stress (τ) and the physical

[1] Substantial part of this chapter has been recently published in the following journal article:
Karki, P., R. Li and A. Bhasin (2014). "Quantifying overall damage and healing behavior of asphalt materials using continuum damage approach." *International Journal of Pavement Engineering*, DOI: 10.1080/10298436.2014.942993. [R. Li contributed the verification tests described in section 3.5.2.2 in this chapter, and A. Bhasin supervised the overall research.]

strain (γ) at time t are expressed in terms of convolution integrals, wherein $G(t)$ and $J(t)$ represent relaxation modulus and creep compliance in shear, and ξ represents the time variable.

$$\tau(t) = \int_0^t G\,(t-\xi, t)\frac{\partial\gamma(\xi)}{\partial\xi}d\xi \qquad 3.1$$

$$\gamma(t) = \int_0^t J\,(t-\xi, t)\frac{\partial\tau(\xi)}{\partial\xi}d\xi \qquad 3.2$$

As can be seen in these relations, one needs to know the relaxation or creep behavior of the material to quantify its stress or strain response. Researchers use mechanical (e.g. Maxwell, Wiechert, Kelvin, etc.) or phenomenological models (e.g. power law) to describe such responses. Models that describe linear viscoelastic response of asphalt materials typically follow the time-temperature superposition principles, thereby facilitating computation of combined responses due to different loading and temperature conditions. The specific models that adequately described the linear viscoelastic properties of fine aggregate matrices used in this study are provided in corresponding sections of this dissertation.

3.1.2 Schapery's Extended Correspondence Principles

Typical boundary value problems with viscoelastic materials can be solved by using Laplace transform or simple correspondence principles with the solutions for similar problems for linear elastic solids. However, such transformations are not applicable to problems wherein the traction or displacement boundary conditions change with time (e.g. crack growth or crack closing with time). To address such situations, Graham (1968) presented the elastic-viscoelastic correspondence principles that Schapery (1984) extended to solve viscoelastic problems in which the traction and displacement boundaries remain intact (CP-I) or change (CP-II and CP-III) with time. In particular,

these extended principles transform the time-dependent stresses and strains in viscoelastic media into the time-independent stresses and strains of an equivalent or reference elastic material, and solve the viscoelastic problems in a pseudo-elastic domain. Schapery categorically provided the generalized expressions for such transformations in an earlier study (Schapery 1984). Researchers have applied Schapery's extended correspondence principles to describe asphalt material traction boundary value problems such as crack growth (Park and Schapery 1997), fatigue damage (Lee and Kim 1998b; Lundström and Isacsson 2003; Park et al. 1996) and healing (Bhasin and Little 2007; Bhasin et al. 2008; Lee and Kim 1998a; Palvadi et al. 2012) among many others.

In torsional shear tests performed for this part of the study, the selected modified correspondence principle, $CP-II$ (Schapery 1984, 1989) transforms the viscoelastic shear variables into the pseudo-elastic variables (denoted by superscript, R) as follows:

$$\tau^R \equiv \tau \tag{3.3}$$

$$\gamma^R \equiv \frac{1}{G^R}\int_0^t G\,(t-\xi,t)\frac{\partial\gamma(\xi)}{\partial\xi}d\xi \tag{3.4}$$

The quantity, G^R used in these transformation expressions represents an arbitrary modulus in the transformed space, and is taken as unity in this study. The following inverse relations can transform the pseudo shear strain and pseudo shear stress back into time-dependent shear stress and shear strain (Kim and Little 1990):

$$\tau \equiv \tau^R \tag{3.5}$$

$$\gamma \equiv G^R\int_0^t J(t-\xi,t)\frac{\partial\gamma^R(\xi)}{\partial\xi}d\xi \tag{3.6}$$

Using the extended correspondence principles, $CP-II$ (Schapery 1984), and the steady state stress condition (Ferry 1980; Tschoegl 1989) for a material subjected to

sinusoidal load, the amplitudes of pseudo shear stress and pseudo shear strain at the k^{th} load cycle can be given by these simplified relations (Underwood and Kim 2013b; Underwood et al. 2006, 2010):

$$\tau_{oc,k}^{R} \equiv \left(\frac{\beta+1}{2}\right)\tau_{pp,k} \tag{3.7}$$

$$\gamma_{oc,k}^{R} \equiv \left(\frac{\beta+1}{2}\right)\left(\frac{\gamma_{pp,k} \,.\, |G^*|_{LVE}}{G^R}\right) \tag{3.8}$$

The subscript oc refers to the peak amplitude of pseudo shear stress or the peak amplitude of pseudo shear strain that are responsible for fatigue cracking in the k^{th} shear load cycle; the subscript pp refers to corresponding peak-to-peak magnitude of viscoelastic shear stress and shear strain as shown in Figure 3.1. The notation, $|G^*|_{LVE}$ in the pseudo shear strain definition refers to the linear viscoelastic dynamic shear modulus of the given material that is measured by applying a small level of strain or stress within the linear viscoelastic range of the material. Similarly, the parameter, β refers to a correction factor to account for the portion of the stress-strain history that is responsible for crack growth in a given cycle (Underwood and Kim 2013b; Underwood et al. 2010). The concept of such correction was also used in some earlier studies related to uniaxial load in which the researchers used half (Daniel 2001) or quarter (Daniel and Kim 2002) of stress-strain history. In a torsional shear test, the full portion of each load cycle is responsible for shear damage in the material. Due to symmetry, $\beta = 0$ is used for calculating the pseudo shear strain that is responsible for damage accumulation in each semi-cycle.

In a stress-controlled cyclic shear test, the shear stress amplitude divided by the shear strain amplitude at a given steady state load cycle yields the dynamic shear

modulus of the material. In the pseudo-elastic realm, the secant slope of pseudo stress-strain curve is defined as the pseudo-stiffness of the material corresponding to that cycle:

$$C_{s,k}^{R}(S_s) \equiv \frac{\tau_{oc,k}^{R}}{\gamma_{oc,k}^{R}} \qquad 3.9$$

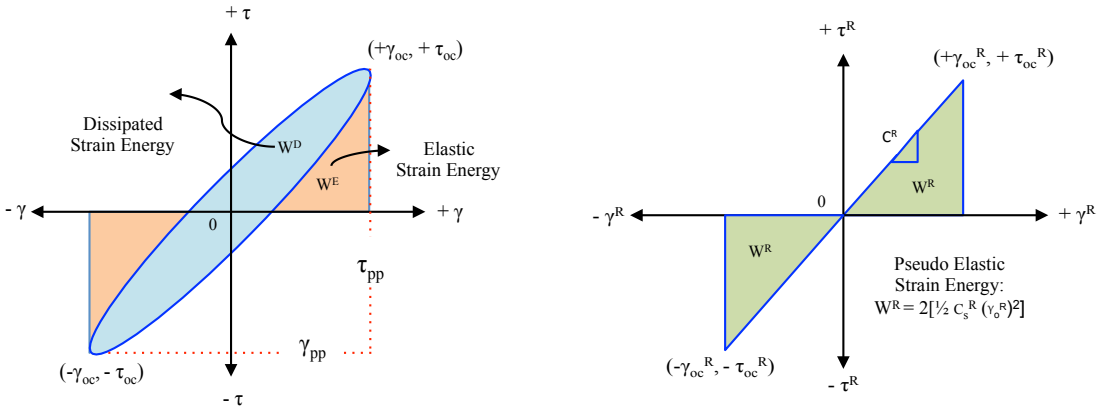

Figure 3.1: Schematic of stress and strain histories in (a) viscoelastic and (b) pseudo-elastic domains

The value of pseudo-stiffness depends on the change in the internal state of the material (represented by S_S), and therefore is denoted as $C_s^R(S_s)$ wherein the subscript s refers to the shear mode of loading. A more robust method to compute pseudo-stiffness requires time-integration on the stress-strain history without assuming the steady state definition. Researchers (Underwood and Kim 2013b; Underwood et al. 2010) have also proposed a mixed use of time-integration to determine pseudo-stiffness based on transient effects. They have attributed this need to the transient effects due to the sudden application of damage-inducing load from zero. However, the sinusoidal shear tests conduced for this work resulted in very similar stress and strain amplitudes above and below the a zero-mean axis in a given cycle, obeying a steady state definition. Therefore,

for the purpose of this study, the simplified definition of pseudo-stiffness as given was used, wherein a correction factor (I) accounts for sample-to-sample variability.

$$C_{s,k}^{R}(S) = \frac{|G^*|_k}{|G^*|_{LVE}} . \frac{G^R}{I} \qquad 3.10$$

3.1.3 Thermodynamic-based Work Potential Theory

Researchers have used thermodynamics-based work potential theory to describe the structural changes due to loading and unloading (Schapery 1987, 1990). This theory relates structural changes with the change in a set of internal state variables, ISVs (Schapery 1986, 1987, 1990). The change in this variable is associated with a change in a work potential that describes the energy released or absorbed by the material to manifest that change. According to this theory, the sum of work potentials associated with each internal state variable and the elastic strain energy density constitute the total work potential of the material.

Work potential theory states that the thermodynamic force (or stress) required to bring a change in material structure via a specific damage or failure mechanism is equal to the rate of change of dissipated strain energy density with respect to the displacement (or strain) associated with corresponding damage mechanism (Pineda and Waas 2013). In a pseudo-elastic domain, the relationship of thermodynamic pseudo force or pseudo shear stress, τ^R with the pseudo strain energy in shear, W_s^R, and the pseudo shear strain, γ^R is given by (Schapery 1984, 1987, 1990):

$$\tau^R = \frac{\partial W_s^R}{\partial \gamma^R} \qquad 3.11$$

Similarly, assuming isothermal condition, the work potential theory (Schapery 1987, 1990) also expresses pseudo shear stress and pseudo shear strain energy, W_s^R as

functions of the internal state variable for damage, S_s and the shear strain, γ^R (or angular displacement) associated to shear damage:

$$\tau_s^R = \tau_s^R\ (\gamma^R, S_s) \tag{3.12}$$

$$W_s^R = W_s^R(\gamma^R, S_s) \tag{3.13}$$

Based on these theories, the pseudo shear stress and pseudo shear strain energy responsible for the shear damage in each half of the k^{th} load cycle (see Figure 3.1) can be expressed as:

$$\tau_{oc,k}^R = I.C_{s,k}^R.\gamma_{oc,k}^R \tag{3.14}$$

$$W_{s,k}^R = \frac{I}{2}.C_{s,k}^R.\left(\gamma_{oc,k}^R\right)^2 \tag{3.15}$$

3.1.4 Rate-type Damage Evolution Law

A model based on continuum damage mechanics (Kachanov 1958) is used to quantify damage in terms of an internal state variable (S_s) assuming that the body under damage is a homogeneous continuum that is much larger than the flaw sizes (Lee and Kim 1998b; Underwood et al. 2010). For time-dependent materials, Schapery et al. (1994; 1996; 1986, 1990) proposed the rate of damage evolution as the $\alpha^{th}-$ power function of change in pseudo strain energy in shear with respect to the internal state variable for damage, wherein the slope (α) refers to a material damage evolution rate parameter. Mathematically, the power law form for the damage evolution rate can be expressed as:

$$\frac{dS_s}{dt} = \left(-\frac{\partial W_s^R}{\partial S_s}\right)^{\alpha} \tag{3.16}$$

This function is analogous to the crack growth law in elastic materials (Paris and Erdogan 1963; Paris et al. 1961) and is based on the fact that crack growth obeys a power relation in local J_v-integral (Schapery 1984, 1990). By using the relations from the work potential theory and applying the chain rule of derivatives, the aforementioned damage evolution law can be simplified to quantify total damage at the N^{th} cycle of shear load (Park et al. 1996):

$$S_{s,N} \cong S_{s,0} + \sum_{k=1}^{N}\left[\Delta S_{s,k}\right] \cong S_{s,0} + \sum_{k=1}^{N}\left[\left\{-I\left(\Delta C_{s,k}^{R}\right).\left(\gamma_{oc,k}^{R}\right)^{2}\right\}^{\frac{\alpha}{1+\alpha}} .\left(\Delta t_k\right)^{\frac{1}{1+\alpha}}\right] \quad 3.17$$

In this expression, $S_{s,0}$ is the value of internal state variable for shear damage at the beginning of loading. The incremental term in the above relation signifies the total damage due to a complete load cycle (see Figure 3.1 for the pseudo shear strain energy formulation). For a specimen without any pre-existing damage, the initial damage value can be set to zero, as is the case in this study. The internal state variable for shear damage S_s starts with the lowest value (set to zero in the undamaged state) and increases with time, signifying the progressive damage growth due to shear, while the pseudo-stiffness $C_s^R(S_s)$ starts with its highest stiffness value (unity after normalization) and keeps decreasing with time.

The VECD model has been widely used in describing deterioration of asphalt composites during uniaxial monotonic tests (Kim and Little 1990; Lundström and Isacsson 2003; Park et al. 1996) and uniaxial cyclic tests (Kim et al. 1997; Kutay et al. 2009; Lundström and Isacsson 2003; Underwood and Kim 2013b; Underwood et al. 2010), but only occasionally in cyclic shear tests. Kim et al. (2003) used modified correspondence principles and work potential theory to study damage and healing in shear mode (Kim et al. 2003), but only a recent study (Palvadi et al. 2012) utilized the

damage evolution law in asphalt composites under shear. However, none of these studies explored the full potential of VECD model to address the issues investigated in this study, i.e., to use this theory to characterize healing and fatigue cracking characteristics.

Furthermore, due to the verified test condition independency of the characteristic damage curve, $C_S^R(S_s)$, it can be used to predict the number of cycles required to degrade an asphalt material to a certain level of stiffness (or pseudo-stiffness, C_x) or to accumulate a certain degree of damage, S_x when subjected to any arbitrary loading condition (e.g. new strain amplitude, γ_{oc}^R or new loading frequency, f) as given by:

$$N \cong f.\sum_{k=1}^{x}\left[\left\{-I.(\Delta C_{s,k}^R).\left(\gamma_{oc,k}^R\right)^2\right\}^{-\alpha}.\left(\Delta S_{s,k}\right)^{(1+\alpha)}\right] \qquad 3.18$$

3.2 TEST MATERIALS

All tests in this study were conducted using the mortars prepared from fine aggregates and an asphalt binder. The fine aggregate matrix (FAM) composites and the full asphalt concrete (AC) mixtures differ only in length scale but follow the same material constitutive model, therefore the methods used in this study are expected to be implementable for full mixtures. Underwood and Kim (2013a) mentioned that consistently fabricated FAMs can be used for comparative studies. The researchers also mentioned that only the fine aggregates matrix that truly replicates the matrix phase present in full mixtures should be used in micromechanics models. A recent study demonstrated that FAMs can be an efficiently fabricated and used to compare the effect of rock asphalts on the overall properties and performances of asphalt composites at temperatures (Li et al. 2014). Based on suggested efficacy, this particular study uses FAMs to develop models based on continuum damage mechanics that was initiated by

Kachanov (1958) and continuously evolved through years. More information about the design, the benefits and the limitations of FAMs are available in some recent studies (Aragao et al. 2010; Karki 2010; Karki, Li, et al. 2014; Li et al. 2014; Palvadi et al. 2012; Underwood and Kim 2013a).

Table 3.1 presents the composition of fine aggregate matrix composites used in this particular study and Figure 3.2 presents the corresponding gradation of the aggregates. As can be seen, aggregates passing ASTM Sieve No. 16 (maximum aggregate size of 1.18 mm) and Superpave© performance graded asphalt binders were used to prepare two different types of FAMs for this study. The two FAMs are named as ARC22 and UM22 after their aggregate sources and binder grades. The ARC22 fine aggregate matrices were prepared using the Limestone aggregates and PG67-22 asphalt binder (9.0 % by weight of total FAM). The UM22 fine aggregate matrix was prepared using aggregates from a different source and modified PG67-22 asphalt binder (11% by weight of total FAM); natural asphalt (UM) was used to modify this binder. The maximum aggregate size and the percentage of binder in these composites were selected based on an earlier study (Karki 2010). It is important to note that ARC22 was used as the base material for the study described in this chapter, UM22 were used for additional verification of the proposed methodology.

Table 3.1: Constituent proportion in the selected asphalt composites

FAM Material	Proportion of aggregates by weight of total aggregates in the mix (%)						Binder % by total wt. of mix
	>#16	#30	#50	#100	#200	Pan	
ARC	0.0	30.3	17.3	13.0	15.2	15.2	9.0
UM	0.0	30.0	21.4	0.0	26.4	11.2	11.0

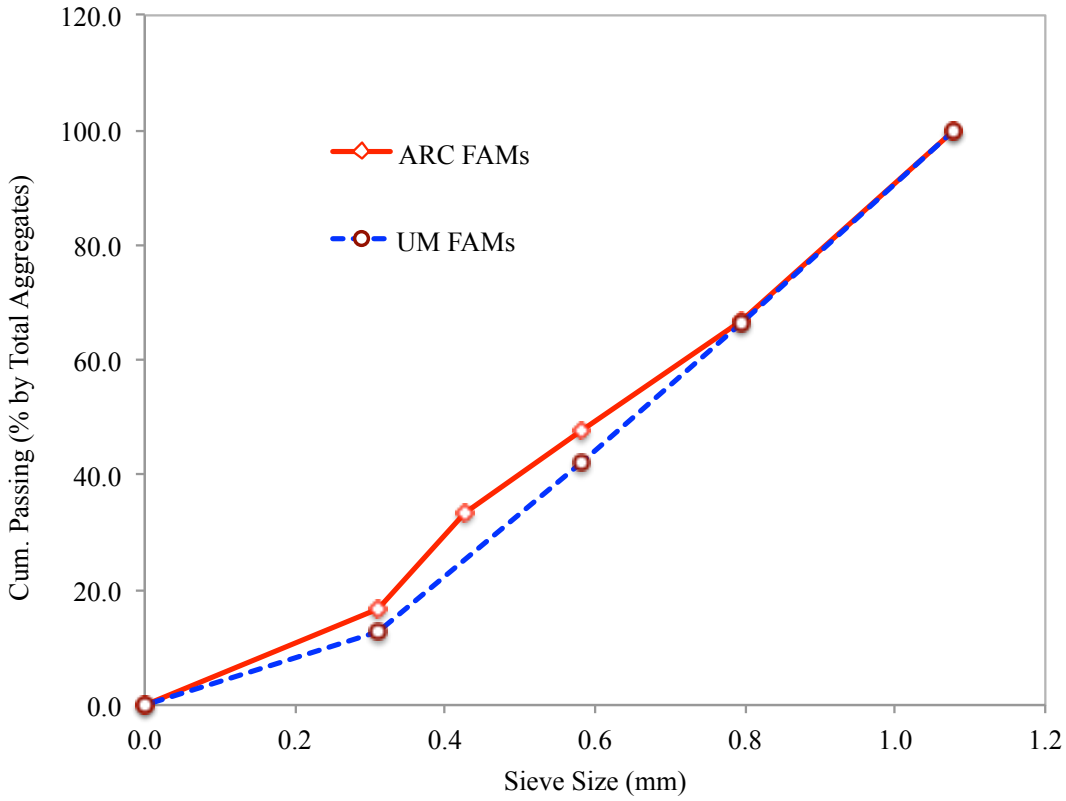

Figure 3.2: Aggregate gradation in the selected asphalt composites

Using a Superpave© gyratory compactor, the laboratory mixed fine aggregate matrices were compacted into cylindrical samples that measured 150.0 mm in diameter and 70.0 mm in height, and contained 1.5% air void by total volume. Cylindrical test specimens, measuring 12.25 mm in diameter and 45.0 mm in height, were extracted from the compacted samples and used for the tests. As shown in Figure 3.3, the compacted sample was sliced into three parts and the middle 45-mm portion was used to extract the cylindrical specimens with aforementioned geometry.

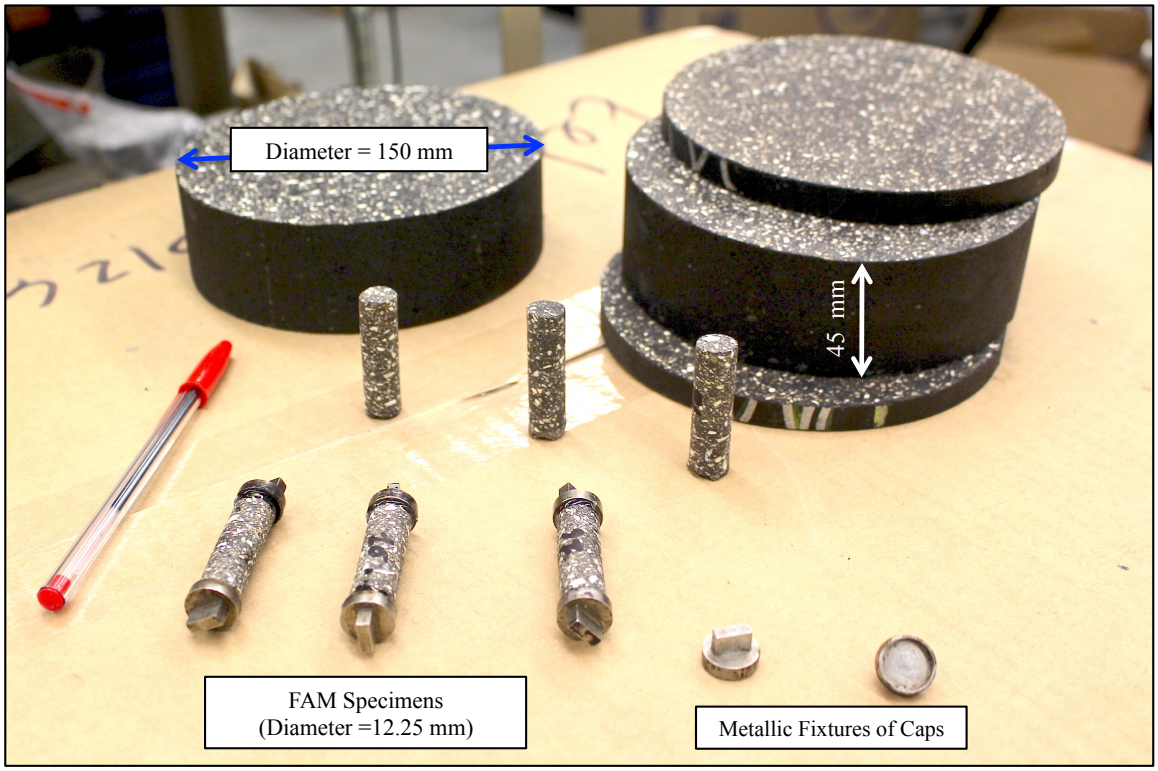

Figure 3.3: Superpave© gyratory compacted fine aggregate matrixes and specimens

The dimensions of test specimens were selected so that the specimens could be glued to metallic fixtures on the two ends using a 5-minute epoxy and mounted onto a dynamic shear rheometer (TA Instruments: AR2000ex). Precautions were also taken to make sure that the specimen dimensions were large enough to prevent undue influence of aggregate size on overall properties. For example, the diameter of the specimen (12.25 mm) was more than 10 times the maximum aggregate size of the largest fine aggregate particle (1.18 mm) in this study. One more benefit of using FAM, besides easier fabrication, is the faster rate of temperature equilibrium due to smaller specimen size and consequently smaller volume of environmental test chamber (ETC). These benefits are very important in countering any changes in the material properties due to the high

temperature susceptibility of asphalt mixtures, and maintaining isothermal conditions for a more accurate assessment of damage and healing.

3.3 TEST METHODS

For this part of the study, each selected FAM specimen was subjected to two linear viscoelastic (non-damage) tests followed by a cyclic damage test with or without rest period in shear. The AR2000ex dynamic shear rheometer from TA Instruments, as seen in Figure 3.4 was used to perform the cyclic shear tests.

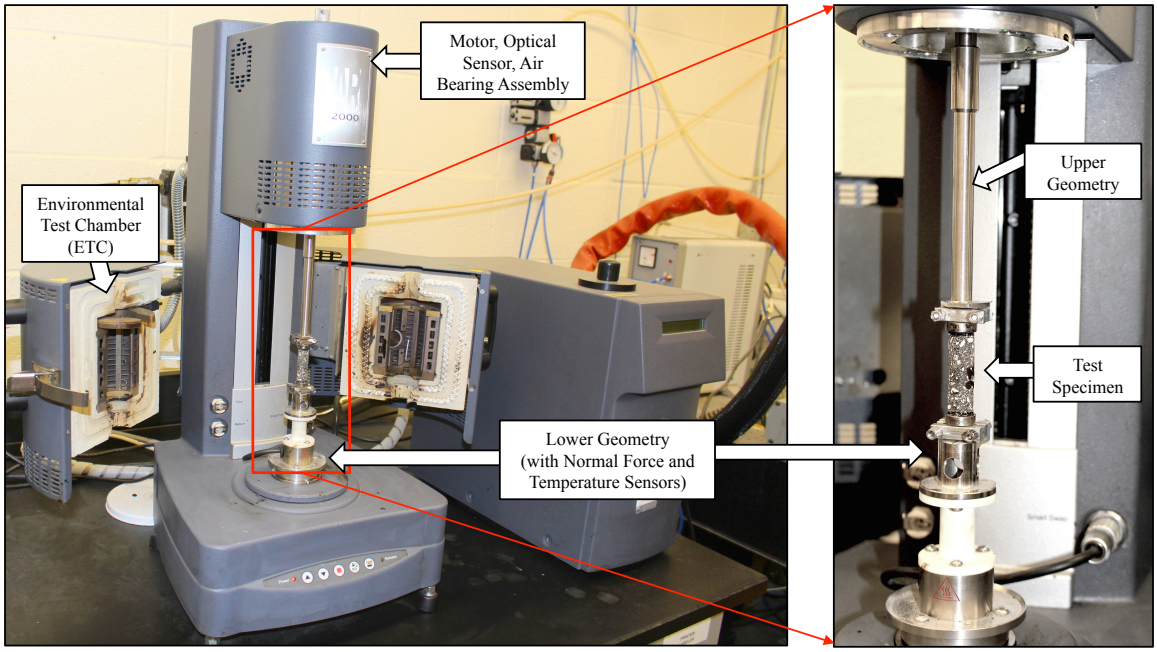

Figure 3.4: AR2000ex dynamic shear rheometer and a cylindrical test specimen

Before each test, a 30-minute equilibrium time without any load was allowed to prevent the any unintended influence of loading history on subsequent loading results and to reach thermal equilibrium. Since this study intends to model only the total recovery in stiffness due to the duration and stiffness condition of a rest period, the continuous

recovery of torsional strain during the zero-load rest periods was not recorded. More detailed descriptions of these tests are provided in the following sections.

3.3.1 Linear Viscoelastic Property Tests

The value of control variable was chosen so that the material would behave linearly throughout these tests; the linear behavior was confirmed using additional tests at slightly higher and lower loading (stress or strain) levels. The specimens were again allowed to rest for thirty minutes without any load to avoid carrying over any loading history into ensuing tests. Both of these linear viscoelastic property tests were conducted on each test specimen before performing fatigue damage and healing tests on them.

3.3.1.1 Creep Compliance Tests

The selected test specimens were subjected to torsional stress of 75-kPa for 30 seconds at 25°C in the AR20000ex dynamic shear rheometer to determine the creep parameter (m) as described below. Following the loading step, the specimen was allowed to recover the creep strain for more than thirty minutes without any external load. The applied shear stress and resultant shear strain were continuously recorded during these steps. The resultant torsional shear strain (γ) over the applied shear stress (τ_o) yields the creep compliance history of the material. In this study, a simple power-law model adequately characterized the linear viscoelastic creep response of the fine aggregate matrix in torsional shear mode:

$$J(t) = \frac{\gamma(t)}{\tau_o} = J_o + J_1 t^m \qquad 3.19$$

where, J_o, J_1 and m are the material creep constants.

3.3.1.2 Dynamic Shear Modulus Tests

The quantity, $|G^*|_{LVE}$ refers to the absolute value of shear stiffness of a viscoelastic material at a given frequency and temperature. To measure this quantity, the specimens previously used for the creep and recovery tests were subjected to sinusoidal shear strain of 0.008%-controlled amplitude for thirty seconds at 10 Hz and 25ºC using the AR2000ex dynamic shear rheometer. The recorded stress and strain amplitudes were then used to compute corresponding stiffness:

$$|G^*| = \frac{\tau_o}{\gamma_o} \tag{3.20}$$

After the stress- or strain-controlled linear viscoelastic tests, each specimen was again allowed to rest for another thirty minutes.

3.3.2 Fatigue Damage and Healing Tests

Previous studies (Palvadi et al. 2012) used different test specimens to obtain damage and healing characteristics (as a function of the duration of rest period and the preceding level of damage) of an asphalt composites. In particular, the researchers used one specimen to quantify damage and three specimens to quantify healing by introducing rest periods at three different levels of damage on each specimen (not counting replicates). The main objective of this study was to develop a procedure to obtain both damage and healing characteristics of the material using the same specimen in lieu of using the previously proposed four-specimen test procedure. To this end, damage and healing tests were conducted using a "single specimen" based on the proposed procedure and "multiple specimens" following the previous procedure and

3.3.2.1 Multiple-Specimen Test Method

Thirty minutes after measuring the linear viscoelastic properties, the test specimens used for the linear viscoelastic property tests were ultimately subjected to

higher shear stress amplitudes to induce fatigue damage. Stress amplitudes ranging from 250 to 400 kPa at 5 or 10 Hz and 25ºC were applied to different test specimens without any rest period until the stiffness reduced to 60% of its initial value (see Figure 3.5). It must be noted that the decrease in stiffness is not the same as the decrease in pseudo-stiffness due to different corrections required as described in the theoretical background section. The use of pseudo-stiffness actually eliminates the contribution of time-dependency and more accurately captures the progression of damage (Lee and Kim 1998b). In order to obtain the healing characteristics, three different test specimens were subjected to sinusoidal torsion with amplitude of 250 kPa until their stiffness reduced to 80%, 70% or 60% of their initial stiffness due to continuous load cycles After the specimen reached the designated value of initial stiffness (80%, 70% or 60%), a rest period of 40 minutes was introduced.

Immediately after the rest period, loading was resumed until the specimen once again reached the same designated fraction of its initial stiffness as before. However, this time the duration of the rest period was reduced to 20 minutes. The process was repeated for rest periods of 10 and 5 minutes. Figure 3.5 illustrates a schematic profile of stiffness for each of the four target sequences. This procedure was repeated for another set of FAM specimens, except this time an oscillatory load with amplitude of 350 kPa was applied to induce damage before and after the rest periods. Also, some additional specimens were tested at 225, 275 and 400 kPa and at 5Hz. The tests with different amplitudes and frequencies were included to verify that the healing characteristics obtained from the analysis of these test results were independent of the loading conditions.

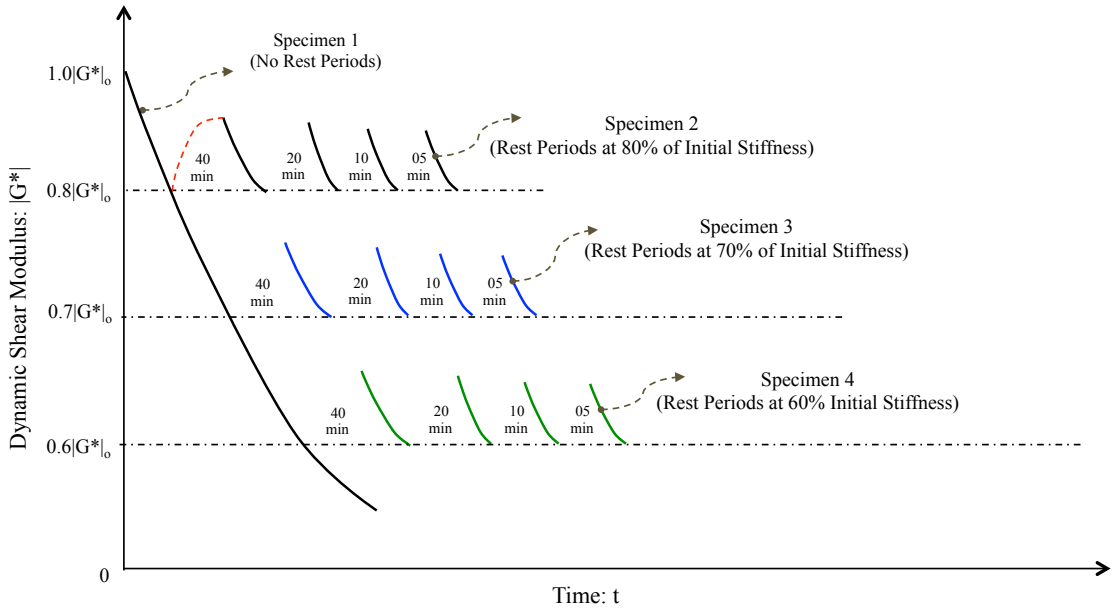

Figure 3.5: Schematic illustration of multiple-specimen test method

3.3.2.2 Single-Specimen Test Method

The goal of this study was to determine whether the above protocol could be simplified to measure both fatigue damage and healing characteristics of the FAM using the same specimen. Figure 3.6 presents the improved testing protocol that requires only a single specimen unlike the earlier protocol that required at least four specimens. As shown in this figure, each test specimen was subjected to oscillatory stress with an amplitude of 250 kPa until the material stiffness reduced to 80% of its initial value. At this point, a rest period of 40 minutes was introduced. Loading was resumed immediately after this rest period until the specimen once again degraded to 80% of its initial modulus. As before, a rest period was introduced at the same preceding level of damage but with a reduced duration, 20-minute in this case. The process was repeated for rest periods of 10 and 5 minutes. This sequence of introducing different rest periods was carried out for each predesignated level of reduced stiffness (70% and 60%) using the same specimen

(see Figure 3.6). Also, as before, some additional specimens were tested at 225, 275 and 400 kPa and at 5 Hz.

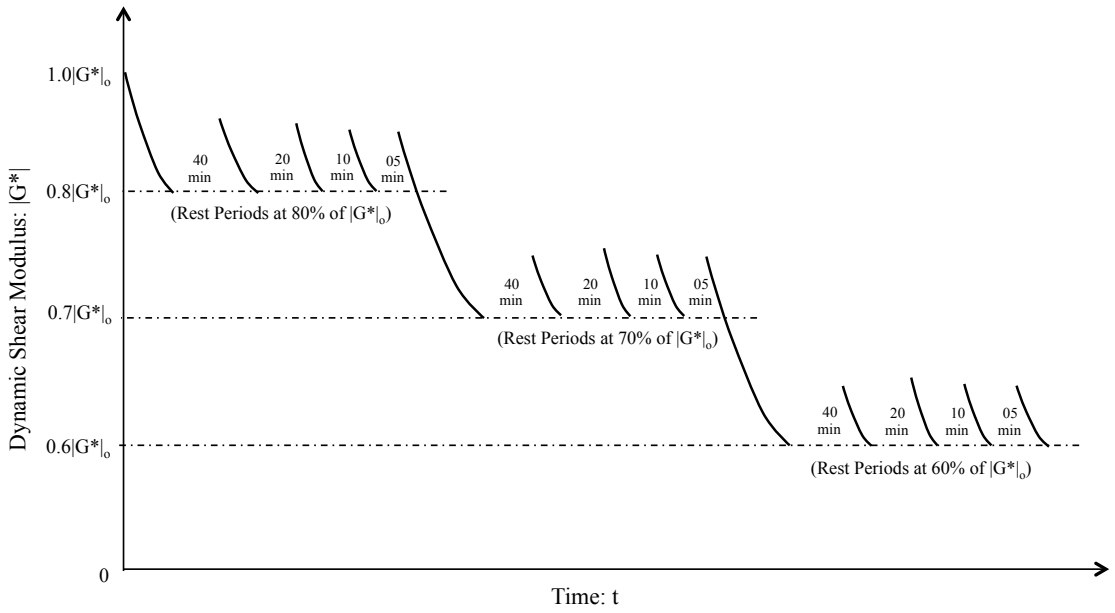

Figure 3.6: Schematic illustration of single-specimen test method

For additional verification of the proposed test method, similar specimens from UM22 were tested at 25ºC by following the single-specimen protocol at the 250 kPa-stress-amplitude, 10 Hz and 25ºC, and multiple-specimen protocol at 225 and 275 kPa-stress-amplitudes at 5 Hz and 25ºC.

3.4 DATA ANALYSIS

3.4.1 Damage Analysis

Based on Schapery's extended correspondence principles, the applied shear stress, measured shear strain and dynamic shear modulus from cyclic shear tests were first transformed into their pseudo counterparts, as illustrated in Figure 3.1. The conversion was carried out for all cases - with and without rest periods and for both multiple-

specimen and single-specimen protocols. The power-law constant for damage evolution, α can take a value of $1/m$ or $1 + 1/m$. Studies (Park et al. 1996 p. 19; Schapery 1975a, 1990) have suggested a value of $1 + 1/m$ for the materials with constant fracture energy and fracture stress, and $1/m$ for the materials with constant fracture energy and fracture process zone size. Similarly, researchers (Daniel and Kim 2002; Kutay et al. 2009; Lee and Kim 1998b; Underwood et al. 2010) have used $1 + 1/m$ for controlled cross-head displacement (CX) tests and 1/m for controlled stress (CS) tests. Following these previous studies, $1/m$ was used for the controlled stress tests conducted in this study to estimate an initial value of α. The damage evolution rate parameter, pseudo shear strain, and pseudo-stiffness were used with the damage accumulation model to determine the characteristic $C\ vs\ S$ curve for the test specimen subjected to fatigue loading without any rest periods (as a part of the multiple-specimen protocol). In the case of fatigue test with rest periods (single-specimen procedures as seen in Figure 3.6), a different procedure as described below was used to recreate a curve that represents damage evolution without any rest period.

For single-specimen tests with rest periods, the pseudo-stiffness data corresponding to the time sweep data falling in between different target stiffness levels was horizontally shifted to the left. The shift was carried out in succession such that the starting point of each portion of the shifted data coincided with the end point of the previous data. In other words, the data corresponding to the stiffness reduction from 80% to 70% of initial stiffness (Curve B in Figure 3.7) and the data corresponding to the stiffness reduction from 70% to 60% of initial stiffness (Curve C in Figure 3.7) were conjoined into a smooth curve along with the first time sweep data (Curve A in Figure 3.7). The resultant stress, strain and stiffness data in the single curve constructed by shifting the sections as described above were further processed to construct the pseudo-

stiffness versus time ($C\ vs\ t$) and pseudo-stiffness versus damage ($C\ vs\ S$) curves using the extended elastic-viscoelastic correspondence relations and the time-dependent damage accumulation relation. Based on the hypothesis discussed earlier, it is expected that the $C\ vs\ S$ curve that is created by horizontal shifting of the segments from individual time sweep curves with rest periods will be similar to the $C\ vs\ S$ curve obtained directly from a fatigue test without any rest periods.

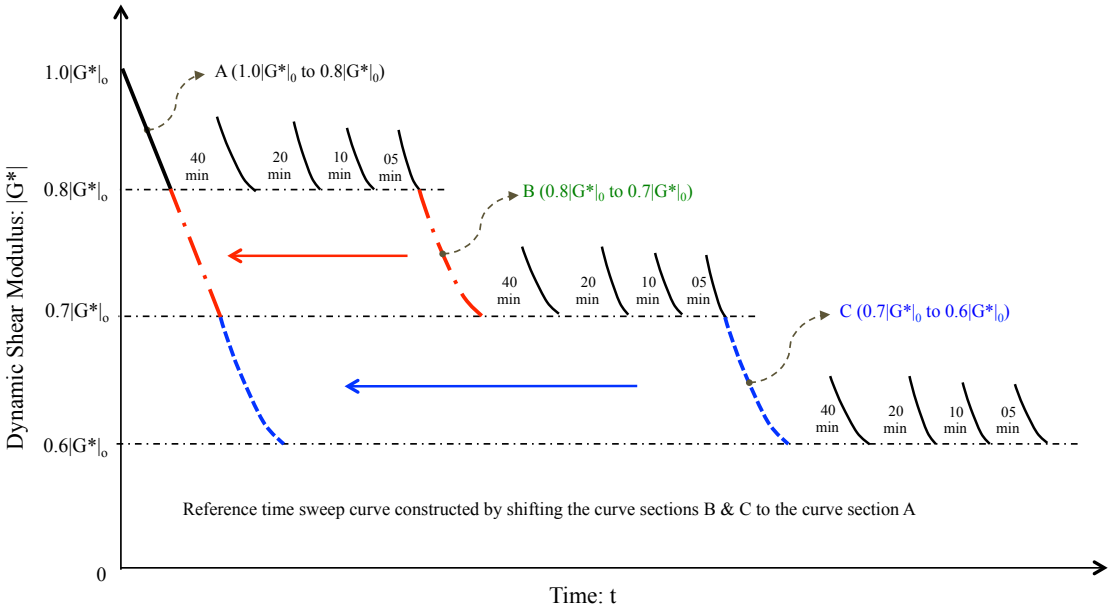

Figure 3.7: Schematic of reference curve construction using single-specimen test data

3.4.2 Healing Analysis

The analytical procedure used to determine healing characteristics was similar for both single and multiple-specimen protocols and is described in this section. Figure 3.8 illustrates a schematic of a typical segment of a time sweep test with a rest period, *RP* introduced in between the loading steps. Let C_i be the initial pseudo-stiffness immediately preceding the rest period of interest at time, t_i (data point, Q' in Figure 3.8).

Let C_f be the pseudo-stiffness measured immediately after the rest period at time, t_f (data point, P in Figure 3.8). The time sweep is resumed after the rest period until the pseudo-stiffness reduces from C_f to at least C_i at time, $t_i + \Delta t$ (data point, Q in Figure 3.8). The value of Δt and the corresponding gain in number of load cycles reflects the benefits of healing. In other words, if there were no healing, the pseudo-stiffness after rest period, C_f would be equal to the pseudo-stiffness before rest period, C_i and Δt would be equal to zero. The time sweep curve after rest period is then horizontally shifted to the left such that the data referring to the pseudo-stiffness, C_i from this curve and the reference curve coincide with each other as illustrated in Figure 3.8. In other words, the data point, Q on the time sweep curve after rest period would coincide with the data point, Q' on the reference curve. The pseudo-stiffness at the beginning of the time sweep segment immediately after the rest period, C_f (data point, P' in Figure 3.8) is much higher than the pseudo-stiffness value at the same time from the reference curve, C_f' (data point, P" in Figure 3.8). The increase in pseudo-stiffness value, from C_i to C_f, represents the effect of partial healing the material undergoes during the rest period. This apparent increase in stiffness is finally normalized to an equivalent increase in stiffness with respect to the original curve. The pseudo-stiffness value corresponding to the normalized increase in stiffness is illustrated as C_f' in Figure 3.8.

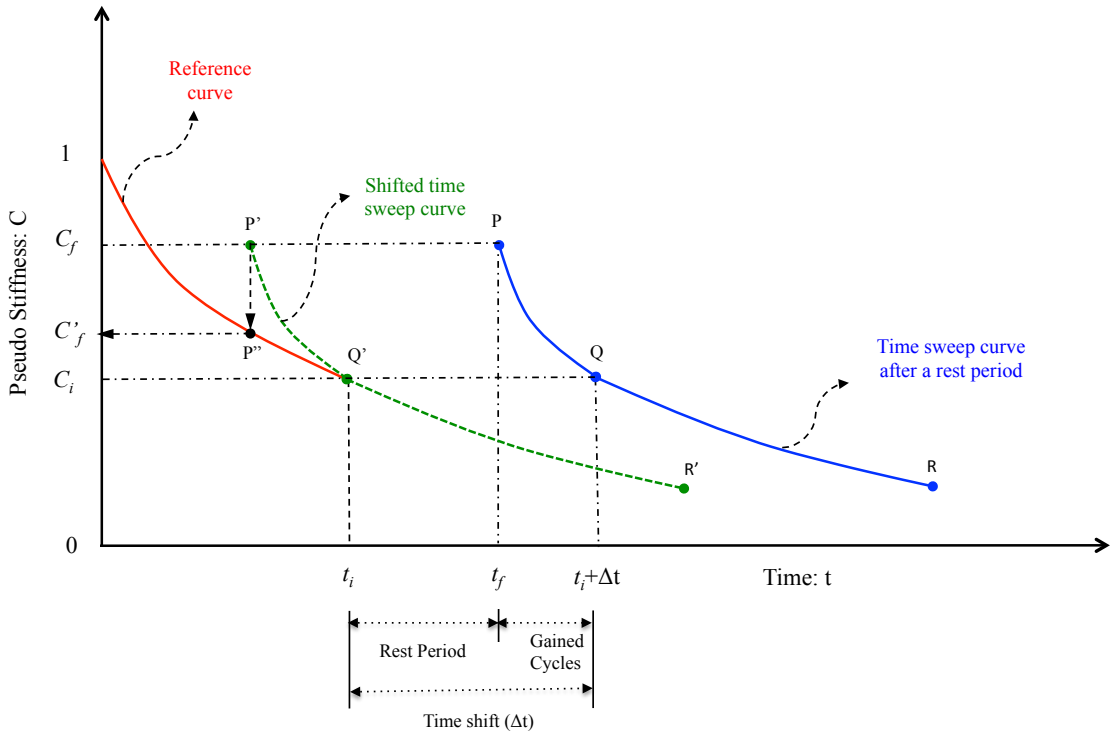

Figure 3.8: Schematic illustration of shifting the time sweep curve for calculating healing potential

The fatigue life of the material is increased by the number of loading cycles gained due to the rest period. However, the number of load cycles gained is not a true material property because it is dependent on the loading conditions. To avoid this shortcoming, the pseudo-stiffness values C_f' and C_i after and before healing, respectively are traced back in the $C\ vs\ S$ curve for the unhealed specimen to obtain corresponding levels of damage, S_f' and S_i respectively (see Figure 3.9). The percent change in accumulated damage before and after the rest periods is defined as healing potential as follows:

$$\%Healing \equiv \frac{S_i - S_f{}'}{S_i} x\ 100\% \qquad 3.21$$

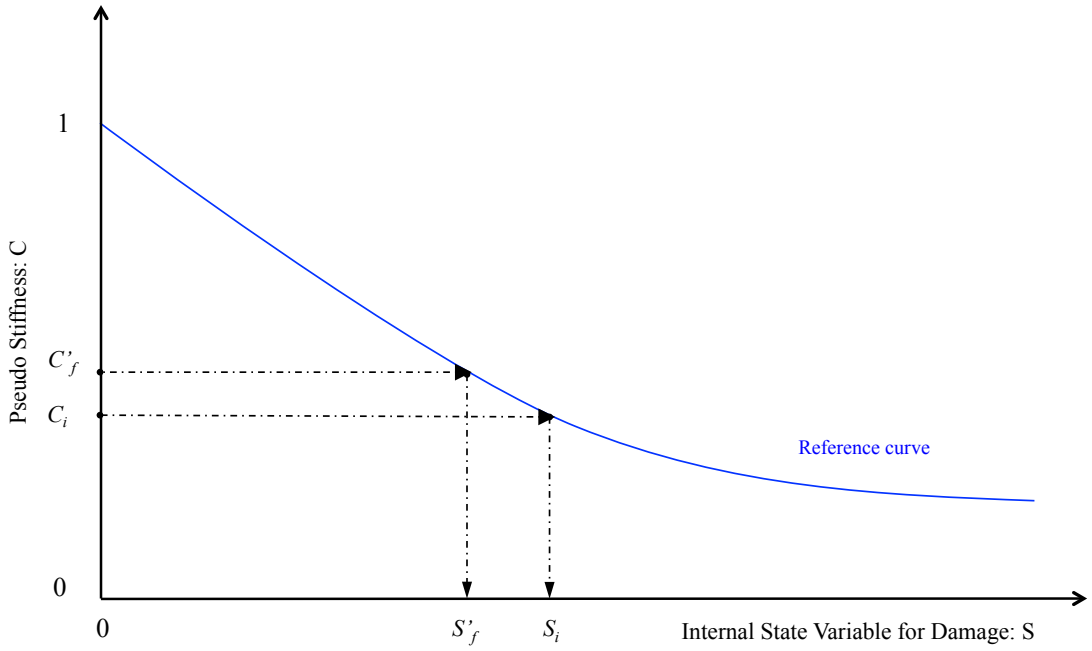

Figure 3.9: Schematic of healing calculation from a reference C vs. S curve

The above procedure was repeated for each combination of rest period and pseudo-stiffness. For the time sweep tests with a single specimen, the reference curve refers to the curve constructed by shifting and combining the sections of curves using the data in between the pre-designated damage levels. In case of the multiple-specimen test protocol, an independent specimen was used to obtain the reference curve.

3.5 Results and Discussion

3.5.1 Linear Viscoelastic Properties

The linear viscoelastic dynamic modulus value of the ARC22 specimens averaged 1.10 ± 0.09 GPa at 10Hz and 25ºC while the m-value averaged 0.430 ± 0.108. As mentioned earlier, these values are required for ensuing calculation of pseudo-stiffness and damage.

3.5.2 Damage Characteristics

3.5.2.1 Fatigue Damage in Shear: An Example

Step 1. Figure 3.10 presents the stiffness history of an ARC22 specimen subjected to a series of time sweep steps in cyclic shear with four different rest periods at three different stiffness levels following the proposed single-specimen test and analysis method. As seen in the figure, the pseudo-stiffness was comparatively higher upon resuming the loading after each rest period but then decreased rapidly until the material resumed the same damage evolution rate as the one just before the rest period. After resuming this damage rate, the specimen continued to lose its stiffness without showing any effect of rest period.

Step 2. The stiffness data affected by healing from each loading step were trimmed away (seen as solid lines in the time sweep steps in Figure 3.11) and the remaining data that is unaffected by healing data (seen as dotted lines in the time sweep steps in Figure 3.11) were moved to the stiffness data obtained from the very first time sweep step to construct a single curve as seen in Figure 3.11 and also in Figure 3.12.

Step 3. Figure 3.13 presents the pseudo-stiffness and damage history obtained using the data from Figure 3.12, the modified elastic-viscoelastic correspondence principles and viscoelastic continuum damage model (with $\alpha = 2.331$).

Figure 3.14 presents the pseudo-stiffness versus damage curve. It is assumed here that it agrees with similar curves constructed directly from cyclic tests without rest periods. The veracity of this assumption will be demonstrated in ensuing sections.

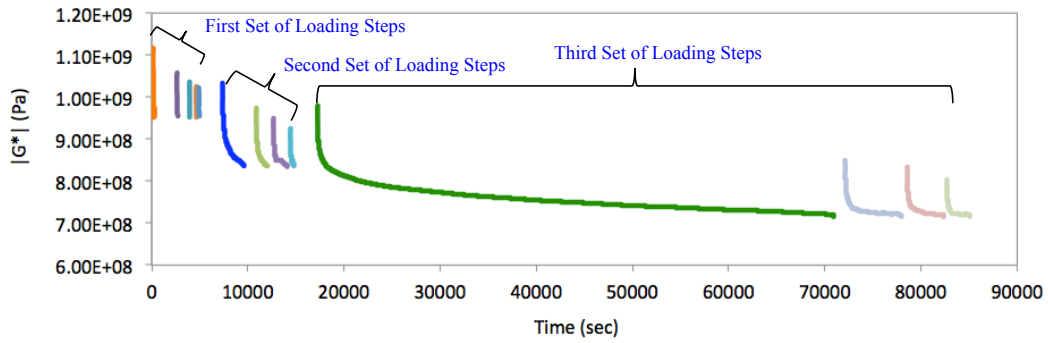

Figure 3.10: Time sweep steps with rest periods

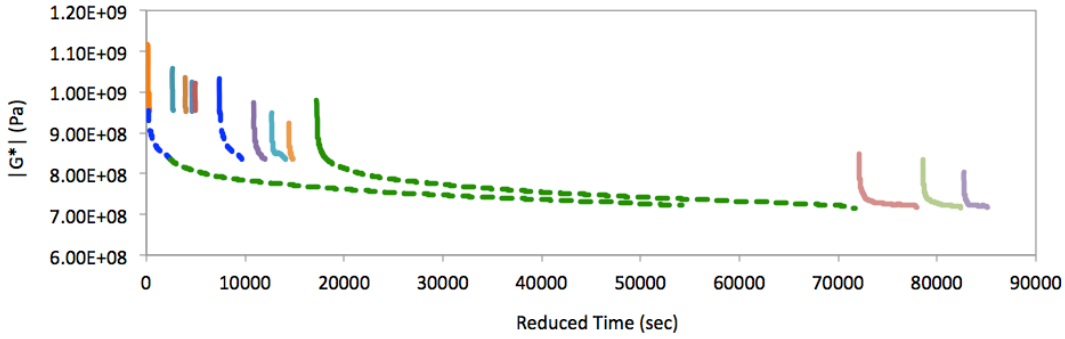

Figure 3.11: Superposition of the data between 100%, 80%, 70% and 60% stiffness

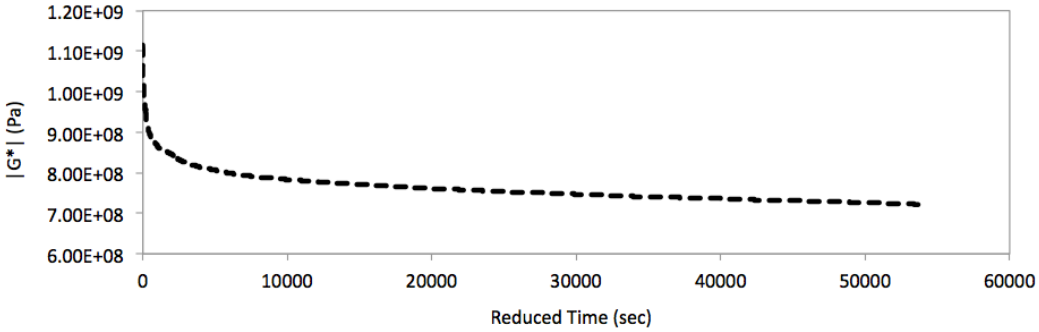

Figure 3.12: Superimposed stiffness history without the effect of rest periods

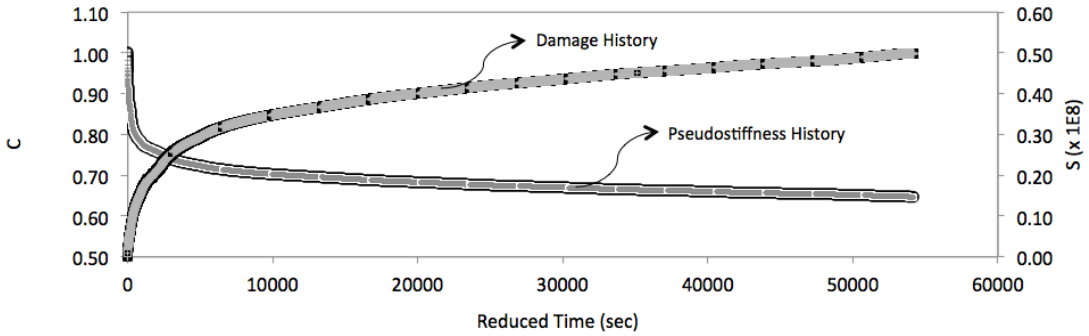

Figure 3.13: Pseudo-stiffness and damage histories without effect of rest periods

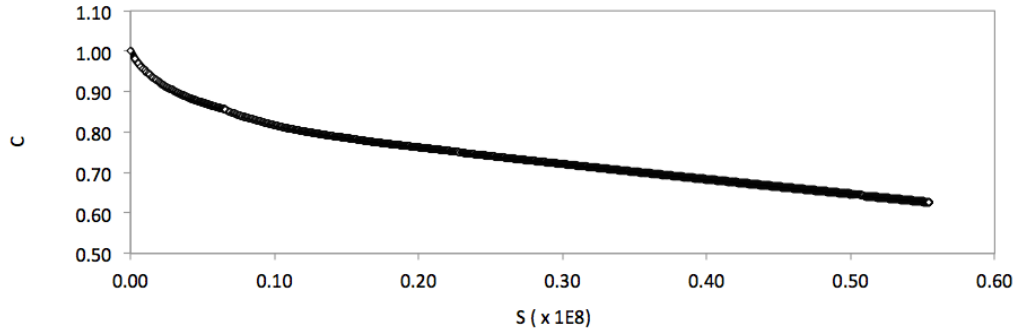

Figure 3.14: The resultant pseudo-stiffness vs. damage parameter curve constructed from the single specimen method

3.5.2.2 Fatigue Damage of Different Materials

Figure 3.15 demonsrates multiple ARC22 and UM22 pseudo-stiffness time-history profiles (for different stress amplitudes in controlled stress cyclic tests) constructed by following the proposed single-specimen test and analysis procedure, as illustared in Figure 3.10 through Figure 3.14. The loading frequency and temperature were 10 Hz and 25ºC unless stated otherwise in the figure. As can be seeen, none to negligible discontinuity of damage is observed at 80%, 70% and 60% of initial stiffness despite the introduction of multiple rest periods at those points. Results from both FAMs consistently demonstrated this characteristic, hence confirming the restoration of intrinsic

damage evolution rate as hypothesized in this study. Continuity in damage evolution rate some time after resuming the loading following a rest period is an important characteristic that allows the construction of the characteristic damage curve even when rest periods are introduced in the test protocol. This observation strongly illustrates that it is possible to filter away the effect of rest periods and create a smooth damage evolution curve for a given material despite the intermittent introduction of rest periods.

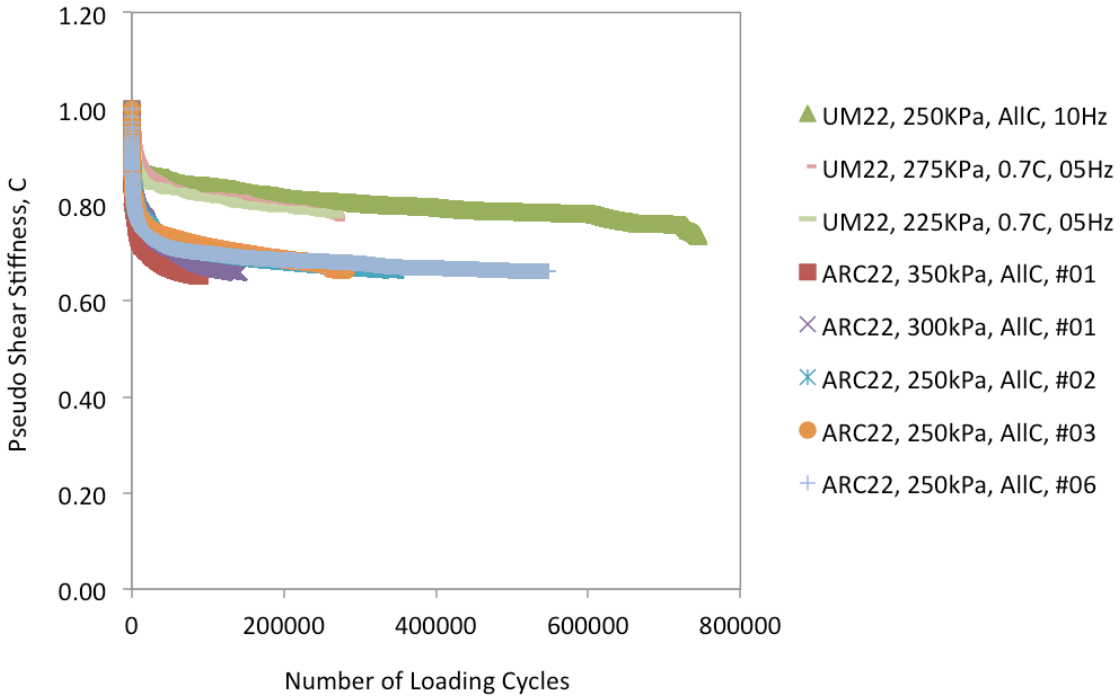

Figure 3.15: Pseudo-stiffness histories constructed from the cyclic tests at 25ºC. Note: (1) The frequency of 10 Hz was used for all cases unless stated otherwise. (2) "AllC" refers to results from the single-specimen tests that include rest periods unless stated otherwise.

Figure 3.16 presents the ARC22 and UM22 pseudo-stiffness vs. damage parameter profiles determined using the pseudo-stiffness history obtained from the single-specimen test results and Equation 3.17. The figure demonstrates that the damage

characteristic curve obtained for each composite was same irrespective of the loading amplitudes and more importantly irrespective of whether or not a rest period was introduced during the fatigue testing. Figure 3.16 reinforces the hypothesis that it is possible to obtain the damage characteristics of the material from the proposed single-specimen test procedure despite the introduction of rest periods.

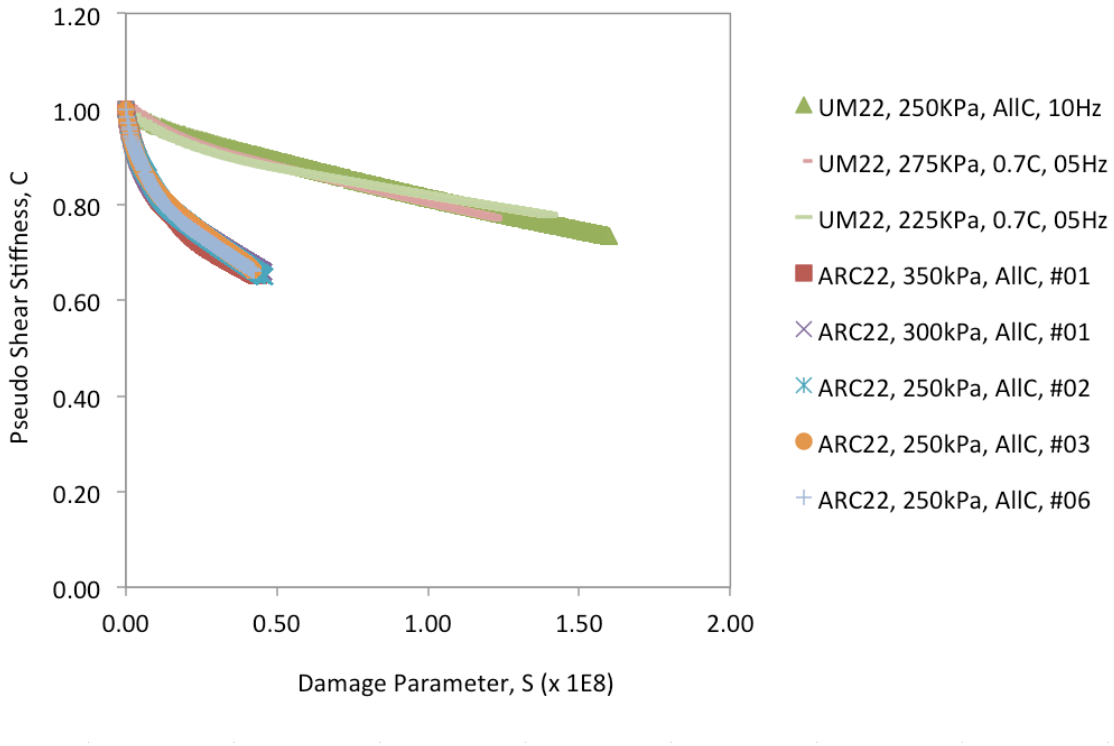

Figure 3.16: Pseudo-stiffness vs. damage parameter curves constructed from the cyclic tests at 25ºC. Note: (1) The frequency of 10 Hz was used for all cases unless stated otherwise. (2) "AllC" refers to results from the single-specimen tests that include rest periods unless stated otherwise.

3.5.2.3 Fatigue Damage of ARC22 Matrix

Figure 3.17 below presents the ARC22 pseudo-stiffness vs. damage curves obtained from eighteen specimens using the proposed single-specimen protocol and other

twenty-two specimens using the multiple-specimen protocol. The same $\alpha = 2.331$ was used for all these cases. The figure reveals consistent $C\ vs\ S$ profiles irrespective of multiple specimens, applied load levels, and rest period durations for the given material. This observation strongly suggests that the $C\ vs\ S$ profile is an inherent material property, and therefore does not depend on applied loading amplitudes.

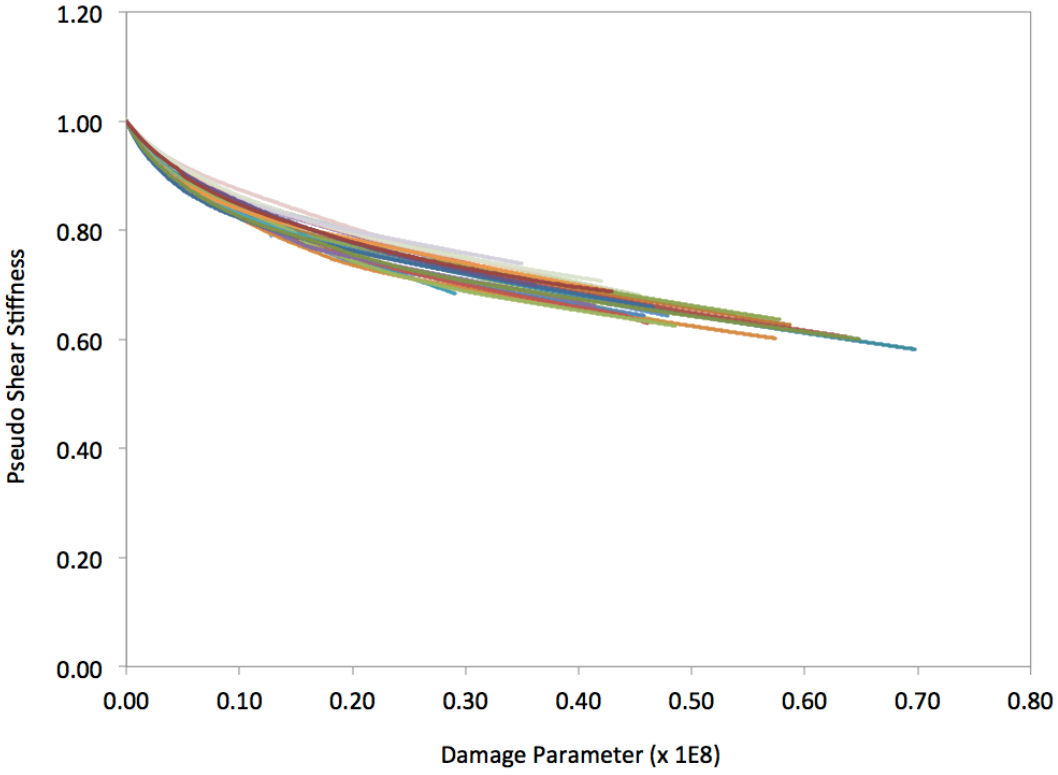

Figure 3.17: Pseudo-stiffness vs. damage parameter curves obtained using a total of forty different specimens; eighteen specimens were tested using the proposed single-specimen method (with rest periods to measure healing) and other twenty-two specimens were tested using the multiple-specimen method (separate specimens for fatigue tests without rest period and tests with rest periods at different levels of initial stiffness); stress-amplitudes of 250, 275, 350 and 400 kPa were used with different specimens at 10 Hz and 25ºC. The same $\alpha = 2.331$ was used for all these cases.

Also previously in Figure 3.16**,** UM22 pseudo-stiffness vs. damage parameter curves obtained from the single-specimen tests (with constant stress amplitude of 250 kPa at 10 Hz and 25ºC) and the multiple specimen tests (with constant stress amplitudes of 225 and 275 kPa at 5 Hz and 25ºC) were in good agreement with each other.

3.5.3 Healing Characteristics of ARC22 Matrix

Healing characteristics of the selected FAM were measured using the multiple-specimen protocol (different specimens for healing rate at each damage level) as well as the single-specimen protocol. As mentioned earlier, the amplitude of loading to induce damage was varied in the study to verify that the characteristics determined were independent of the loading type or history. Figure 3.18 illustrates the average values of healing potential for the selected FAM, measured by inducing damage following the multiple-specimen and single-specimen protocols under different stress amplitudes.

As seen in Figure 3.18, results obtained from both test protocols under different loading amplitudes show that the composites healed more during longer rest periods and less during shorter rest periods. Similarly, a higher percent of healing was observed when rest periods were introduced at a lower level of damage than at a higher level. The observations reinforce the fact that healing behavior is a function of the duration of rest period and the damage level preceding the rest period. In other words, the sooner the rest periods are introduced before significant stiffness reduction, the higher is the healing potential. The standard deviations for rest periods introduced after higher levels of damage are typically greater.

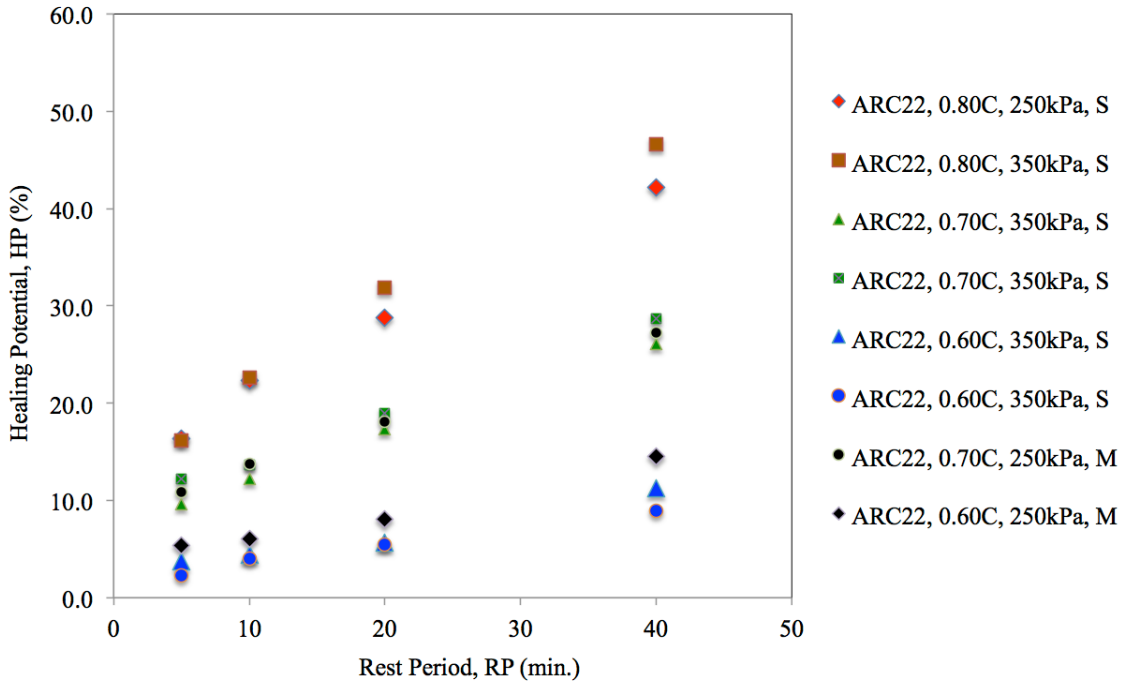

Figure 3.18: Healing potential from multiple-specimen (as referred by suffix "M") and single-specimen cyclic fatigue tests (as referred by suffix "S") under different stress amplitudes at 10 Hz and 25ºC.

Figure 3.18 also illustrates that the healing behavior obtained from the proposed single-specimen experimental and analytical method was very similar to the behavior obtained using the multiple-specimen protocol irrespective of the loading amplitude. This observation clearly signifies that the damage and healing of viscoelastic materials obtained in this manner are independent of loading sequences and amplitudes. In summary, the results obtained from the proposed experimental and analytical method revealed that damage and healing behavior are properties of materials that are independent of the amplitude, and sequence of loading. However, healing characteristics were dependent on the duration of rest period and the damage level preceding the rest period. Also, the values for percentage healing are small and demonstrate higher

variability from specimen to specimen noticeably at lower levels of stiffness or higher levels of damage in contrast to the values at higher levels of stiffness or lower levels of damage. Since only four rest periods were used in this study, phenomenological models to fit healing potential with rest period were not explored.

Chapter 4: Damage and Healing in Tension-Compression

Fatigue cracking due to tension is one of the most common distresses that shorten the useful life of flexible pavements. Cracking that starts at the bottom of an asphalt concrete layer due to localized tensile stress and moves progressively towards the surface is a good example of fatigue cracking due to tension. Different types of mixture tests are used to estimate the life of pavement materials subjected to different distresses and thereby facilitate the selection of the most durable materials. However, methods that are typically used to characterize fatigue behaviour due to uniaxial as well as shear loading use different test procedures and different metrics that are influenced by applied test conditions. To counter this dependency, this study investigates whether the same method and metrics used in Chapter 3 involving shear fatigue can be applied to measure fatigue damage as well as healing properties in uniaxial tension-compression mode of loading. In other words, this portion of this study examines the viability of using similar specimens, test procedures and metrics in the tension-compression mode of loading as those used in the shear mode of loading. The existing test methods only deal with only one mode of loading – monotonic or cyclic uniaxial mode, cyclic shear mode, flexural mode of loading (Kutay et al. 2008, 2009; Lee et al. 2000; Lee and Kim 1998a; b; Lundström and Isacsson 2003; Park et al. 1996; Tarefder et al. 2013; Underwood and Kim 2012, 2013b; Underwood et al. 2006, 2010).

This chapter explains the implementation of the proposed method in uniaxial mode of loading to measure:

- damage characteristics independent of the loading conditions used to induce damage or the sequence of rest periods introduced during such measurements, and

- healing characteristics due to rest periods independent of the loading conditions used to induce damage preceding the rest periods.

To this end, this chapter describes fatigue damage and healing behaviour of two different fine aggregate matrices using the proposed test method and the viscoelastic continuum damage mechanics (VECD) models. The following section will review the viscoelastic constitutive models required to understand damage and healing behaviors of asphalt materials subjected to uniaxial load cycles.

4.1 THEORETICAL BACKGROUND

4.1.1 Linear Viscoelastic Constitutive Model

The stress or strain response of a linearly viscoelastic asphalt material subjected to uniaxial loading without causing damage can be explained in terms of convolution integrals that represent the hereditary behaviour of viscoelastic materials:

$$\sigma(t) = \int_0^t E\ (t-\xi, t)\frac{\partial \varepsilon(\xi)}{\partial \xi} d\xi \qquad 4.1$$

$$\varepsilon(t) = \int_0^t D\ (t-\xi, t)\frac{\partial \sigma(\xi)}{\partial \xi} d\xi \qquad 4.2$$

The notations $\sigma(t)$ and $\varepsilon(t)$ in these integrals refer to time-dependent uniaxial stress and strain; $E(t)$ and $D(t)$ refer to relaxation modulus and creep compliance of the material. The computation of linear viscoelastic response needs the characteristic functions that describe the relaxation modulus and creep compliance of the material.

4.1.2 Schapery's Extended Correspondence Principles

The extended correspondence principle, $CP-II$ (Schapery 1984) transforms the time-dependent uniaxial stress and uniaxial strain into elastic equivalent uniaxial pseudo stress, σ^R and uniaxial pseudo strain, ε^R as given by:

$$\sigma^R \equiv \sigma \tag{4.3}$$

$$\varepsilon^R \equiv \frac{1}{E^R}\int_0^t E\,(t-\xi,t)\frac{\partial\varepsilon(\xi)}{\partial\xi} \tag{4.4}$$

The quantity, E^R in these equations is an arbitrary constant that is taken as unity in this study. The superscript, R refers to the pseudo-elastic domain for the reference elastic material. The substitution of integral terms in the correspondence equations with the hereditary definitions of stress and strain directly corresponds to the stress-strain relation of a pseudo-elastic media. Therefore, E^R represents the elastic modulus of the pseudo or reference elastic material hypothesized by the correspondence principles. There also exist inverse relations between the viscoelastic and pseudo-elastic quantities as given by (Schapery 1984):

$$\sigma \equiv \sigma^R \tag{4.5}$$

$$\varepsilon \equiv E^R\int_0^t D(t-\xi,t)\frac{\partial\varepsilon^R(\xi)}{\partial\xi}d\xi \tag{4.6}$$

Using the extended correspondence principle, $CP-II$ (Schapery 1984), and the steady state condition (Ferry 1980; Tschoegl 1989), the pseudo stress and pseudo strain values corresponding to the uniaxial stress and uniaxial strain amplitudes at the k^{th} load cycle can be expressed as (Underwood and Kim 2013b; Underwood et al. 2006, 2010):

$$\sigma^R_{ot,k} \equiv \left(\frac{\beta+1}{2}\right)\sigma_{pp,k} \tag{4.7}$$

$$\varepsilon^R_{ot,k} \equiv \left(\frac{\beta+1}{2}\right)\left(\frac{\varepsilon_{pp,k}\,.\,|E^*|_{LVE}}{E^R}\right) \tag{4.8}$$

The subscript, ot in these steady state correspondence definitions refers to the amplitude of pseudo stress or pseudo strain that is responsible for fatigue cracking at the

k^{th} load cycle whereas the subscript, pp refers to the peak-to-peak magnitude of stress or strain in that corresponding cycle. The notation $|E^*|_{LVE}$ refers to the dynamic modulus value measured by applying a small level of strain or stress within the linear viscoelastic range of the material. Similar to shear tests, β is a correction factor for accounting the portion of stress-strain history that is responsible for fatigue cracking as before; this correction factor can take any value from -1 to $+1$ depending upon the applied load cycle (sinusoidal, haversine, etc.) and the resultant material response (Underwood and Kim 2013b; Underwood et al. 2010). For example, in a sinusoidal load cycle, only one half of stress-strain history of a given cycle corresponds the tensile behavior that is responsible for cracking behavior of the material due to tension. It is assumed that damage does not accumulate during the stress-strain history corresponding to compression. Therefore, a zero value of β is used to analyze the effective strain, strain, stiffness and damage in each load cycle. In the elastic equivalent space, the value obtained by dividing pseudo stress amplitude over pseudo strain amplitude in a given load cycle represents the secant slope of stress-strain hysteresis loop. This secant slope represents the pseudo-stiffness of the pseudo-elastic material in the same way the uniaxial dynamic modulus (physical stress over physical strain) represents the stiffness of the actual viscoelastic material. In a steady state uniaxial test, the definition of pseudo-stiffness can be calculated using the following expression:

$$C_{uk}^{R}(S) \equiv \frac{\sigma_{ot,k}^{R}}{\varepsilon_{ot,k}^{R}} \cdot \frac{1}{I} \qquad 4.9$$

In the above expression, I accounts for the specimen-to-specimen variability in the initial stiffness. The subscript, u is used to distinguish the uniaxial cyclic tests described herein from the shear tests described in the earlier chapter.

4.1.3 Thermodynamics-based Work Potential Theory

The work potential theory of elastic media explains the structural change in asphalt material specimens that are subjected to uniaxial load cycles on the basis of thermodynamics. This theory expresses the pseudo strain energy density (W_u^R) and the resultant pseudo stress in an axially loaded specimen as the functions of applied pseudo strain, applied temperature and internal state variable (S_u) that represent the structural changes due to uniaxial loading. In an isothermal condition, the pseudo strain energy and the pseudo stress relations at the k^{th} load cycle follow as:

$$\sigma_{ot,k}^R = I.C_k^R.\varepsilon_{ot,k}^R \quad 4.10$$

$$W_{u,k}^R = \frac{I}{2}.C_k^R.\left(\varepsilon_{ot,k}^R\right)^2 \quad 4.11$$

4.1.4 Rate-type Damage Evolution Law

Similar to shear tests, the rate of structural changes due to uniaxial loading can be expressed as the power function of pseudo strain energy density (W_u^R) and an internal state variable (S_u) associated with damage due to uniaxial load cycles (Park et al. 1996; Schapery 1986):

$$\frac{dS_u}{dt} = \left(-\frac{\partial W_u^R}{\partial S_u}\right)^{\alpha} \quad 4.12$$

The $\alpha-$ value is a material damage rate parameter associated with uniaxial loading. Using the energy, stress and damage rate relations of the reference pseudo-elastic material, the total amount of damage accumulated until the N^{th} load cycle ($S_{u,N}$) can be computed using the following relation (Park et al. 1996):

$$S_{u,N} \cong S_{u,0} + \sum_{k=1}^{N}\left[\Delta S_{u,k}\right] \cong S_{u,0} + \sum_{k=1}^{N}\left[\left\{-\frac{I}{2}.\Delta C_{u,k}^R.\left(\varepsilon_{ot,k}^R\right)^2\right\}^{\frac{\alpha}{1+\alpha}}.(\Delta t_k)^{\frac{1}{1+\alpha}}\right] \quad 4.13$$

The notation, $S_{u,0}$ in this model refers to the value of internal state variable at the very beginning of load cycles. As shown above, the simplified definitions of pseudo-quantities used in this model are exclusively based on steady state conditions. The use of this damage model is justified as long as the micro-cracks do not localize and form larger macro-cracks (Underwood et al. 2010). More discussions on this issue will be provided in the result and discussion section.

4.2 TEST MATERIALS AND TEST PREPARATION

For this part of the study, the previously used ARC22 matrix that contained PG67-22 asphalt binder and another fine aggregate matrix ARC16 that contained PG64-16 asphalt binder were selected. The two matrices differed only in the selected grade of the binder but had same volumetric properties. The geometry of the specimen selected was the same as used earlier for cyclic shear tests, i.e., 12.25 mm in diameter and 45 mm in length. More details on the fabrication of these specimens can be found in Chapter 3.

A dynamic mechanical analyzer, ElectroPuls™ E1000 as seen in Figure 4.1 from Instron Engineering Corporation was used to conduct the uniaxial tests on the test specimens. Metallic jigs or caps were glued to the two ends of the specimens using a 5-minute epoxy to clamp them on the instrument. The selected epoxy was significantly stiffer than the material being tested. This allowed the measurement of specimen deformation using a built-in displacement transducer by measuring the end-to-end dimension change instead of using strain or displacement gauges mounted on a specimen. While gluing the specimens to the metallic grips, precautions were taken to avoid axial eccentricity. Similarly, precautions were also taken while clamping the specimens on the instrument using the metallic caps to prevent eccentricity and stresses/ strains before the actual test started.

Before starting any of these tests, the specimens were first conditioned for thirty minutes at 25ºC without applying any external stresses or strains. An environmental test chamber (ETC), solid state air condition and a temperature sensor as seen in Figure 4.1 along with a heat source were continuously used to maintain the target temperature during the conditioning, loading and resting periods. The conditioning step gives the specimen time to reach isothermal condition as required to use continuum mechanics. Also, this step allows the specimens to offset stress or strain histories, if any, during specimen handling and linear viscoelastic tests, thereby preventing the transfer of unwarranted strains to ensuing tests.

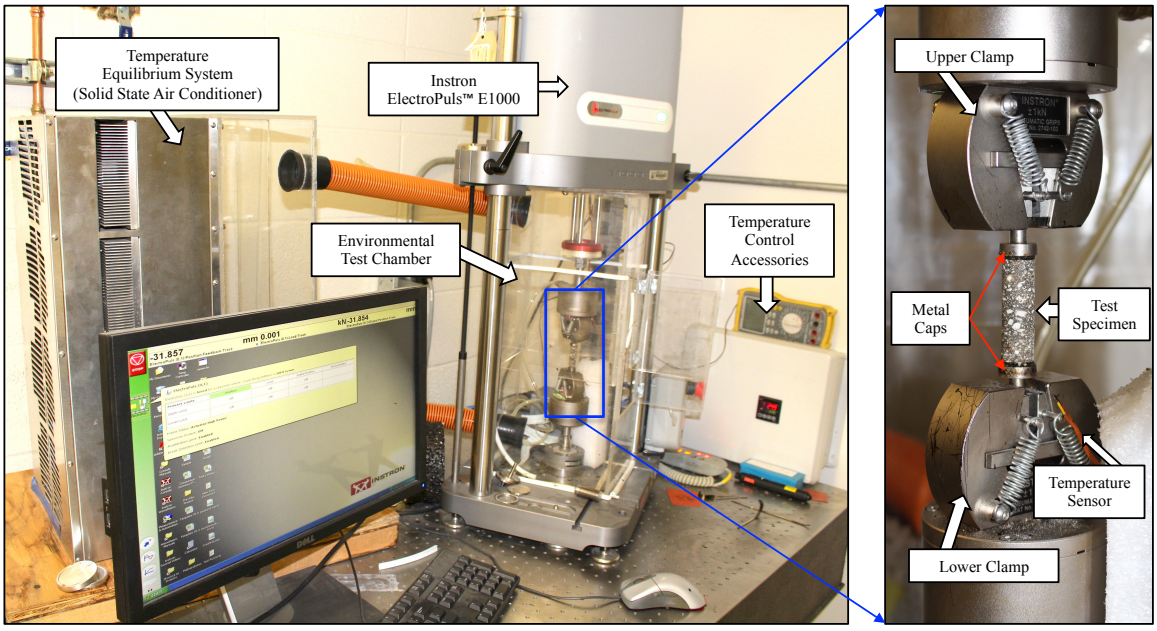

Figure 4.1: Tension-compression test set-up with a magnified view of test specimen

Similarly, during the conditioning period, the force and displacement calibration were performed using the specimen and the instrument assembly. The resultant calibration constant was used in the actual test to ensure that the instrument would

execute the commanded force or displacement control from the very beginning of the test. A well-calibrated test can avert the transient effects that can arise due to the sudden application of load on the specimen, thereby avoiding artifacts during the computation of damage. Therefore, in this study, calibration was performed for each specimen and test condition.

4.3 TEST METHODS

Each selected test specimen from both materials was subjected to a uniaxial creep test, a uniaxial dynamic modulus test and a damage-inducing uniaxial cyclic test in series. A feedback system inbuilt in the instrument was used to control the load and displacement as intended. A digital data acquisition system was used to measure and record the load-displacement data with micrometer resolution at millisecond time intervals. The following sections provide the specific descriptions of the three tests.

4.3.1 Linear Viscoelastic Property Tests

Force-controlled uniaxial creep tests and displacement-controlled dynamic modulus tests were performed to determine the material creep parameter, m and the linear viscoelastic dynamic modulus, $|E^*|_{LVE}$, respectively. Both of these properties are essential to analyze overall damage and healing due to fatigue cracking using the VECD models. It must be noted that only one of the creep, relaxation or frequency sweep tests is required to determine the LVE properties (Ferry 1980; Gross 1953; Tschoegl 1989). However, the two separate LVE tests added redundancy but improved accuracy compared to determining one directly from test and one indirectly from the viscoelastic transformations.

4.3.1.1 Creep Compliance Tests

The material parameter, m signifies the rate dependency of the compliance of a material when subjected to a constant uniaxial load at a given temperature. To obtain this parameter, each specimen was first subjected to a 3.0-N tensile force at 25^0C for thirty seconds and then allowed to recover the residual arbitrary strain for another six hundred seconds at zero loads. The magnitudes of applied loads and the durations of loading and recovery were selected based on multiple trial tests performed on specimens using the same materials at lower and higher tensile loads to ensure that the materials response within its linear limits. In some cases, two creep and recovery tests were randomly conducted back to back for additional verifications.

In this study, the creep compliance history data for each specimen followed a generalized power-law relation with time of loading.

$$D(t) = \frac{\varepsilon(t)}{\sigma_o} = D_o + D_1 t^m \qquad 4.14$$

The parameters, D_o, D_1 and m as seen above are the material constants related to creep in uniaxial direction. After each creep and recovery test, the specimens were allowed 30-minute equilibrium time.

4.3.1.2 Dynamic Modulus Tests

After a 30-minute equilibrium time, the specimens that were previously used for the creep tests were once again used to determine the linear viscoelastic dynamic modulus, $|E^*|_{LVE}$. To this end, each specimen was subjected to 20 sinusoidal cycles with 0.005-mm amplitude ($\varepsilon_o = 0.011\%$) in tension-compression mode at a frequency of 5 or 10 Hz and the temperature of 25°C. Unlike the shear tests, uniaxial tests were conducted at one additional frequency of 5 Hz.

To assure linear viscoelastic response, the selected number of load cycles and the amplitudes of controlled displacements (or strains) were based on similar tests performed at lower and higher amplitudes for different load cycles. By definition, the stress amplitude (force amplitude per unit cross-sectional area of the specimen) divided by the strain amplitude (or displacement amplitude per unit length of the specimen) corresponding to the same load cycle yields the dynamic modulus (stress over strain) of the material.

$$|E^*| = \frac{\varepsilon_o}{\sigma_o} \tag{4.15}$$

The average of these moduli obtained from the first few cycles is herein denoted as $|E^*|_{LVE}$. After the dynamic modulus tests, the specimens were allowed another 30-minute long conditioning or equilibrium time.

4.3.2 Fatigue Damage and Healing Tests

The loading frequencies and the test temperature that were previously used for the LVE tests of a given material were again used for the uniaxial cyclic test with and without rest periods. In these tests, each specimen was subjected to a number of sinusoidal load cycles with a constant loading frequency and displacement amplitude. The applied amplitude of uniaxial strain was selected high enough to induce damage in the materials. The force required to achieve the commanded displacement was continuously recorded during this process. Figure 4.2 demonstrates the stress-strain history obtained from one of the displacement-controlled cycles at 10 Hz and 25ºC. Since strain is a ratio of displacement and the length of the specimen, both "displacement-control" and "strain-controlled" terms are used alternatively in this study.

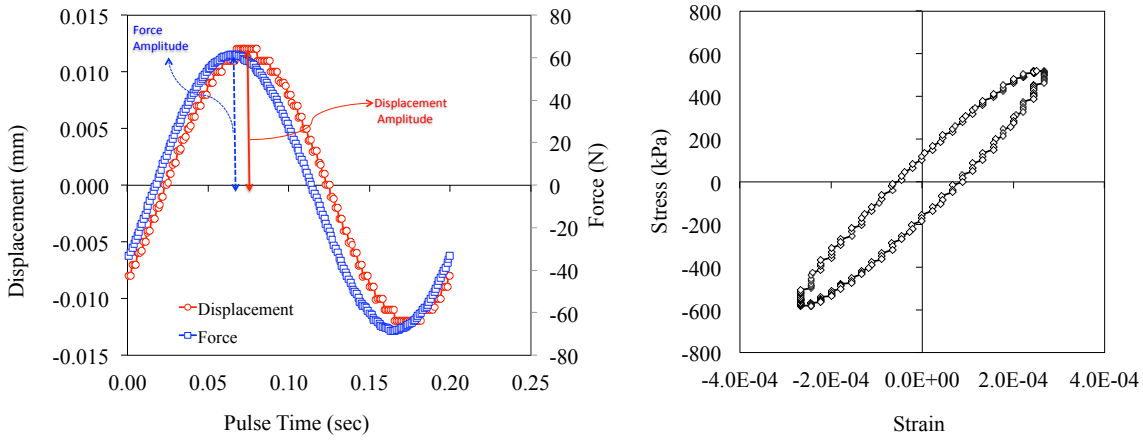

Figure 4.2: Uniaxial Test: (a) Displacement and force histories, and (b) Stress-strain hysteresis at 5 Hz and 25ºC

Continued application of load cycles induces damage in a material, which in turn reduces the material stiffness or increases its compliance. For example, Figure 4.3 provides the schematic of a fatigue test of a FAM specimen that continuously loses its stiffness (corresponding to from data point A_1 to data point A_3). In this particular study, displacement (or strain) amplitude was controlled. Figure 4.3 also presents a schematic of the proposed test method in which a number of rest periods are introduced when the stiffness of the material reduces by certain percentages of initial stiffness as assigned. ElectroPuls™ E1000 instrument allowed the percentage allocations only with respect to initial stiffness of a particular loading segment. This means that a rest period was started as soon as the stiffness of the material in a given time sweep step reduced by a certain percentage of the initial stiffness of the same time sweep step. For example, Figure 4.3 illustrates a condition in which a rest period would start as soon as the material stiffness drops its stiffness by $\Delta|E^*|_{wrt\,B1}$ with respect to stiffness at data point B_1 and reaches the stiffness corresponding to data point B_2.

To ensure that new rest periods would successively initiate at lower levels of stiffness, the relative reduction value for each loading step was assigned greater than the stiffness recovered during the preceding rest period. Figure 4.3 demonstrates that a new rest period would start as soon as the stiffness drop associated with $(B_1 - B_2)$ would be greater than the stiffness surge associated with data points $(B_1 - A_2)$. Therefore, the relative stiffness reduction assigned for each loading step plays a vital role in fixing the stiffness to initiate rest periods. Since the assigned stiffness reduction for a given loading step is based on the initial stiffness of the same loading step, and since this initial stiffness varies from specimen-to-specimen due to different level of healing, the rest periods would initiate at slightly different levels of stiffness. However, since the proposed method of data analysis is independent of the testing conditions, the exact value of stiffness at which rest period is introduced is not absolutely critical. In fact, consistent results in the measured healing properties despite the variations in the level of stiffness at which rest periods are introduced from one specimen to another can be used as an indicator of the efficacy of this test method. To decide the value of stiffness reductions, some additional tests were conducted using several different stiffness reduction percentages.

To be specific, the uniaxial cyclic tests with or without rest periods in this study were performed using three different displacement or strain amplitudes (0.010 mm, 0.012 mm and 0.015 mm displacement amplitudes that respectively correspond to 0.022%, 0.027% and 0.033% strain amplitudes) at two frequencies (5 Hz 10 Hz) and 25ºC. Rest periods ranged from 5 minutes to 40 minutes while stiffness reductions ranged from 0.19 to 0.32 GPa. For damage and healing computations, the force-displacement amplitude data was recorded at each cycle of loading steps.

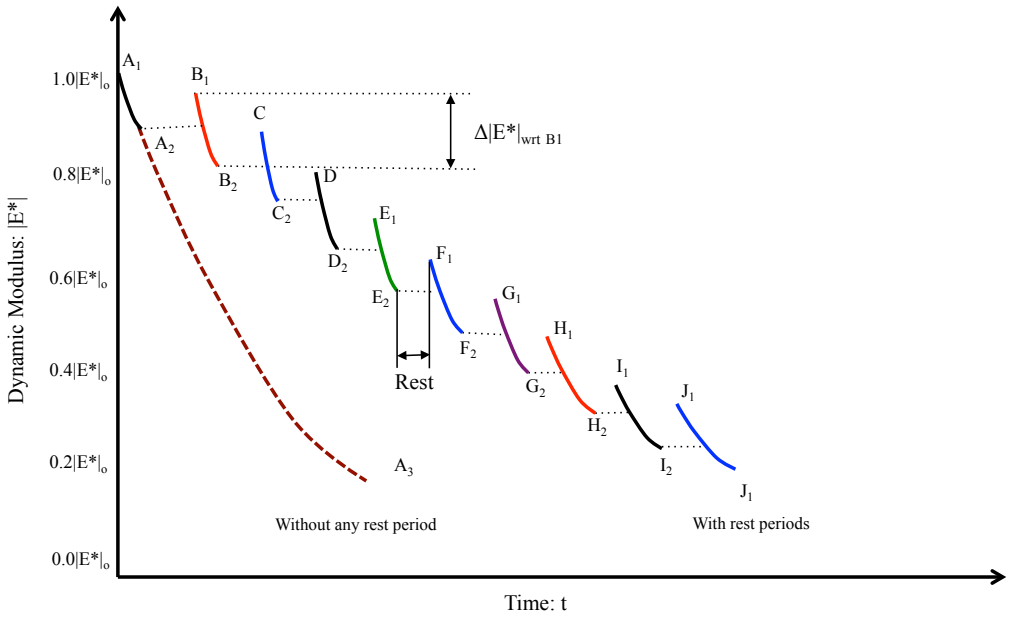

Figure 4.3**:** Schematic of the fatigue test with and without rest periods

4.4 DATA ANALYSIS

The computation of accumulated damage in uniaxial cyclic tests without rest periods involves the use of damage model derived using Schapery's correspondence principles, work potential theory and rate-type damage evolution law. The test method with four rest periods at three different stiffness levels in shear using the same specimen as proposed in Chapter 3 was modified to be more flexible to include multiple number of rest periods at several different stiffness levels in this chapter. As such, the extraction of damage properties from cyclic tests with rest periods in tension-compression needs a little bit more analysis although it follows the same fundamental process in Chapter 3.

Figure 4.4 schematically demonstrates the construction of a single curve using the separate batches of data obtained from the fatigue test with multiple rest periods using the

same specimen. As seen, the illustrated test contains eight rest periods introduced between nine consecutive time sweep steps (represented by curves A to J); each time sweep curve starts at a stiffness greater than the stiffness preceding the rest period and ends at a stiffness lower than the stiffness preceding the rest period. For example, the stiffness preceding the second rest period (denoted by data point B_2 Figure 4.4) is lower than the stiffness at which the third time sweep step starts (denoted by data point C_1 in Figure 4.4) and greater than the stiffness at which it ends (denoted by data point C_2 in Figure 4.4). As such, there lies a point (denoted by point "P" in Figure 4.4) in the time sweep history with stiffness equal to the value corresponding to stiffness at B_2. This study assumes that the data contained between the points "P" and "C_2" is free from healing effects, and therefore can be moved to conjoin with similar sections from other time sweep steps. This process of data shifting and stitching is similar to the process earlier used in Chapter 3.

Healing analysis method and model used in this part of the study is fundamentally the same as the one used in Chapter 3. The only difference is the different mode of damage growth.

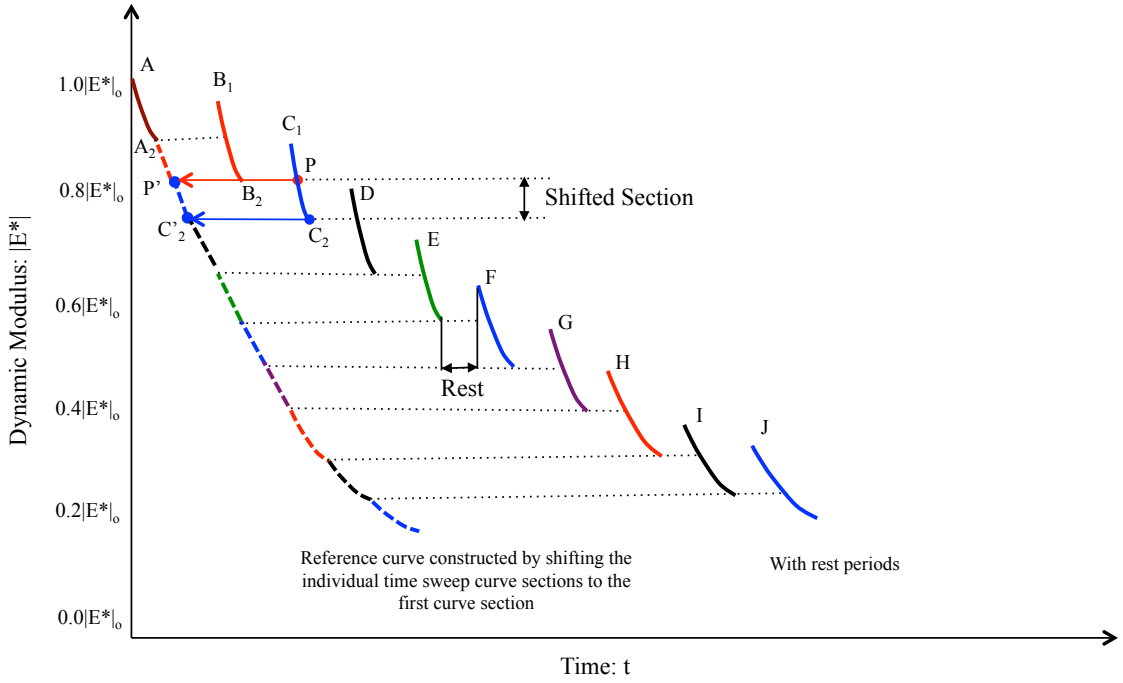

Figure 4.4: Schematic of constructing a single time sweep curve from fatigue tests with multiple rest periods

4.5 Results and Discussion

4.5.1 Linear Viscoelastic Properties

Figure 4.5(a) present the ARC16 and ARC22 linear viscoelastic creep parameters (m) and corresponding damage evolution rate parameter (α) calculated using the m-values. As mentioned earlier, the slope parameters, m were obtained from the creep tests at 3.0 N tensile forces. Similarly, Figure 4.5(b) presents the ARC16 and ARC22 dynamic moduli ($|E^*|_{LVE}$) obtained from the dynamic modulus tests conduced at a strain amplitude of 0.005 mm and frequencies of 5 Hz and 10 Hz. As can be seen, the ARC22 material has higher stiffness and lower m-value than the ARC16 materials. Consequently,

the damage parameter of the softer material, i.e., ARC22 is higher than the damage parameter for the stiffer material, i.e., ARC16 as expected.

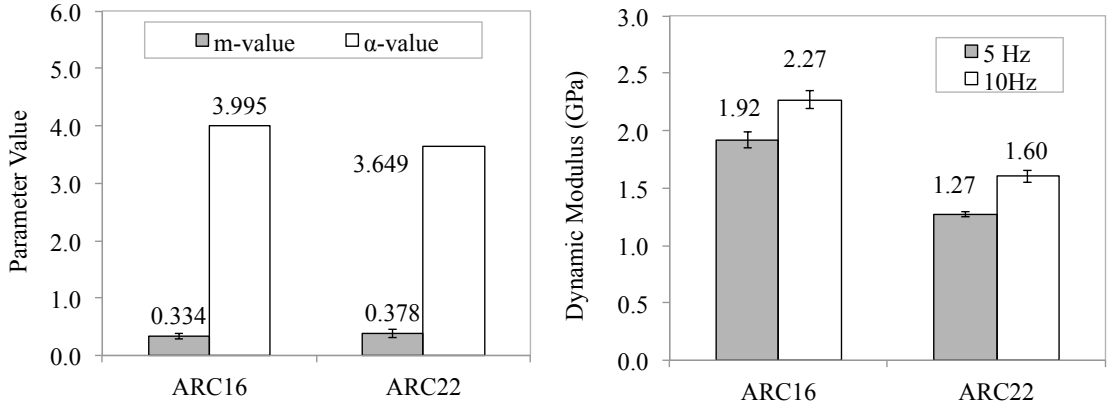

Figure 4.5: Results from the linear viscoelastic property tests of ARC16 and ARC22 materials at 25°C: (a) m-values with selected alpha, (b) dynamic moduli at 5 and 10 Hz

4.5.2 Damage Characteristics

4.5.2.1 Fatigue Damage in Tension-Compression: An Example

The following steps first exemplify the process used in this study to construct the pseudo stiffness versus damage parameter curve ($C\ vs\ S$) of FAM specimen subjected to the uniaxial test with multiple rest periods. The procedure described below was implemented in analyzing fatigue tests with as well as without rest periods. In case of the tests without rest periods, the rest periods were considered zero.

Step 1. Figure 4.6 presents the tensile and compressive stress and strain amplitudes obtained from a strain-controlled fatigue test with rest periods. In this particular test, a strain amplitude of 0.027% (or displacement amplitude of 0.012 mm), a frequency of 10 Hz, the temperature of 25°C and the rest periods of 5, 10, 20 and 40 minutes (represented by the gaps in the Figure 4.6) were used. As shown in

this figure, the input strain and the output stress symmetrically oscillate across the zero-mean axis with constant amplitudes. Figure 4.7 presents the history of uniaxial dynamic modulus computed using the stress and strain amplitudes. The modulus values were calculated using the strain and stress amplitudes above the zero-mean axis due to the symmetry across the mean axis. Figure 4.7 clearly demonstrates that the selected test specimen lost its stiffness during each loading step and partially recovered this loss during each rest period. Figure 4.7 also shows a faster rate of stiffness reduction immediately after a rest period but a slower rate some time after resuming the load cycles following the rest period. This change in rate can be attributed to the fact that the number of cycles needed to regrow the micro-cracks that healed during the rest periods is smaller than the number of cycles needed to start new micro-cracks. It is therefore reasonable to assume that new micro-cracks form only after full regeneration of healed micro-cracks.

The work potential theory defines stiffness (or pseudo-stiffness) as a function of accumulated damage. Based on this theory, it is plausible to assume that the stiffness level at which the healed micro-cracks are fully recreated and new micro-cracks are about to initiate is actually equal to the same stiffness level that precedes the rest period. In other words, the material restarts forming micro-cracks at a rate equal to its characteristic damage evolution rate as soon as the stiffness degrades to a value equal to the stiffness preceding the rest period. Therefore, a new rest period can be applied again since there is no effect of healing after resuming the damage rate. This fact also makes it possible to stitch the stiffness sections unaffected by healing into one single curve; the resultant

characteristic curve should represent the material response without any rest period.

Step 2. For computing the damage from fatigue tests using the proposed model, the stiffness data obtained from each time sweep step was horizontally shifted towards the stiffness data obtained from the very first time sweep step such that the data that is unaffected by healing align in a single smooth curve as seen in Figure 4.8. While shifting the stiffness data, the original time gap between each data point from a given loading step was maintained. The horizontal shifting and tail-to-tail stitching of the individual time sweep sections reduced the total time originally taken by the cyclic test with rest periods (see Figure 4.6 and Figure 4.7) by almost three times (see Figure 4.8). The sharp drops and bends seen in Figure 4.8 represent the material response affected by healing.

Step 3. The stiffness data assumed to be affected by healing from each loading step were then trimmed away leaving behind the data that is assumed free from healing effect. Figure 4.9 presents the stiffness history constructed by moving and stitching the data unaffected by healing for the given example specimen. As seen in the figure, the curve shows negligible number of kinks as if the corresponding data was obtained directly from a cyclic test without rest periods. This single curve can also be constructed by first trimming the data affected by healing, and only then moving and stitching the remaining data. In case of cyclic tests without rest periods, steps 2 and 3 were not required.

Step 4. The stiffness history corresponding to Figure 4.9 was then converted into pseudo-stiffness history using the modified elastic-viscoelastic correspondence principles. Similarly, the strain amplitudes corresponding to the data in Figure 4.9 were converted into pseudo strain amplitudes. Using the calculated pseudo quantities

and viscoelastic continuum damage model described above, the internal state variable for damage or simply damage parameter history was obtained. Figure 4.10 presents the pseudo-stiffness and damage parameter histories constructed. As seen in the figure, the test specimen had maximum stiffness (or pseudo-stiffness) and zero damage at the beginning of the test. But, the specimen kept accumulating damage while losing stiffness with more number of load cycles, a typical behavior shown by viscoelastic material subjected to continuous stress or strain without rest period.

Step 5. The pseudo-stiffness was then plotted against damage parameter to obtain the characteristic curve of the material based on VECD. Figure 4.11 presents the pseudo-stiffness vs. damage parameter curve for the ARC16 specimen used in this example.

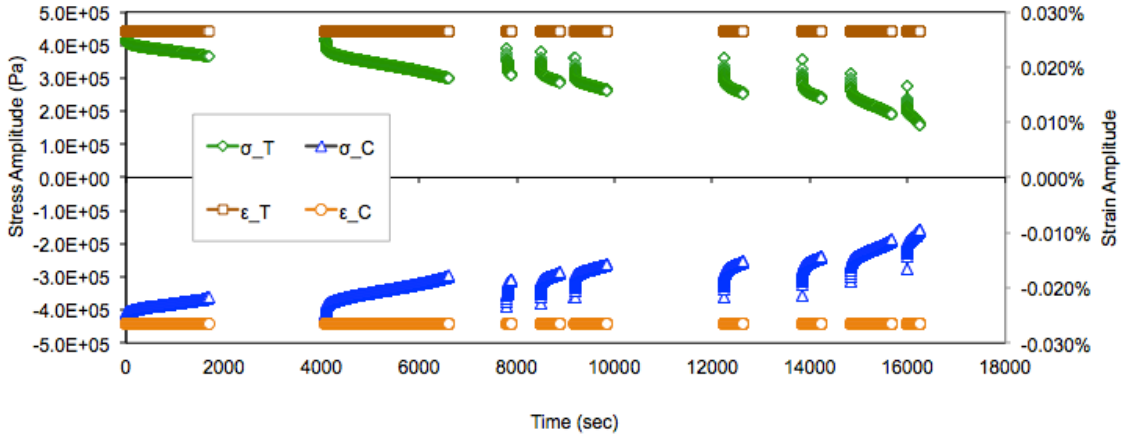

Figure 4.6: Typical results from a uniaxial cyclic test with rest periods

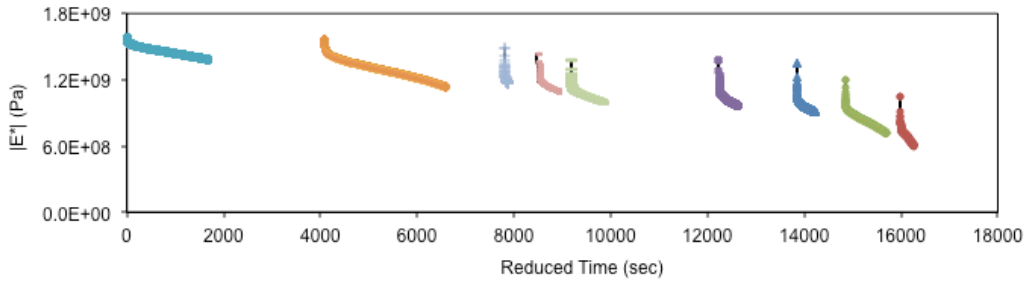

Figure 4.7: Dynamic modulus history obtained using stress and strain amplitudes

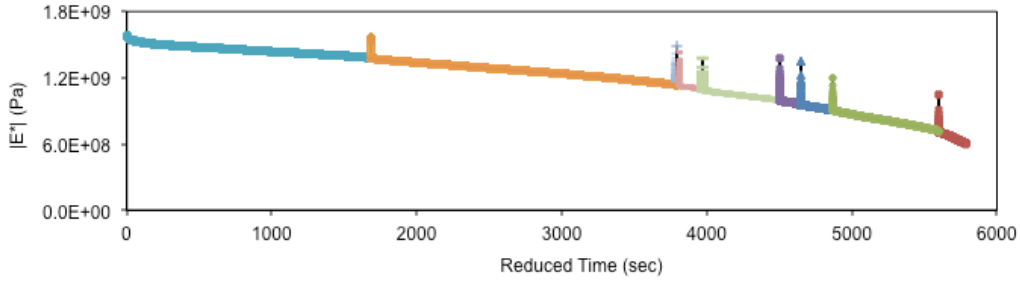

Figure 4.8: Dynamic modulus history after horizontal shifting

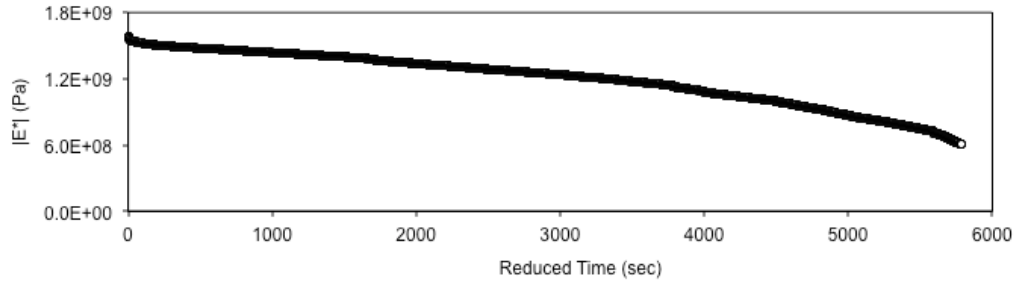

Figure 4.9: Dynamic modulus history after trimming the effect of healing

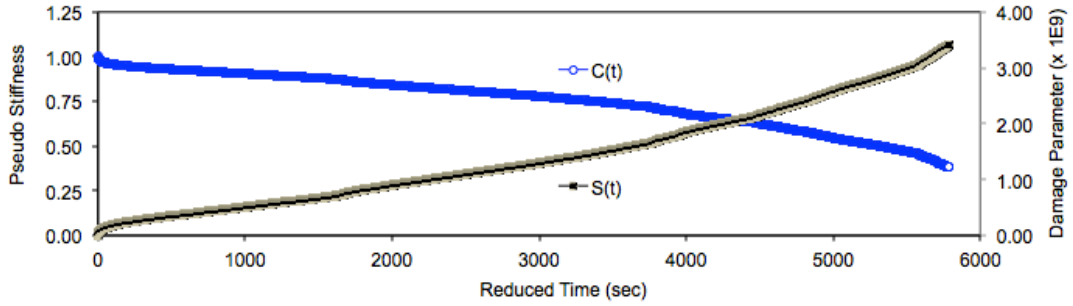

Figure 4.10: Pseudo-stiffness and damage parameter histories from the proposed method

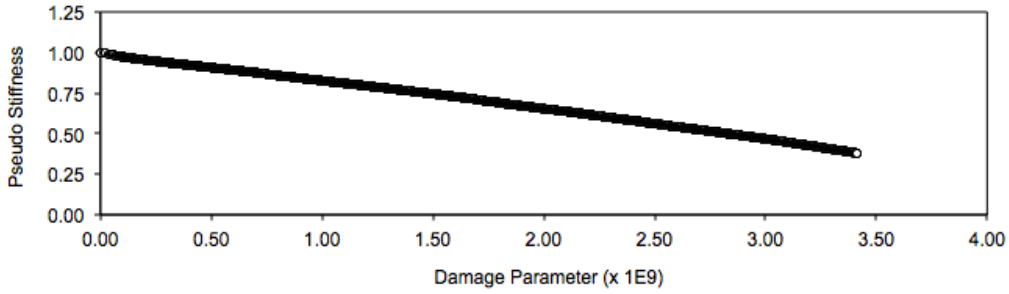

Figure 4.11: Pseudo-stiffness vs. damage parameter curve obtained from VECD-analysis

The following sections will provide evidence to support that the $C\ vs\ S$ curves obtained from the fatigue tests with rest periods using the just-demonstrated analytical process agree with the $C\ vs\ S$ curves obtained directly from the fatigue tests without rest periods.

4.5.2.2 Fatigue Damage in Tension-Compression without Rest Periods

Figure 4.12 presents the pseudo-stiffness vs. damage parameter curves obtained from the uniaxial cyclic tests of ARC16 and ARC22 specimens without any rest periods. As can be seen, the curves obtained from the uniaxial cyclic tests of a given material agree with each other despite the use of different strain amplitudes (0.018%, 0.022%,

0.027% and 0.033%) and loading frequencies (5 Hz and 10 Hz). This observation demonstrates that the damage characteristics obtained using the VECD model is independent of applied strain and frequency conditions. Similarly, the $C\ vs\ S$ curves obtained from ARC16 specimens are different than the $C\ vs\ S$ curves obtained from ARC22 specimens. Therefore, it can be asserted that the $VECD$ model yields the true material properties that are independent of test conditions - strain amplitudes and loading frequencies to be specific.

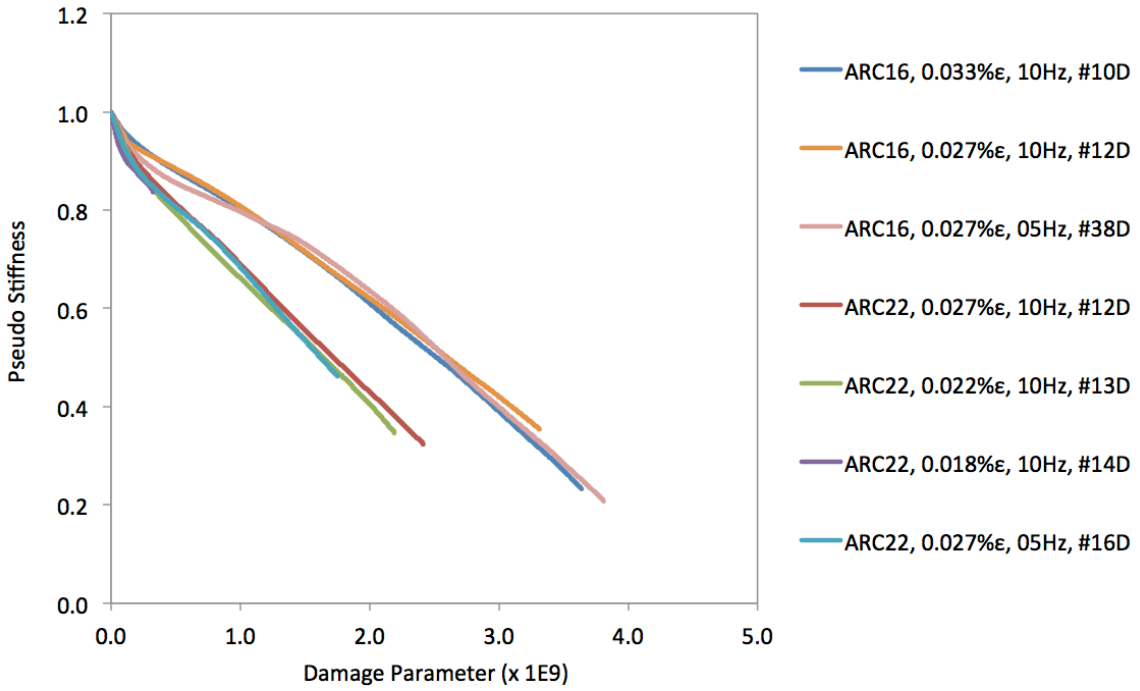

Figure 4.12: Characteristic $C\ vs\ S$ curves for ARC16 and ARC22 matrices

4.5.2.3 Fatigue Damage of ARC16 Matrix with Rest Periods

Figure 4.13 presents the pseudo-stiffness vs. damage parameter ($C\ vs\ S$) curves constructed from the displacement-controlled uniaxial cyclic tests of ARC16 specimens with and without rest periods at 25ºC. In particular, the uniaxial cyclic tests with rest

periods (denoted by suffix "H" in Figure 4.13) were conducted using five specimens at strain amplitude of 0.027% and loading frequency of 5 Hz. During these tests, the rest periods of 40, 20, 10 and 5 minute durations were introduced at decreasing order of stiffness levels. The stiffness levels at which such rest periods would initiate were randomly varied from specimen-to-specimen by allowing the first initial stiffness of a given time sweep step to reduce by different amount from step-to-step and specimen-to-specimen. As mentioned earlier, such variation indirectly helps demonstrate the validity of VECD-based damage model. Figure 4.13 also presents the $C\ vs\ S$ obtained from the uniaxial cyclic tests without any rest periods (denoted by suffix "D" in Figure 4.13) – two specimens at 5 Hz and 0.027% strain amplitude, one specimen at 10 Hz and 0.027% strain amplitude, and another one specimen at 10 Hz and 0.033% strain amplitude.

Figure 4.13 demonstrates that $C\ vs\ S$ curves constructed from fatigue tests with rest periods are consistently smooth, except in some cases with minor kinks where the data from two consecutive loading steps were stitched. This observation is evident in all $C\ vs\ S$ curves obtained from the cyclic tests with rest periods irrespective of applied loading and resting conditions. Figure 4.13 also demonstrates a close agreement between the $C\ vs\ S$ curves obtained from the cyclic tests involving different durations of rest periods and different stiffness levels preceding the rest periods as well as different loading conditions. Furthermore, these curves are coherent with the curves obtained from the cyclic tests without rest periods at different loading conditions.

As before, the agreement between the $C\ vs\ S$ curves constructed from cyclic tests with rest periods and the $C\ vs\ S$ curves obtained directly from cyclic tests without rest periods strongly suggests that the VECD damage model is not only independent of loading conditions but is also independent of rest conditions. This observation proves that the asphalt materials fully recover their damage evolution rate some time after resuming

the load cycles following the rest period. Furthermore, $C\ vs\ S$ curves constructed from the cyclic tests with rest periods are consistently similar to each other and the ones obtained from the cyclic tests without rest periods irrespective of different strain amplitudes, frequencies, rest periods and stiffness preceding the rest periods. This behavior reinforces the test condition independency of VECD damage model. As such, the method to quantify damage and healing in shear was successfully implemented in tension-compression mode. The above observations strongly verify that the same method can be used to extract fatigue damage and healing properties of asphalt mixtures simultaneously from the same specimen irrespective of the mode of loading.

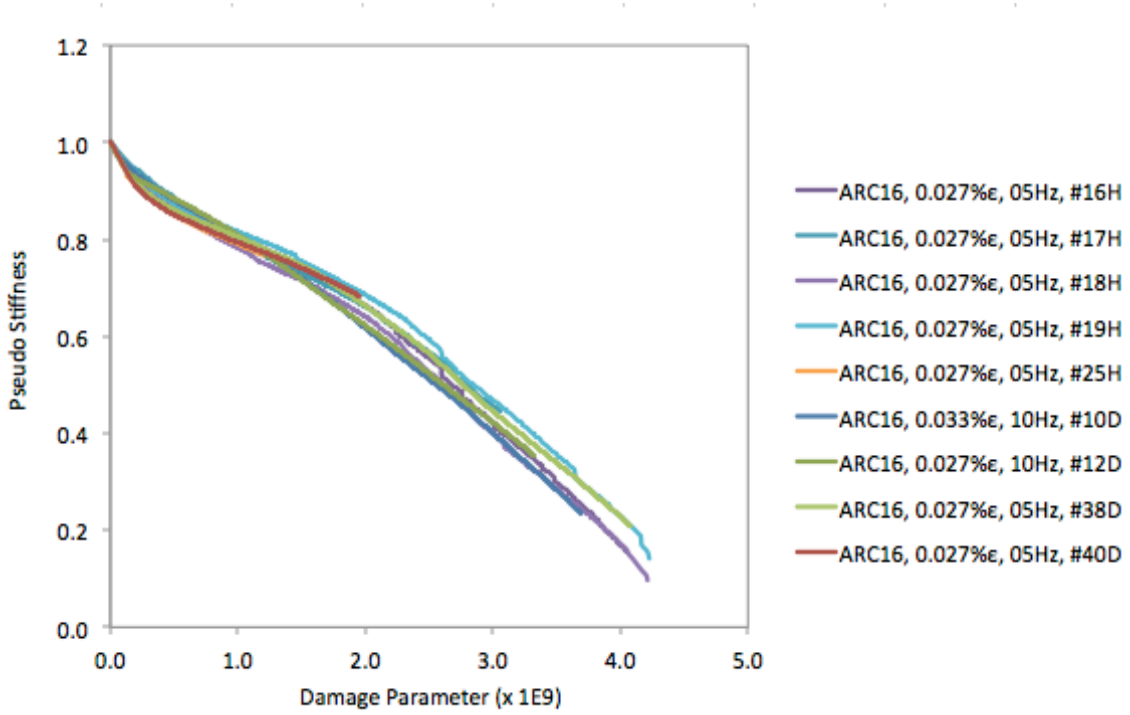

Figure 4.13: ARC16 results from cyclic tests: Without rests, "D" and with rests, "H"

However, the assertions made above are true only until micro-cracks do not localize and form macro-cracks or flaws. The use of the continuum-based damage model after localization therefore does not represent true material property. Formation of macro-cracks usually causes a quicker reduction in material stiffness and equivalent escalation in damage. But the majority of ARC16 specimens used in uniaxial cyclic tests resulted in consistently similar $C\ vs\ S$ curves with minor discrepancy as seen in Figure 4.13.

4.5.2.4 Fatigue Damage of ARC22 Matrix with Rest Periods

Figure 4.14 presents the pseudo-stiffness vs. damage parameter curves ($C\ vs\ S$) of ARC22 specimens subjected to uniaxial load cycles at different loading and rest situations. Similar to ARC16 composites, different strain-amplitudes (0.018%, 0.022%, 0.027% and 0.033%), loading frequencies (5 Hz and 10 Hz) were applied on the ARC22 specimens at 25ºC. Eight cyclic tests with rest periods and five cyclic tests without rest periods in uniaxial mode of loading were performed to obtain the $C\ vs\ S$ curves in Figure 4.14. For healing, rest periods of 40, 20, 10 and 5 minutes were intermittently and randomly introduced during the cyclic tests while varying the stiffness levels at which these rest periods would initiate.

As can be seen in Figure 4.14, the $C\ vs\ S$ curves constructed using the results from cyclic tests with rest periods at different loading and healing conditions are smooth with very few kinks. The curves constructed from cyclic tests with rest periods are similar to the $C\ vs\ S$ curves obtained from cyclic tests without rest periods irrespective of different strain amplitudes and frequencies. The consistently similar $C\ vs\ S$ curves strongly suggest that $C\ vs\ S$ represents the true material properties that do not depend on applied test conditions, and that the damage evolution rate recovers some time after resuming the load cycles following the rest periods as hypothesized. Moreover, the

possibility of extracting the true material properties, i.e., C vs S curves from cyclic tests with rest periods in addition to healing due to rest periods makes the proposed method very promising. However, it is noted here that ARC22 specimens showed a slightly higher specimen-to-specimen variability than ARC16 specimens after certain level of stiffness reduction, hinting the annulment of continuum due to localized macro-cracks. As the ARC22 specimens are softer than ARC16 materials, such variability was expected. Equally important is the verification that the proposed method could be used in tension-compression mode as efficiently as in shear mode.

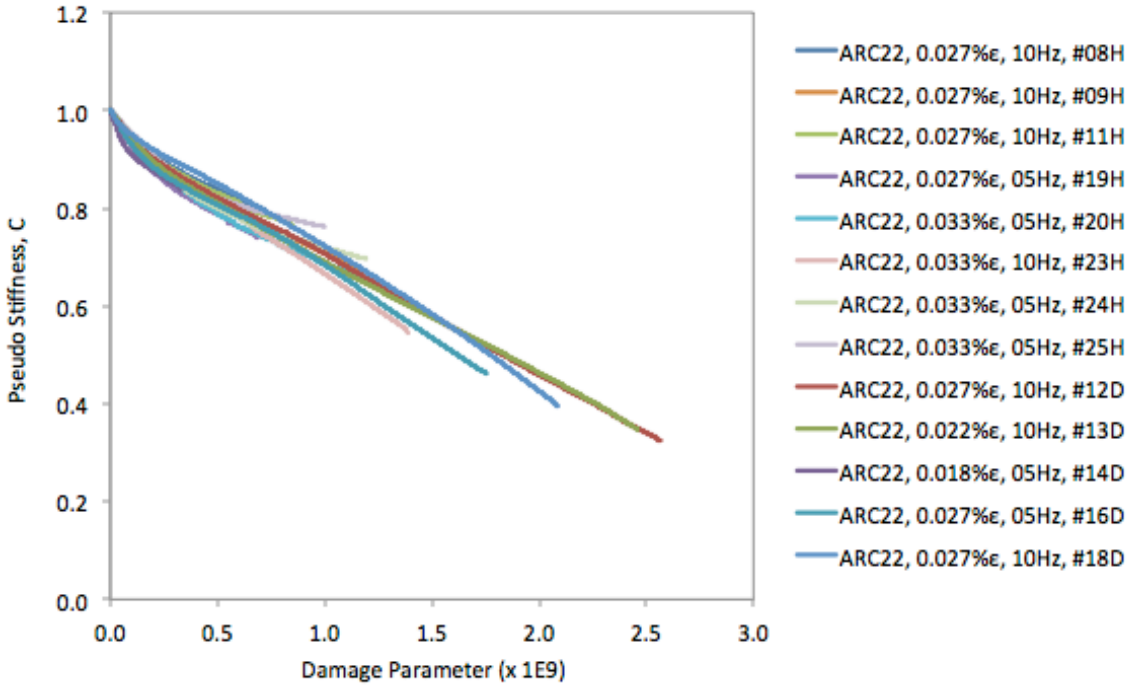

Figure 4.14**:** ARC22 results from cyclic tests: Without rests, "D" and with rests, "H"

In summary, Figure 4.13 and Figure 4.14 reveal that (a) C vs S curves are indeed material properties that are independent of loading conditions (such as strain amplitudes,

frequencies, and temperatures) as well as rest conditions (such as the number and duration of rest period and the stiffness preceding the rest period). The test condition independency of $C\ vs\ S$ curves provides the possibility of quantifying damage from cyclic tests with rest periods using the same specimen without the need of any additional tests. The results from both ARC16 and ARC22 thus reemphasize the findings obtained in Chapter 3 and demonstrate that the proposed method can be applied to understand and measure fatigue cracking due to shear as well as uniaxial load cycles.

4.5.3 Healing Characteristics

Figure 4.15 presents the healing potential of ARC16 and ARC22 materials as a function of stiffness levels at which 40-minute long rest periods were introduced. The healing potential values shown in this figure were calculated using the equivalent change in accumulated damage corresponding to the change in stiffness before and after a rest period. The 20, 10 and 5 minute rest periods introduced in the specimen did not yield in reasonable and repetitive results.

As can be seen in Figure 4.15, the healing potential of both materials calculated from fatigue tests with rest periods at different loading conditions demonstrate a decreasing trend with decrease in the stiffness value preceding the rest period. This behavior suggests that VECD-based healing properties are independent of applied strain amplitudes and frequencies similar to the VECD-based damage properties ($C\ vs\ S$). Having defined healing potential in terms of an internal state variable for damage that does not depend on loading condition, this behavior of healing was expected. In a cyclic test with rest period, healing is calculated by tracing the damage parameters corresponding to stiffness values before and after a rest period from the pseudo-stiffness vs. damage parameter curve that is constructed by filtering healing effect. Therefore, the

healing potential of a material due to a rest period introduced at a higher level of damage does not depend on the amount of healing the material experiences during a rest period introduced at lower level of damage.

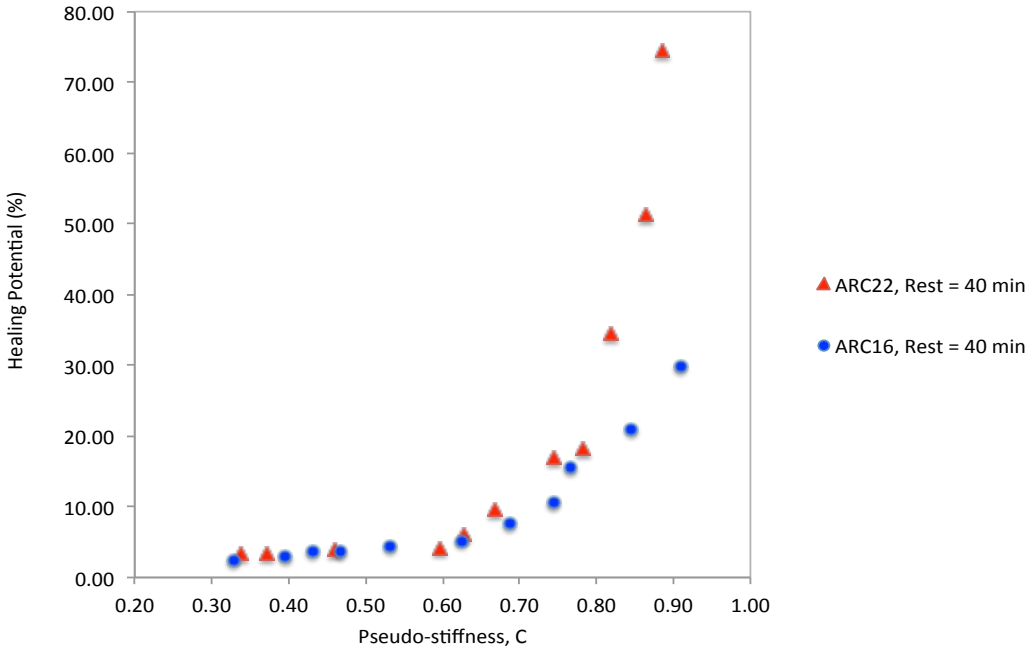

Figure 4.15: Healing potential results for ARC16 and ARC22 composites

Figure 4.15 also shows that the healing potential of the two composites was influenced by the stiffness at which the rest periods were introduced. When the rest periods were introduced at higher levels of stiffness (or before accumulating more damage), the materials regained a larger fraction of the stiffness lost during the preceding loading step. In contrast, when rest periods were introduced at lower levels of stiffness (or after accumulating more damage), the materials regained much smaller portion of the lost stiffness. The rest periods of 20, 10 and 5 minutes resulted in inconsistent results for a given stiffness level, indirectly implying that the rest periods do influence the amount

of healing. As such, unlike VECD-based damage model, the VECD-based healing model is independent of the loading conditions used to induce fatigue damage but dependent on the duration of rest periods and the extent of damage preceding the rest periods.

Also notable in Figure 4.15 is a higher healing potential of ARC22 specimens than that of the ARC16 specimens. This can be attributed to the fact that ARC22 materials were softer than the ARC16 materials, and therefore possessed characteristics that promoted faster damage recovery compared to the ARC16 materials. This behavior corresponds to the level of ease with which micro-cracks can be rejoined together in a given material. In summary, the duration of rest periods and the stiffness at which these rest periods are introduced influence the healing potential of a given material. Equally important is the demonstration that the same method used in cyclic shear tests could be used to extract healing potential with similar properties, that is independent of loading conditions and dependent on rest conditions.

4.5.4 Fatigue Life Prediction using the VECD Models

The most important feature of the VECD method is that the damage ($C\ vs\ S$) and healing characteristic curves of a given material are independent of loading conditions. As a corollary, these characteristic curves can be used to predict the fatigue cracking response of the material under any arbitrary combination of loading conditions and rest periods. This section describes the integrated use of damage and healing models to predict the fatigue life of a material with or without rest periods; the follow-up section will discuss the results obtained using this method in uniaxial damage mode:

Step 1. The proposed method with rest periods results in:

a. Linear viscoelastic dynamic modulus of the material: $|\mathrm{E}^*|_{\mathrm{LVE}}$
b. Material-specific damage parameter: α

c. Damage characteristics that are independent of test conditions:

$$C_u \cong C_u(S_u) \tag{4.16}$$

d. Healing characteristics that are independent of loading conditions but dependent on rest conditions:

$$HP \cong HP\ (RP, C_u(S_u)) \tag{4.17}$$

The damage and healing characteristics can be fitted with representative functions that best describe their shapes (Kutay et al. 2008; Palvadi et al. 2012).

Step 2. For a known stiffness (or pseudo-stiffness) level at which a rest period (RP) would be introduced ($C_{u,B}$ in Figure 4.16), the corresponding amount of damage (S_B in Figure 4.16) can be determined from the characteristic damage function, that is, $C_{u,B} \cong C_u\left(S_{u,B}\right)$. Similarly, based on the duration of rest period (RP) and the stiffness preceding the rest period ($C_{u,B}$), the healing potential (HP) can be determined form the characteristic healing function, that is, $HP_{u,B} \cong HP_u\left(RP, C_{u,B}\right)$.

Step 3. As shown in Figure 4.16, the asphalt material partially recovers its pseudo-stiffness by offsetting an equivalent amount of damage during the rest period, thereby resulting in a higher stiffness and a lower damage level after the rest period than before the rest period. The healing model (seen in Equation 3.21) in Chapter 3 can be furthermore simplified to predict the amount of damage remaining in the material after healing:

$$S'_{u,A} \cong (1 - HP).S_{u,B} \tag{4.18}$$

Step 4. Using the fitted $C\ vs\ S$ function, the pseudo-stiffness (or simply the stiffness) level reached after the rest period can be computed, i.e., $C_{u,A} \cong C_u\ (S'_{u,A})$. This pseudo-stiffness level refers to the stiffness value in the virgin (unhealed) specimen (see Figure 3.8).

Step 5. Also, the VECD damage model can be furthermore modified to estimate the number of cycles needed to degrade a given material to a certain level of pseudo-stiffness, $C_{u,x}$ (or to accumulate certain amount of damage, $S_{u,x}$) when subjected to an arbitrary frequency (f) and controlled strain amplitude (ε_0):

$$N_{C_{u,x}} \cong f. \sum_{k=1}^{Until\ C_{u,x}} \left[\left\{ -\frac{1}{2}.\left(\Delta C^R_{u,k}\right).\left(\varepsilon^R_{ot,k}\right)^2 \right\}^{-\alpha} .\left(\Delta S_{u,k}\right)^{(1+\alpha)} \right] \quad 4.19$$

This incremental relation can be also simplified using the selected $C\ vs\ S$ function.

$$N_{C_{u,x}} \cong f.\left[\frac{1}{2}.\left(\varepsilon^R_{ot,k}\right)^2\right]^{-\alpha} .\left[\int_0^{S_x} \left(-\frac{\partial C_u(S_u)}{\partial S_u}\right)^{-\alpha} dS_u\right] \quad 4.20$$

The use of step-wise or continuous function can be used to predict the number of cycles needed to degrade the initial stiffness (or the initial pseudo-stiffness) to the stiffness level preceding the rest period ($N_B$in Figure 4.16) as well as to the stiffness level reached after rest period due to healing (N_A in Figure 4.16). In this particular study, the step-wise formulation was used in the ensuing section for simplicity.

Step 6. The difference between the numbers of cycles needed to degrade the pseudo-stiffness from the recovered level to the pseudo-stiffness level preceding the rest period gives the number of load cycles gained due to a rest period (see Figure 4.16).

$$\Delta N_{BA} = N_B - N_A \quad (4.21)$$

Step 7. The increased fatigue life can be calculated by summing up the number of cycles gained due to healing with the number of cycles corresponding to the stiffness preceding the rest period and the rest period itself (see Figure 4.16).

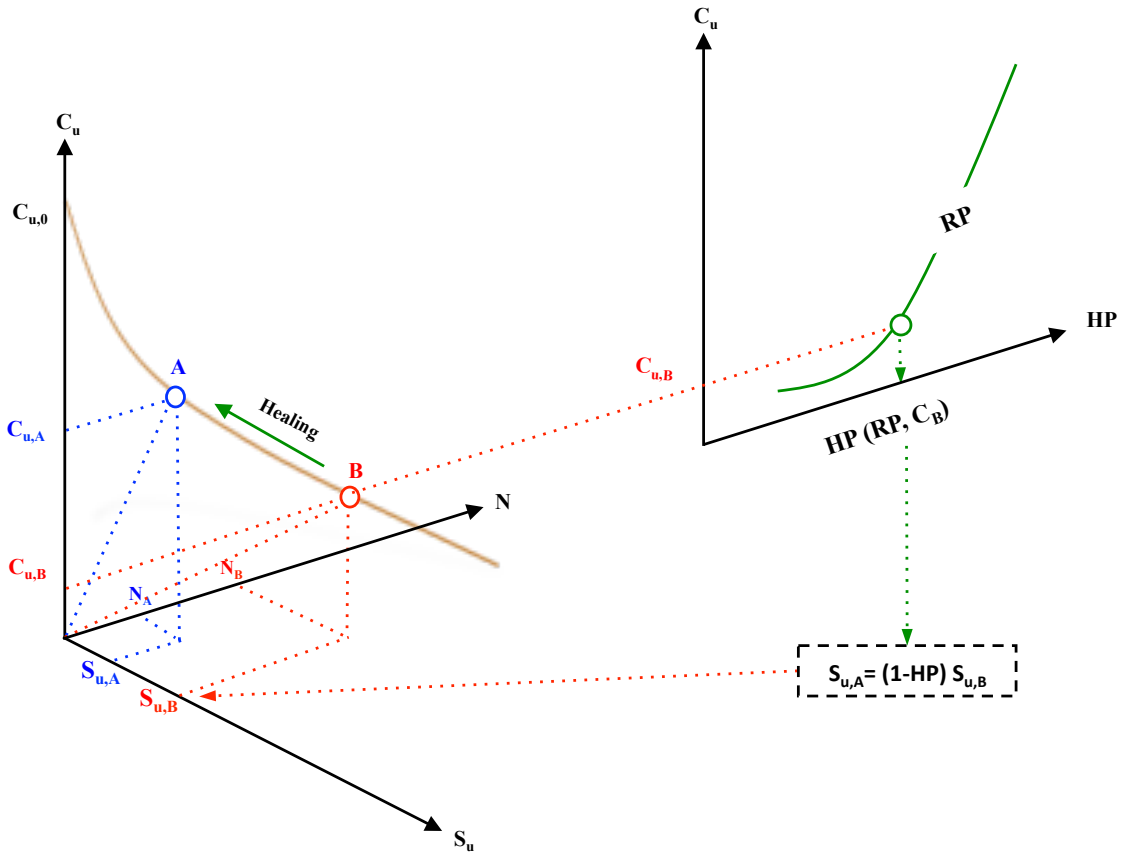

Figure 4.16: Schematic illustration of the integrated use of damage and healing models to predict the fatigue life with and without rest periods

4.5.4.1 Fatigue Life Prediction without Rest Periods

For this study, the measured properties (characteristic damage and healing curves) and the predictive steps described above were finally used to estimate the fatigue life with

and without rest periods. The predictions were performed for three different strain amplitudes (0.025%, 0.027% and 0.030%) at two different loading frequencies (5 and 10 Hz). The cases involving 0.027% strain amplitudes were selected for verification purposes.

Figure 4.17 presents the predicted number of cycles required to degrade the initial stiffness of ARC16 and ARC22 matrices by 25% when subjected to uniaxial cyclic tests at different loading conditions without any rest periods. The 25% stiffness reduction was chosen within the conventional fatigue failure criteria of 50% stiffness reduction (Tayebali et al. 1994). Figure 4.17 demonstrates that the ARC22 material subjected to strain amplitude of 0.025% and loading frequency of 5 Hz at 25ºC needs the maximum number of strain cycles to lose its initial stiffness by 25%. In contrast, the ARC16 material subjected to strain amplitude of 0.030% and loading frequency of 10 Hz resulted in the minimum number of strain cycles to reduce its initial stiffness by the same amount. Similarly, Figure 4.17 also shows that the stiffer ARC16 material needs fewer load cycles than the softer ARC22 material to degrade its stiffness by a certain amount at a given frequency, temperature and strain condition. However, the difference between the number of cycles to reduce the initial stiffness of ARC16 and ARC22 by 25% at loading frequencies of 5 Hz was comparatively larger than the corresponding difference at 10 Hz at a given controlled-strain condition. These observations were successfully verified with the measured number of cycles and their trends at 0.027% controlled strain conditions. As such, it can be concluded that the VECD model is capable of capturing the material-specific damage evolution and predicting accurate number of cycles for selected level of stiffness degradations.

Similarly, Figure 4.17 demonstrates that, at a given frequency, the number of cycles required to degrade a material by a certain amount increases with a decrease in

applied strain amplitude and vice versa. Furthermore, the same figure also illustrates that, at a given strain control condition, the number of cycles required to degrade a material by a certain amount increases with a decrease in applied frequency and vice versa. These observations are consistent with several other earlier research studies (Adhikari and You 2010; Fakhri et al. 2013; Mollenhaue et al. 2009), thereby verifying the possibility of predicting fatigue life at arbitrary loading conditions using the VECD method.

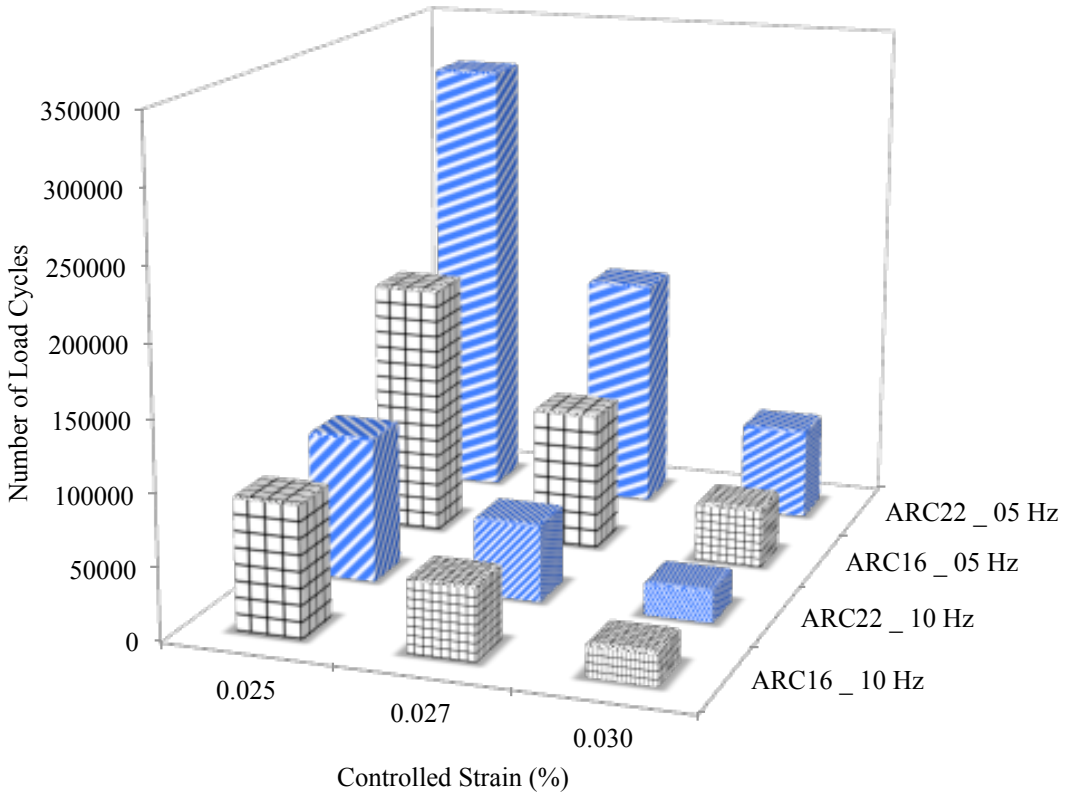

Figure 4.17**:** Predicted number of load cycles to reduce initial stiffness by 25% at 25ºC

4.5.4.2 Fatigue Life Prediction with Rest Periods

Figure 4.18 presents the gain in fatigue life due to a 40-minute rest period introduced at 75% of the initial pseudo-stiffness. As shown in this figure, the ARC22 specimen subjected to loading frequency of 5 Hz and strain amplitude of 0.025% would gain the highest number of load cycles during the given duration of rets period in compliance with its better healing capacity. In contrast, the ARC16 material subjected to loading frequency of 10 Hz and strain amplitude of 0.030% would gain the least number of load cycles in compliance with its lower healing potential.

Additionally, Figure 4.18 illustrates that, for a given frequency and strain-amplitude, the ARC22 material would gain a higher number of load cycles than the ARC16 material. This observation is consistent with the longer fatigue life and higher healing potential of the ARC22 material than the ARC16 material subjected to the same loading conditions as verified in the case of 0.027% strain amplitude conditions. Similarly, the same figure shows that, for a given material, the number of cycles gained due to a 40-minute rest period decreases with an increase in applied strain amplitude but increases with a decrease in applied strain amplitude. Furthermore, for a given strain amplitude, the predicted gain in fatigue life was higher at lower frequencies than at higher frequencies. The process was also applied to predict the total gain in load cycles due to multiple rest periods by summing up the increase in load cycles due to each individual rest periods. Figure 4.19 presents the total number of cycles due to five consecutive 40-minute long rest periods introduced at the pseudo-stiffness corresponding to 75% of the initial stiffness.

The above observations strongly verify that (a) the same experimental and analytical procedure method used for shear loading in Chapter 3 can yield the damage and healing properties related to uniaxial loading, (b) the same specimen can yield both

damage and healing properties of an asphalt material due to a given mode of loading, (c) the VECD-based damage models and metrics are independent of applied test conditions, (d) the VECD-based healing models and metrics are also independent of applied test conditions but dependent of applied rest durations and the stiffness preceding the rest periods, (e) damage and healing models together can yield fatigue life at any other arbitrary loading and rest conditions.

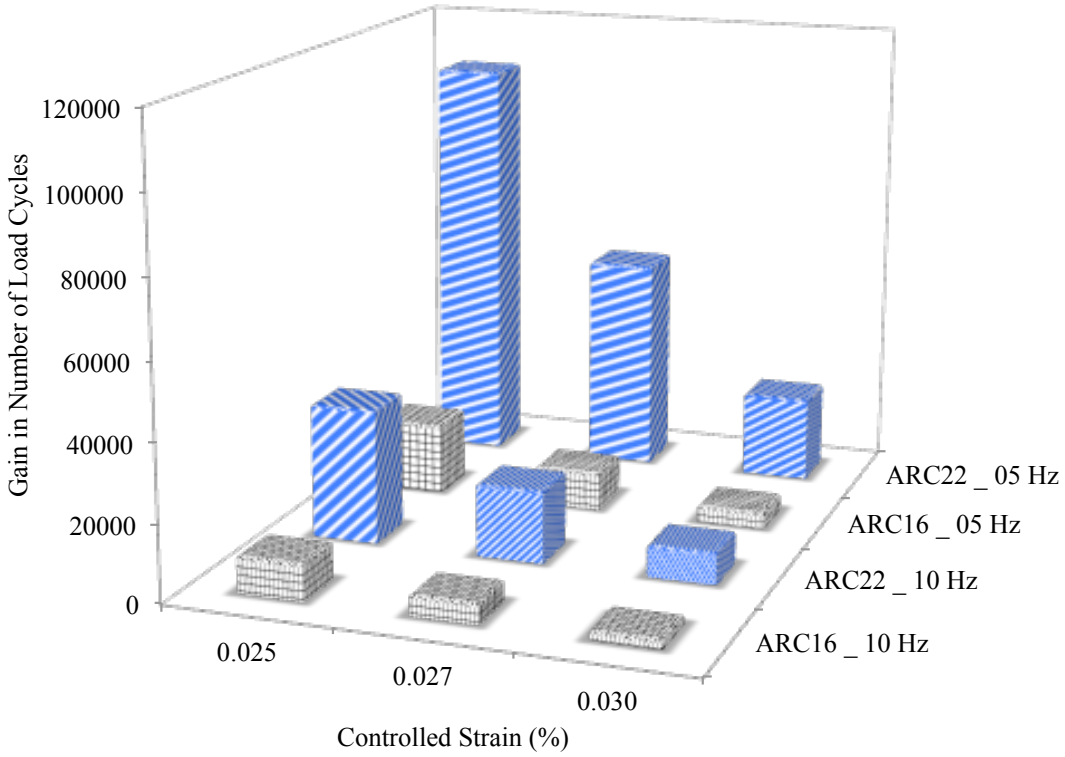

Figure 4.18: Predicted gain in the number of load cycles to reach 75% of initial stiffness at 25ºC after a 40-min long rest period at 0.75C

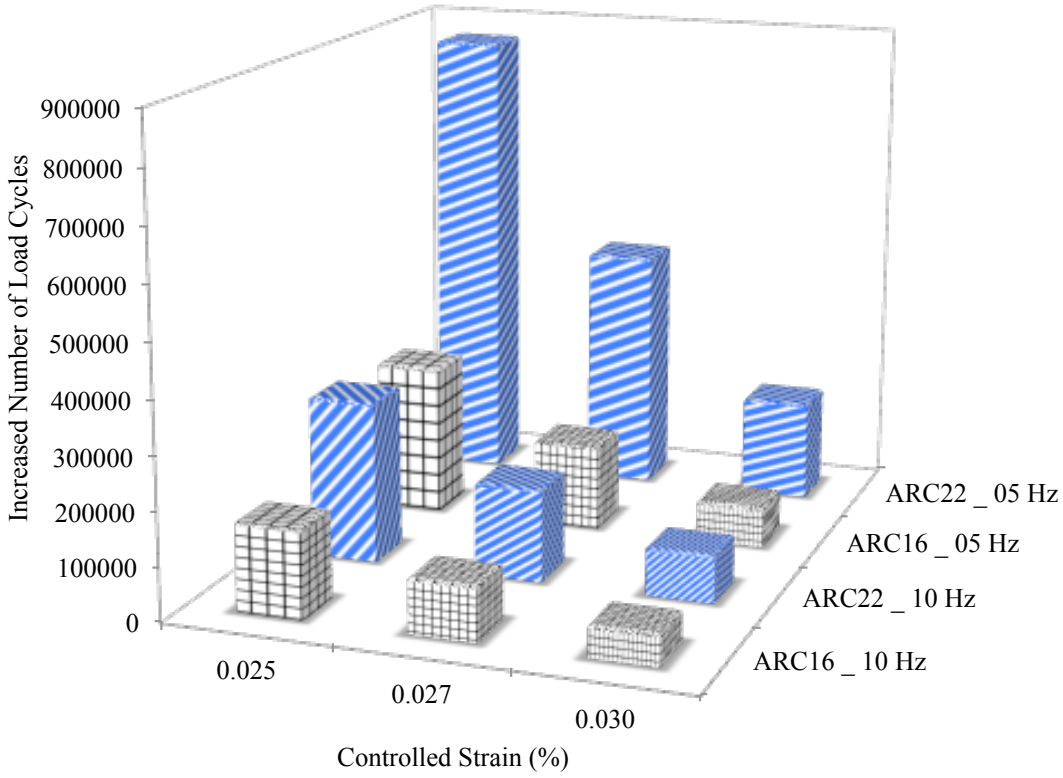

Figure 4.19: Predicted number of load cycles to reach 75% of initial stiffness at 25ºC after five 40-min long rest periods at 0.75C

Chapter 5: Summary and Conclusions

The primary goal of this research was to devise an integrated method to measure and model both fatigue damage and healing in asphalt composites using the same specimen. The preceding chapters presented the synopses of conventional methods, the associated limitations and proposed a methodology that addresses these limitations. As shown in the foregoing chapters, the experimental part of the proposed method involved cyclic tests of asphalt materials with a number of rest periods introduced during the same test run. Similarly, the analytical part of the proposed method involved extraction of material-specific fatigue damage and healing characteristics using the test results.

The following are the conclusions drawn from the implementation of the integrated method in cyclic shear tests and cyclic uniaxial (tension-compression) tests.

5.1 Damage Characteristics

1. *Pseudo-stiffness vs. damage parameter characteristic curve is independent of the loading conditions.*

For a given material, the pseudo-stiffness versus damage parameter curves obtained from the cyclic shear tests conducted at different stress amplitudes and without rest periods agreed with each other. Similarly, the pseudo-stiffness versus damage parameter curves obtained from the cyclic uniaxial tests at different strain amplitudes, loading frequencies and without rest periods agreed also with each other.

In this study, since the mechanisms of crack growth in shear tests and uniaxial tests are different, this dissertation did not compare the pseudo-stiffness vs. damage parameter curves constructed from the two types of tests. Nonetheless, the consistently similar $C\ vs\ S$ curves for any given mode of loading (shear or tension-compression) suggest that the $C\ vs\ S$ curve is independent of loading amplitudes and loading

frequencies. This conclusion reinforces the earlier assertions (Kim et al. 1997; Lee and Kim 1998b; Underwood et al. 2010).

2. *Pseudo-stiffness vs. damage parameter* ($C\ vs\ S$) *characteristic curve is independent of the history of healing*.

The pseudo-stiffness versus time curves constructed by horizontally shifting the data segments from cyclic shear tests involving rest periods introduced at different levels of damage or stiffness produced smooth pseudo-stiffness vs. damage parameter curves. Furthermore, these curves agreed with each other as well as with the $C\ vs\ S$ curves constructed from the cyclic tests without any rest period. Also, this resemblance was true irrespective of loading conditions - stress amplitudes and frequencies.

Similarly, the $C\ vs\ S$ curves constructed from the cyclic uniaxial tests involving a number of rest periods introduced at random stiffness levels (until 20% of initial stiffness in some cases) also agreed with each other as well as with the $C\ vs\ S$ curves obtained from the similar tests without rest period. As in the case of shear tests, uniaxial tests also demonstrated this coherence irrespective of applied loading conditions - frequencies and strain amplitudes.

This similarity strongly supports the hypothesis that the damage evolution ($C\ vs\ S$) is a unique material characteristic that resumes its rate some time after recommencing the load cycles following a rest period. As such, it can be concluded that damage growth does not depend on the total number of rest periods as well as the duration and condition of each rest period. In other words, $C\ vs\ S$ characteristic is independent of the history of rest periods in addition to loading conditions.

3. *Pseudo-stiffness vs. damage parameter* ($C\ vs\ S$) *characteristic is a material-specific property.*

As mentioned above, the pseudo-stiffness vs. damage parameter curve for a given material was independent of the applied loading conditions as well as the history of healing. But, the $C\ vs\ S$ curves of a given material were quite different from the $C\ vs\ S$ curves of any other material. This dependence of $C\ vs\ S$ curve on material type was evident in both shear and uniaxial cyclic tests. Therefore, it can be concluded that VECD-based pseudo-stiffness versus damage parameter characteristic is an exclusive material property.

5.2 HEALING CHARACTERISTICS

1. *Healing potential depends on the stiffness (or damage) level preceding the rest period.*

For a given duration of a rest period introduced during the cyclic shear test, the ARC22 matrix specimens healed more when the rest period was introduced at a higher stiffness (or lower damage) than when the rest period was introduced at a lower stiffness (or higher damage). In the uniaxial cyclic tests, both ARC16 and ARC22 matrices showed noticeable healing only after applying a 40-minute long rest period. Nonetheless, the dependence of healing percentage on the stiffness level preceding a rest period was clearly evident. Similar to the results from the cyclic shear tests, the rest periods introduced at a higher stiffness resulted in more healing than the rest period of a similar duration introduced at a lower stiffness in a cyclic uniaxial test.

These results strongly illustrates that healing potential depends on the stiffness preceding the rest period. To be specific, as more damage accumulates (or stiffness drops), the less is the healing capacity of the material to heal. As such, in order to

maximize the benefits in fatigue life due to healing, it is imperative to introduce a rest period before a material reaches a state of significant damage.

2. *Healing potential depends on the duration of the rest period.*

For the same level of stiffness preceding a rest period, a material heals more during a longer duration of rest period than during a shorter duration of rest period. This was evident in the shear tests at all three levels of stiffness (60%, 70% and 80% of initial stiffness).

In uniaxial tests, healing was insignificant and inconsistent during the shorter durations of rest periods (5, 10 and 20 minutes) while consistent and significant together in longer duration of rest periods (40 minutes). This exhibition of noticeable healing in uniaxial tests only after slightly longer duration of rest periods implicitly demonstrated that microcracks healed at different rates in the two tests. This distinction can be attributed to the different modes of crack growth in the shear versus uniaxial tests.

Nonetheless, both shear tests and uniaxial tests signify the dependence of healing potential on the duration of rest period. This dependence of shear healing is consistent with earlier observations (Lytton et al. 1993; Palvadi et al. 2012).

3. *Healing potential does not depend on the history of healing.*

For a given material, the healing percentages obtained from the single-specimen cyclic shear tests were in good agreement with the healing percentages obtained from the multiple-specimen protocol, wherein a separate specimen was used to obtain the healing behaviour at different levels of damage preceding the rest period. Similarly, for a given material, the healing percentages obtained from the cyclic uniaxial test procedures with different rest periods at variable stiffness levels converged into the same curve

This observation demonstrates that the history of healing at lower levels of damage did not affect the healing behaviour at subsequent higher levels of damage. In other words, VECD-based healing characteristic model is independent of the history of healing.

4. Healing potential is independent of the loading conditions.

For a given material, a given rest period introduced at the same stiffness preceding the rest period, the percentage of healing remained similar irrespective of different values of loading frequencies and amplitudes applied during the time sweep test preceding the rest periods. This observation was evident in both shear and uniaxial tests.

The independence from loading conditions can be explained by the VECD-based definition of healing in terms of change in internal state variable. In other words, healing potential inherits the independence of $C\ vs\ S$ curve from the loading conditions.

5. Healing potential is a material property.

For the same duration of rest period introduced at the same stiffness during a uniaxial test, the matrix with higher damage evolution rate (ARC16) exhibited a lower potential to heal than a matrix with lower damage evolution rate (ARC22). Since binder grade was the only difference between the two matrixes used in the uniaxial tests, this difference in healing potential implicitly reflects the corresponding effect of binder grades in the composites.

5.3 Expected Benefits

1. The integrated method can eliminate the redundancy related to damage-only tests.

The prospect of constructing a single pseudo-stiffness versus time as well as a single pseudo-stiffness versus damage parameter ($C\ v\ s\ S$) by selectively shifting and

stitching the individual time sweep test data based on continuum damage mechanics is the most notable of the integrated method. The close agreement between the $C\ v\ s\ S$ curves constructed from this method with multiple rest periods and the ones constructed from the conventional tests without a rest period suggest that damage-only tests are redundant.

2. *The integrated method can eliminate the redundancy related to separate rest periods*.

This research verified that damage evolution rate resumes some time after recommencing the load cycles following a rest period. Additionally, the research also verified that the percentage of healing during a given duration of rest period at a given stiffness level does not depend on the history of previous periods. As such, one can introduce a new rest period at the stiffness lower than or equal to the stiffness preceding the preceding rest period as long as the material regains its inherent damage rate. The integrated method does not need specimens and test runs for each rest condition unlike the conventional methods.

3. *The integrated method can eliminate the redundancy related to the loading conditions*.

The dissertation showed that VECD-based damage and healing models are independent of applied loading conditions and healing histories. This independence suggests that the results obtained for a given loading and healing conditions using the integrated method can be used to predict the fatigue life with and without healing at any arbitrary loading and healing conditions. This predictive capacity of the integrated method eliminates the need for conducting tests under different loading conditions.

4. *The integrated method can be used in both cyclic tests in shear and tension-compression.*

This research successfully implemented the integrated method to determine overall fatigue damage and effective healing in asphalt materials in cyclic shear tests (under controlled torsional stresses) as well as in the cyclic uniaxial tests (under controlled tension-compression strains). This fact strongly suggests that the integrated experimental and analytical method can be extended to study fatigue damage and healing under different modes of loading.

5. *The integrated method can be extended to analyze or compare full mixtures.*

This research analyzed the damage and healing properties of different fine aggregate matrices that differed in constituent proportions, but followed the same material constitutive models. Since fine aggregate matrices used in this study and asphalt concrete mixtures used in conventional tests differ in constituent proportion but follow the same material constitutive models, it is expected that the integrated method can be used to analyze and compare the cracking and healing characteristics of full mixtures. The possibility of reducing the number of test runs and specimens of full mixtures is an attractive feature of the proposed method.

5.4 FUTURE WORKS

1. *Temperature effects*

This dissertation did not include the effect of temperature on damage and healing properties of selected materials. As one of the major impetus for damage and healing in actual pavements, the effects of environmental loads or simply temperature on these properties are forwarded to future works.

2. Transient effects

This study assumed a steady state condition in both torsional shear and uniaxial tension-compression tests and used the secant slope of hysteresis curve for pseudo-stiffness analysis. Rigorous models proposed by other researchers (Underwood and Kim 2013b; Underwood et al. 2010) can be used to study the transient effects that might last until a number of load cycles following the initiation of each time sweep steps.

3. Other effects

This study implemented the integrated method to analyze damage and healing in fine aggregate matrices that were separately subjected to torsional shear cycles and tension-compression cycles. Also, this study included only one control mode (strain or stress) in the two tests. Furthermore, this dissertation studied only the effects of rest period of zero loads and four durations. The issues of representative rest periods and load conditions are forwarded for future works.

Bibliography

Abbas, A., Jones, R. H., and Boyd, J. G. (2005). "Modeling of asphalt mastic stiffness using discrete elements and micromechanics analysis." *International Journal of Pavement Engineering*, 6(2), 137–146.

Adhikari, S., and You, Z. (2010). "Fatigue evaluation of asphalt pavement using beam fatigue apparatus." *Technology Interface Journal*, 10(3).

Aragao, F. T. S. (2011). "Micromechanical model for heterogeneous asphalt concrete mixtures subjected to fracture failure." PhD Dissertation, University of Nebraska-Lincoln.

Aragao, F. T. S., Kim, Y., Karki, P., and Little, D. N. (2010). "Semi-empirical, analytical, and computational predictions of dynamic modulus of asphalt concrete mixtures." *Transportation Research Record: Journal of Transportation Research Board*, 2181, 19–27.

Aragao, F. T. S., Lee, J., Kim, Y., and Karki, P. (2010). "Material-specific effects of hydrated lime on the properties and performance behavior of asphalt mixtures and asphaltic pavements." *Construction and Building Materials*, 24, 538–544.

Barenblatt, G. I. (1962). "Mathematical theory of equilibrium cracks in brittle fracture." *Advances in Applied Mechanics*, 7, 55–129.

Bazin, P., and Saunier, J. (1967). "Deformability, fatigue and healing properties of asphalt mixes." *International Conference on the Structural Design of Asphalt Pavements*.

Bhasin, A., and Little, D. N. (2007). "Exploring mechanisms of healing in asphalt mixtures and quantifying its impact." *Self-healing materials: An Alternative Approach to 20 Centuries of Materials Science*, Springer Series in Materials science, S. van der Zwaag, ed., Springer Netherlands, 205–218.

Bhasin, A., Little, D. N., Bommavaram, R., and Vasconcelos, K. L. (2008). "A framework to quantify the effect of healing in bituminous materials using material

properties." *Road Materials and Pavement Design*, Special issue on asphalt technology, 9(1), 219–242.

Bhasin, A., Palvadi, S., and Little, D. N. (2011). "Influence of aging and temperature on intrinsic healing of asphalt binders." *Transportation Research Record: Journal of the Transportation Research Board*, 2207(-1), 70–78.

Bhasin, A., Parthasarthy, A. S., and Little, D. N. (2009). *Laboratory investigation of a novel method to accelerate healing in asphalt mixtures using thermal treatment*. Center for Transportation Research, Austin, TX.

Bommavaram, R., Bhasin, A., and Little, D. N. (2009). "Determining intrinsic healing properties of asphalt binders." *Transportation Research Record: Journal of Transportation Research Board*, 2126, 47–54.

Bonnaure, F. P., Huibers, A. H. J. J., and Boonders, A. (1982). "A laboratory investigation of the influence of rest periods on the fatigue characteristics of bituminous mixes." *Journal of the Association of Asphalt Paving Technologists*, 51, 104–128.

Buttlar, W., and You, Z. (2001). "Discrete element method modeling of asphalt concrete: microfabric approach." *Transportation Research Record: Journal of the Transportation Research Board*, 1757, 111–118.

Carpenter, S. H., and Shen, S. (2006). "Dissipated energy approach to study hot-mix asphalt healing in fatigue." *Transportation Research Record: Journal of the Transportation Research Board*, 1970, 178–185.

Chehab, G. R. (2002). "Characterization of asphalt concrete in tension using a viscoelastoplastic model." PhD Dissertation, North Carolina State University, Raleigh.

Dai, Q., Sadd, M. H., and You, Z. (2006). "A micromechanical finite element model for linear and damage coupled viscoelastic behavior of asphalt mixture." *International Journal for Numerical and Analytical Methods in Geomechanics*, 30(11), 1135–1158.

Dai, Q., and You, Z. (2007). "Prediction of creep stiffness of asphalt mixture and micromechanics finite-element and discrete models." *Journal of Engineering Mechanics*, 133(2), 163–173.

Daniel, J. S. (2001). "Development of a simplified fatigue test and analysis procedure using a viscoelastic, continuum damage model, and its implementation to WesTrack mixtures." North Carolina State University.

Daniel, J. S., and Kim, Y. R. (2002). "Development of a simplified fatigue test and analysis procedure using a viscoelastic, continuum damage model." *Journal of the Association of Asphalt Paving Technologists*, 71, 619–650.

Edwards, M. A., and Hesp, S. A. . (2006). "Compact tension testing of asphalt binders at low temperatures." *Transportation Research Record: Journal of the Transportation Research Board*, 1962, 36–43.

Fakhri, M., Hassani, K., and Ghanizadeh, A. R. (2013). "Impact of loading frequency on the fatigue behavior of SBS modified asphalt mixtures." Procedia - Social and Behavioral Sciences, 69–78.

Ferry, J. D. (1980). *Viscoelastic properties of polymers*. Wiley, New York, NY.

Ghuzlan, K. A., and Carpenter, S. H. (2000). "Energy-derived damage-based failure criterion for fatigue testing." *Transportation Research Record: Journal of the Transportation Research Board*, 1723, 141–149.

Graham, G. A. C. (1968). "The correspondence principle of linear viscoelasticity theory for mixed boundary value problems involving time-dependent boundary regions." *Quarterly of Applied Mathematics*, 26(167-174).

Gross, B. (1953). *Mathematical structure of the theories of viscoelasticity*. Hermann et Cie, Paris.

Guddati, M. N., Feng, Z., and Kim, Y. R. (2002). "Toward a micromechanical-based procedure to characterize fatigue performance of asphalt concrete." *Transportation Research Record: Journal of the Transportation Research Board*, 1789, 121–128.

Haft-Javaherian, M. (2011). "Virtual microstructure generation of asphaltic mixtures." University of Nebraska-Lincoln, Lincoln, NE.

Jacobs, M. M., Hopman, P. C., and Molenaar, A. A. (1996). "Application of fracture mechanics principles to analyze cracking in asphalt concrete." *Journal of the Association of Asphalt Paving Technologist*, 65, 1–39.

Kachanov, L. M. (1958). "Rupture time under creep conditions." *Proceedings of the USSR Academy of Sciences, Department of Technical Sciences (Izvestiya Akademii Nauk SSSR. Otdelenie Tekhnicheskich Nauk)*, 8, 26–31.

Karki, P. (2010). "Computational and experimental characterization of bituminous composites based on experimentally determined properties of constituents." MS Thesis, University of Nebraska-Lincoln, Lincoln, Nebraska.

Karki, P., Kim, Y., and Little, D. N. (2014). "Dynamic modulus prediction of asphalt concrete mixtures through computational micromechanics." *In Review*.

Karki, P., Li, R., and Bhasin, A. (2014). "Quantifying overall damage and healing behavior of asphalt materials using continuum damage approach." *International Journal of Pavement Engineering*.

Kim, B., and Roque, R. (2006). "Evaluation of healing property of asphalt mixture." *Transportation Research Record: Journal of the Transportation Research Board*, 1970, 84–91.

Kim, H., and Buttlar, W. G. (2009). "Finite element cohesive fracture modeling of airport pavements at low temperatures." *Cold Regions Science and Technology*, 57(2-3), 123–130.

Kim, Y., Little, D. N., and Lytton, R. L. (2003). "Fatigue and healing characterization of asphalt mixtures." *Journal of Materials in Civil Engineering*, 15(1), 75–83.

Kim, Y. R. (1988). "Evaluation of healing and constitutive modeling of asphalt concrete by means of the theory of nonlinear viscoelasticity an damage mechanics." Texas A&M University.

Kim, Y. R., Lee, H. J., and Little, D. N. (1997). "Fatigue characterization of asphalt concrete using viscoelasticity and continuum damage theory." *Journal of the Association of Asphalt Paving Technologists*, 66, 520–569.

Kim, Y. R., Lee, Y. C., and Lee, H. J. (1995). "Correspondence principle for characterization of asphalt concrete." *Journal of Materials in Civil Engineering*, 7(1), 59–68.

Kim, Y. R., and Little, D. N. (1990). "One-dimensional constitutive modeling of asphalt concrete." *Journal of Engineering Mechanics*, 116(4), 751–772.

Kim, Y. R., Little, D. N., and Benson, F. C. (1990). "Chemical and mechanical evaluation on healing mechanism of asphalt concrete." *Proceedings of the Association of Asphalt Paving Technologists*, 59, 240275.

Kim, Y., and Wool, R. P. (1983). "A theory of healing at a polymer-polymer interface." *Macro-molecules*, 16, 1115–1120.

Kutay, M. E., Gibson, N. H., and Youtcheff, J. S. (2008). "Conventional and viscoelastic continuum damage (VECD)-based fatigue analysis of polymer modified asphalt pavements." *Journal of the Association of Asphalt Paving Technologists*, 77, 395–434.

Kutay, M. E., Gibson, N. H., Youtcheff, J. S., and Dongre, R. N. (2009). "Utilizing small samples to predict fatigue lives of field cores using a newly developed formulation based on viscoelastic continuum damage theory." *Transportation Research Record: Journal of Transportation Research Board*, 2127, 90–97.

Lee, H. J., Daniel, J. S., and Kim, Y. R. (2000). "Continuum damage mechanics-based fatigue model of asphalt concrete." *Journal of Materials in Civil Engineering*, 12, 105–112.

Lee, H., and Kim, Y. R. (1998a). "Viscoelastic continuum damage model of asphalt concrete with healing." *Journal of Engineering Mechanics*, 124(11), 1224–1232.

Lee, H., and Kim, Y. R. (1998b). "Viscoelastic constitutive model for asphalt concrete under cyclic loading." *Journal of Engineering Mechanics*, 124(1), 32–40.

Li, R., Karki, P., Hao, P., and Bhasin, A. (2014). "Rheological and low temperature properties of asphalt composites containing rock asphalts." *In Review*.

Little, D. N., Lytton, R. L., and Chen, C. W. (2001). *Microdamage healing in asphalt and asphalt concrete, Volume I: Microdamage and microdamage healing, Project summary report*. Texas Transportation Institution, College Station, TX.

Lundström, R., and Isacsson, U. (2003). "Characterization of asphalt concrete deterioration using monotonic and cyclic tests." *International Journal of Pavement Engineering*, 4(3), 143–153.

Lytton, R. (2000). "Characterizing asphalt pavements for performance." *Transportation Research Record*, 1723, 5–16.

Lytton, R. L., Chen, C. W., and Little, D. N. (1998). *A micromechanics fracture and healing model for asphalt concrete*. Task K - Microdamage Healing in Asphalt And Asphalt Concrete, Texas A&M University, College Station, TX.

Lytton, R. L., Chen, C. W., and Little, D. N. (2001a). *Microdamage healing in asphalt and asphalt concrete, Volume III: A micromechanics fracture and healing model for asphalt concrete*. Texas Transportation Institution, College Station, TX.

Lytton, R. L., Chen, C. W., and Little, D. N. (2001b). *Microdamage healing in asphalt and asphalt concrete, Volume IV: A viscoelastic continuum damage fatigue model of asphalt concrete with microdamage healing*. Texas Transportation Institution, College Station, TX.

Lytton, R. L., Uzan, J., Fernando, E. G., Roque, R., Hiltunen, D. R., and Stoffels, S. M. (1993). *Development and validation of performance prediction models and specifications for asphalt binders and paving mixes*. National Research Council, Washington, D.C.

Masad, E., Muhunthan, B., Shashidhar, N., and Harman, T. (1999). "Internal structure characterization of asphalt concrete using image analysis." *Journal of Computing in Civil Engineering*, 13(2), 88–95.

Masad, E., Somadevan, N., Bahia, H. U., and Kose, S. (2001). "Modeling and experimental measurements of strain distribution in asphalt mixes." *Journal of Transportation Engineering*, 127(6), 477–485.

McElvaney, J., and Pell, P. S. (1973). "Fatigue damage of asphalt - Effect of rest period." *Highways and Road Construction*, 41(1766), 16–20.

Mollenhaue, K., Wistuba, M., and Rabe, R. (2009). "Loading frequency and fatigue: In situ conditions & impact on test results," University of Minho, Portugal.

Nishizawa, T., Shimeno, S., and Sekiguchi, M. (1997). "Fatigue analysis of asphalt pavements with thick asphalt mixture layer." *8th International Conference on Asphalt Pavements*, Seattle, Washington, 969–976.

Palvadi, S., Bhasin, A., and Little, D. N. (2012). "Method to quantify healing in asphalt composites using continuum damage approach." *Transportation Research Record: Journal of Transportation Research Board*, 2296(4), 86–96.

Paris, P. C., and Erdogan, F. (1963). "A critical analysis of crack propagation laws." Journal of Fluids Engineering, 85(4), 528–533.

Paris, P. C., Gomez, M. P., and Anderson, W. E. (1961). "A rational analytic theory of fatigue." *The Trend in Engineering*, 13, 9–14.

Park, S. W. (1994). "Development of a nonlinear thermo-viscoelastic constitutive equation for particulate composites with growing damage." The University of Texas at Austin.

Park, S. W., Kim, Y. R., and Schapery, R. A. (1996). "A viscoelastic continuum damage model and its application to uniaxial behavior of asphalt concrete." *Mechanics of Materials*, 24(4), 241–255.

Park, S. W., and Schapery, R. A. (1997). "A viscoelastic constitutive model for particulate composites with growing damage." *International Journal of Solids and Structures*, 34(8), 931–947.

Pineda, E. J., and Waas, A. M. (2013). "Numerical implementation of a multiple-ISV thermodynamically-based work potential theory for modeling progressive damage

and failure in fiber-reinforced laminates." *International Journal of Fracture*, 182(1), 93–122.

Raithby, K. D., and Sterling, A. B. (1970). "The effect of rest periods on fatigue performance of hot-rolled asphalt under reversed axial loading and discussion." *Journal of the Association of Asphalt Paving Technologists*, 39, 134–152.

Reese, R. (1997). "Properties of aged asphalt binder related to asphalt concrete fatigue life." *Journal of the Association of Asphalt Paving Technologists*, 66, 604–632.

Rice, J. R. (1968). "A path independent integral and the approximate analysis of strain concentration by notches and cracks." *Journal of Applied Mechanics*, 35, 379–386.

Sadd, M. H., Dai, Q., Parameswaram, V., and Shukla, A. (2003). "Simulation of asphalt materials using a finite element micromechanical model with damage mechanics." *Transportation Research Record: Journal of the Transportation Research Board*, 1832, 86–95.

Schapery, R. A. (1973). *A theory of crack growth in viscoelastic media*. Mechanics and Materials Research Center, Texas A&M University.

Schapery, R. A. (1975a). "A theory of crack initiation and growth in viscoelastic media, I. Theoretical development." *International Journal of Fracture*, 11(1), 141–159.

Schapery, R. A. (1975b). "A theory of crack initiation and growth in viscoelastic media, II. Approximate methods of analysis." *International Journal of Fracture*, 11(3), 369–388.

Schapery, R. A. (1975c). "A theory of crack initiation and growth in viscoelastic media, III. Analysis of continuous growth." *International Journal of Fracture*, 11(4), 549–562.

Schapery, R. A. (1984). "Correspondence principles and a generalized J integral for large deformation and fracture analysis of viscoelastic media." *International Journal of Fracture*, 25(3), 195–223.

Schapery, R. A. (1986). "Time-dependent fracture: Continuum aspects of crack growth." *Encyclopedia of materials science and engineering*, Pergamon Press Inc., Elmsford, N.Y., 5043–5053.

Schapery, R. A. (1987). "Deformation and fracture characterization of inelastic composite materials using potentials." *Polymer Engineering and Science*, 27(1), 63–76.

Schapery, R. A. (1989). "On the mechanics of crack closing and bonding in linear viscoelastic Media." *International Journal of Fracture*, 39, 163–189.

Schapery, R. A. (1990). "A theory of mechanical behavior of elastic media with growing damage and other changes in structure." *Journal of Mechanics and Physics of Solids*, 38(2), 215–253.

Song, I., Little, D. N., Masad, E., and Lytton, R. (2005). "Comprehensive evaluation of damage in asphalt mastics using X-Ray CT, continuum mechanics, and micromechanics." *Journal of the Association of Asphalt Paving Technologists*.

Tarefder, R. A., Bateman, D., and Swamy, A. K. (2013). "Comparison of fatigue failure criterion in flexural fatigue test." *International Journal of Fatigue*, 55, 213–219.

Tayebali, A. A., Deacon, J. A., Coplantz, J. S., Harvey, J. T., and Monismith, C. L. (1994). "Mix and mode-of-loading effects on fatigue response of asphalt-aggregate mixes." *Journal of the Association of Asphalt Paving Technologists*, 63, 118–151.

Tschoegl, N. W. (1989). *The phenomenological theory of linear viscoelastic behavior: An introduction*. Springer-Verlag, Berlin.

Tvergaard, V., and Hutchinson, J. W. (1992). "The relation between crack growth resistance and fracture process parameters in elastic-plastic solids." *Journal of the Mechanics and Physics of Solids*, 40(6), 1377–1397.

Underwood, B. S., and Kim, Y. R. (2012). "Simplified viscoelastic continuum damage model as an asphalt concrete fatigue analysis platform." *Transportation Research Record: Journal of the Transportation Research Board*, 2296, 36–45.

Underwood, B. S., and Kim, Y. R. (2013a). "Effect of volumetric factors on the mechanical behavior of asphalt fine aggregate matrix and the relationship to asphalt mixture properties." *Construction and Building Materials*, 49, 672–681.

Underwood, B. S., and Kim, Y. R. (2013b). "Nonlinear viscoelastic behavior of asphalt concrete and its implication on fatigue modeling." *Transportation Research Record: Journal of the Transportation Research Board*, 2373, 100–108.

Underwood, B. S., Kim, Y. R., and Guddati, M. N. (2010). "Improved calculation method of damage parameter in viscoelastic continuum damage model." *International Journal of Pavement Engineering*, 11(6), 459–476.

Underwood, B. S., Kim, Y. R., and Guddati, M. N. (2006). "Characterization and performance prediction of ALF mixtures using viscoelastic continuum damage model." *Journal of the Association of Asphalt Paving Technologists*, 75, 577–636.

Wagoner, M. P., Buttlar, W. G., and Paulino, G. H. (2005a). "Disk-shaped compact tension test for asphalt concrete fracture." *Experimental Mechanics*, 45(3), 270–277.

Wagoner, M. P., Buttlar, W. G., and Paulino, G. H. (2005b). "Development of a single-edge notched beam test for asphalt concrete mixtures." *Journal of Testing and Evaluation, American Society of Testing and Materials*, 33(6), 1–9.

Wang, L., Frost, J., and Shashidhar, N. (2001). "Microstructure study of WesTrack mixes from X-Ray tomography images." *Transportation Research Record: Journal of the Transportation Research Board*, 1767(-1), 85–94.

Williams, D., Little, D. N., Lytton, R. L., Kim, Y. R., and Kim, Y. (2001). *Microdamage healing in asphalt and asphalt concrete, Volume II: Laboratory and field testing to assess and evaluate microdamage and microdamage healing*. Texas Transportation Institution, College Station, TX.

Wool, R. P., and O'Connor, K. M. (1981). "A theory of crack healing in polymers." *Journal of Applied Physics*, 52(10), 5953–5963.

Yoon, C., and Allen, D. A. (1999). "Damage dependent constitutive behavior and energy release rate for a cohesive zone in a thermoviscoelastic solid." *International Journal of Fracture*, (96), 55–74.

You, Z., Adhikari, S., and Kutay, E. M. (2009). "Dynamic modulus simulation of the asphalt concrete using the X-ray computed tomography images." *Materials and Structures*, 42(5), 617–630.